



Doctoral Thesis

**Transformation Dynamics of Amorphous to
Crystalline Carbonates**

submitted by

Florian Konrad

in partial fulfillment of the requirements for the
doctoral degree of natural sciences of
Graz University of Technology

Supervisors

Martin Dietzel - Florian Gallien

Reviewers

Martin Dietzel - Patrick Gane - Attila Demény

Graz, July 2017

Abstract

The versatile industrial applications of carbonate minerals require highly diverse material properties, which are not entirely covered by common natural limestone, chalk and marble. Hence, a high demand exists on synthesizing carbonates with tailored characteristics and properties, but the control on e.g. polymorph development as well as particle size and shape is highly challenging. About two decades ago, it was discovered that many organisms are building their complex calcium carbonate-based skeletons via an amorphous precursor, which points to a potential pathway on how an enhanced control over carbonate mineral formation might be achieved. An understanding of the transformation dynamics of amorphous to crystalline carbonates is therefore advantageous for the development of new synthesis methods and tailored materials. Amorphous calcium carbonate (ACC) - as the calcium end-member precursor - is a hydrated phase forming spherical nanoparticles with a short-range but no long-range order. This absence of a structural order is utilized by organisms to direct polymorphism, particle size and shape of the crystalline transformation product. Many studies have been conducted on the synthesis of amorphous calcium carbonate and its transformation behaviour. But as the amorphous synthesis product mostly transforms within minutes at ambient conditions into a crystalline calcium carbonate individual, polymorph dependent (trans)formation kinetics and mechanisms are difficult to study. In this thesis, the transformation kinetics and mechanisms of additive-free amorphous carbonates, in particular ACC, was experimentally studied to decipher the physicochemical boundary conditions necessary for controlling ACC metastability and its crystallization pathway in air and in aqueous solution. The experimental data indicate that under air exposure the metastability of ACC is governed by the physisorption of H₂O from the gas phase. The uptake of H₂O triggered the transformation of ACC after reaching a critical H₂O level of four monolayers of water on the surface of ACC nanoparticles. The lifetime of ACC was prolonged indefinitely in air-sealed vessels with restricted availability of gaseous H₂O, facilitating the handling of further processing steps. Experimental results of ACC transformation pathways in aqueous solutions show that the formation of distinct calcium carbonate minerals can be controlled by temperature and/or fluid chemistry adjustments of the reactive solution. For instance, ikaite was precipitated from ACC by the adjustment of temperature of the reactive solution. The formation of aragonite through intermediate monohydrocalcite, instead of calcite and vaterite, was triggered by the adjustment of magnesium-concentration in solution. Furthermore, aging experiments of ACC in different (heavy) metal-solutions show high elemental exchange rates with partly complete replacement of calcium during transformation, resulting in the formation of different metal carbonates. This leads to the conclusion that the fate of the amorphous carbonate phase with respect to crystallization pathways and chemical composition depends primarily on the physicochemical conditions during its transformation. Considering the ubiquitous use of calcium carbonates in industrial products, the presented results illustrate new possibilities to enhance control over the crystallization process in order to produce carbonate minerals with tailored material properties.

Outline

Carbonate minerals crystallize from solution by spontaneous ion clustering. According to the classical theory of nucleation, once a critical cluster size has been formed, nucleation starts and the cluster grows by the attachment of ions on the surface. However, in biomineralization the general validity of this classical crystallization theory has been challenged with the finding that organisms can build their carbonate-based skeletons via an amorphous carbonate precursor, which infers a non-classical, particle-mediated nucleation via stable prenucleation clusters. The formation of crystalline carbonates via an amorphous precursor offers new possibilities to unveil certain phenomena, like the natural occurrence of high Mg-calcites that cannot be explained by classical nucleation.

In this thesis, the non-classical nucleation via a stable prenucleation cluster, in particular amorphous calcium carbonate (ACC), and its transformation behaviour into distinct crystalline carbonates was investigated, in an attempt to close some existing gaps and to obtain a better understanding of this newly discovered nucleation pathway.

The present thesis comprises four chapters, one of which was published in 2016 and three of them are prepared for submission. [Chapter 1](#) describes a synthesis method for obtaining additive-free amorphous calcium carbonate in the first place and furthermore focuses on the transformation behaviour of ACC in air and in this respect on the metastabilization of this short-living precursor material. In the following chapters, the previously synthesized and characterized ACC powder was dispersed into aqueous solutions, in order to study the influence of solution chemistry as well as temperature on the transformation of ACC. [Chapter 2](#) focuses thereby on the specific influence of magnesium concentration in solution on the crystallization pathway of additive-free ACC and sheds light on the contribution of fluid chemistry on the metastability of amorphous precursor. [Chapter 3](#) investigates temperature dependent transformation of ACC and discusses the possibility of ikaite formation, a cold temperature indicator mineral, via an amorphous precursor. Finally, [Chapter 4](#) introduces a screening study, in which the general influence of metals in solution on the transformation of ACC into a crystalline carbonate was examined. It further elucidates on the cation sorption capacity of ACC and the possibility to transform the amorphous blank phase into crystalline carbonate minerals with desired chemical compositions and crystal structures.

Table of Contents

Chapter 1 Transformation of amorphous calcium carbonate in air.....	6
1.1 Introduction.....	6
1.2 Experimental.....	8
1.2.1 Synthesis and storage of ACC	8
1.2.2 Methods.....	9
1.3 Results and discussion	11
1.3.1 In-situ monitoring of ACC (trans)formation	11
1.3.2 Characterization of synthesized ACC	12
1.3.3 Metastability and (re)hydration of ACC	14
1.3.4 Crystallization of CaCO₃ polymorphs from ACC transformation	17
1.4 Conclusions.....	19
1.5 Supporting Information	20
1.6 References.....	23
Chapter 2 Influence of solution chemistry on metastability and transformation of amorphous calcium carbonate	28
2.1 Introduction.....	28
2.2 Experimental.....	30
2.2.1 ACC synthesis.....	30
2.2.2 Experimental Setup.....	31
2.2.3 Methods.....	31
2.3 Results	34
2.3.1 Solid phase behaviour in solution	34
2.3.2 Evolution of solid and solution chemistry	36
2.4 Discussion	38
2.4.1 Retardation of ACC transformation in aqueous MgCl₂ solutions.....	38
2.4.2 Distinct carbonate mineral formation controlled by aqueous MgCl₂ content.....	41
2.4.3 Conceptual transformation mechanisms of ACC into different crystalline polymorphs	43
2.5 Conclusions.....	45
2.6 Supporting Information	46
2.7 References.....	47
Chapter 3 Ikaite formation from ACC up to 18 °C questions its use as an indicator of low temperature conditions.....	52
3.1 Introduction.....	52
3.2 Experimental.....	54
3.2.1 Synthesis of ACC.....	54
3.2.2 Experimental Setup.....	54

3.2.3 Methods	55
3.3 Results	56
3.3.1 Phase evolution at distinct temperatures	56
3.3.2 Chemical composition of solids and solution chemistry	60
3.4 Discussion	61
3.4.1 Ikaite formation from an amorphous calcium carbonate precursor	61
3.4.2 Metastability and transformation of ACC at different temperatures	63
3.4.3 Formation of ikaite up to 18 °C and its transformation in air	65
3.5 Conclusions.....	66
3.6 References	67
<i>Chapter 4 Crystallization pathways and cation exchange during transformation of ACC in Me²⁺-solutions</i>	72
4.1 Introduction.....	73
4.2 Experimental.....	74
4.2.1 Synthesis of ACC and experimental setup	74
4.2.2 Analytics	75
4.3 Results and Discussion.....	76
4.3.1 Formation of alkaline earth metal carbonate minerals from ACC	76
4.3.2 Formation of transition metal carbonate minerals from ACC	80
4.3.3 Conditioning transformation pathways of ACC by solution chemistry	81
4.3.4 Implications for natural environments and technical applications	83
4.4 Conclusions.....	84
4.5 Supporting Information	85
4.6 References	87
<i>Chapter 5 Perspectives</i>	93
5.1 Synthesis of amorphous metal carbonates and co-precipitation of different metal ions with ACC.....	93
5.2 Unveiling the individual effects of solid and solution composition on the transformation of amorphous carbonate phases.....	94
5.3 The importance of <i>in-situ</i> observation of reaction processes in aqueous solution...	94
5.4 Adsorption capacity and controlled transformation of ACC.....	95
5.5 References	95
<i>Chapter 6 Afterword</i>	97
6.1 Acknowledgement.....	97
6.2 Curriculum Vitae	98
6.3 Statutory declaration.....	99

Chapter 1

Transformation of amorphous calcium carbonate in air

ABSTRACT: In air, the mechanisms of amorphous calcium carbonate (ACC) transformation into crystalline polymorphs of CaCO_3 and whether the atomic ordering is attributable to a solid-state transformation or a dissolution and re-precipitation process are still under debate. While some studies observed a significant influence of relative humidity on ACC transformation, other studies suggested a dehydration process of ACC prior to crystallization. In the present study, we focus on the metastability of additive-free ACC in air and in particular on its dependence on relative humidity. Our findings indicate that the transformation of ACC into crystalline CaCO_3 is triggered only after the physisorption of a critical H_2O level. Consequently, ACC metastability was prolonged by retarding H_2O uptake and by keeping the physisorbed H_2O below the critical level, ACC remained in its metastable state. Therefore, the conceptual formation of a “thin film” of about 4 monolayers of physisorbed H_2O is considered to govern the transformation of ~ 90 nm sized ACC particles via partial dissolution and re-precipitation. Furthermore, we observed simultaneous formation of calcite, vaterite and aragonite from ACC, where distinct proportions correspond to different H_2O exposure conditions. Thus, polymorph formation from ACC depends also on physicochemical boundary conditions during transformation rather than on pre-structural formation within ACC alone.

1.1 Introduction

Amorphous calcium carbonate (ACC) is of great interest for material science and known to be an important precursor in biomineralisation of crystalline CaCO_3 . It is also of remarkable interest when it comes to crystallization pathways in order to understand how crystals can be formed and grow (Raiteri and Gale, 2010; Rodriguez-Navarro et al., 2016). A large number of studies and synthesis protocols of ACC have, therefore, emerged from a wide variety of different fields. For designing or functionalizing materials, ACC bears great potential, as evidenced by the use of amorphous CaCO_3 as a drug-delivery carrier (Zhao et al., 2015), acting against osteoporosis (Meiron et al., 2011) and by fabricating micropatterned single crystals (Aizenberg et al., 2003) as well as microlens arrays (Lee et al., 2012). In

biomineralisation, ACC has been identified as source for the development of calcium carbonate based shells, spicules or spines (Aizenberg et al., 2002; Addadi et al., 2003; Politi et al., 2004) and offers, for example, an explanation for the fast skeletal re-building of living organisms after moulting (Levi-Kalishman et al., 2002), not least because of its high solubility (Brečević and Nielsen, 1989; Clarkson et al., 1992). Although biogenic ACC contains foreign ions as well as organic ligands, such as amino acids or polysaccharides (Addadi et al., 2003; Gal et al., 2010; Habraken et al., 2015), the interrelationship of inorganic and organic components therein, is so far only poorly understood (Xiao and Yang, 2011). The study of pure additive-free ACC is essential to understand the intrinsic amorphous state and its subsequent transformation behaviour. Determining the actual mechanism of transformation in air and its distinct polymorph formation is of relevance not only for material science but for biomineralisation as well, considering, for example, that the calcite spicules of some sea urchin larval grow from ACC inside a closed membrane separated from aqueous solutions (Beniash et al., 1999; Raz et al., 2003; Devol et al., 2015).

Studies report that in air, additive-free ACC transforms into crystalline CaCO_3 within 1-4 days at ambient temperatures (Lee et al., 2005; Rodriguez-Blanco et al., 2008). By mixing a CaCl_2 - with a Na_2CO_3 -solution in excess ethanol and drying the separated ACC in vacuum, metastabilities of 1-2 months were observed (Gebauer et al., 2010). Another procedure for preserving additive-free ACC up to 6 weeks is documented in Ihli et al. (2013), by freezing a saturated CaCO_3 solution using liquid nitrogen, sublimating the frozen H_2O in a freeze-dryer and, as a result, precipitating ACC as a relict. These extended metastabilities were explained by the removal of physisorbed H_2O from the surface of ACC. Whereas fast transformation of ACC was suggested to be stimulated by loosely bound, physisorbed H_2O at ACC surfaces and/or in cavities between ACC particles, promoting dissolution and re-precipitation (Ihli et al., 2014; Radha and Navrotsky, 2015). Accordingly, faster crystallization of ACC films was found to correlate with elevated relative humidity (RH) conditions (Xu et al., 2006), while the dispersion of ACC in anhydrous alcohol was observed to prevent transformation (Gebauer et al., 2010; Gal et al., 2013). This suggests that humidity is crucial for the metastability of ACC in air, but no systematic study exists on the exact mechanisms.

Herein, we try to elucidate and quantify the role of humidity on the metastability of ACC in air by studying the physisorption of H_2O on ACC particles in respect to different physicochemical boundary conditions. Hence, we synthesized additive- and physisorbed water-free ACC by freeze-drying technique, as it results in extended metastability and reproducible H_2O to CaCO_3 ratios (Brečević and Nielsen, 1989; Ihli et al., 2013) and

quantitatively monitored the evolution of H₂O uptake on ACC particles and its subsequent transformation behaviour to crystalline anhydrous CaCO₃.

1.2 Experimental

1.2.1 Synthesis and storage of ACC

Synthesis of ACC was carried out by mixing two stock solutions prepared with ultrapure Milli-Q water (18.2 MΩcm), where calcium chloride-dihydrate (> 99%, p.a., ACS) and sodium carbonate (> 99.5%, p.a., ACS, Carl Roth) were used as Ca²⁺- and CO₃²⁻-source, respectively. Equimolar concentrations of 0.25 M were chosen for both solutions, with volumes each of 0.08 dm³. The Ca²⁺- and CO₃²⁻-bearing solutions were rapidly mixed (pH ~10) in a beaker at 20 (± 1) °C and immediately transferred into a suction filtration unit. A membrane cellulose acetate filter (0.2 μm pore size, 10 cm diameter) was used for separating the obtaining reaction products from solution. Subsequently the reaction products were washed with 0.1 dm³ of pre-cooled (5 ± 1 °C) ultrapure water and transferred immediately into a freeze-dryer (Figure 1.1). In separate experiments, both solutions were mixed at different concentrations (0.25-1 M) and monitored *in-situ* by Raman spectroscopy to study the duration of metastability of ACC in solution. For monitoring the metastability behaviour in air, freeze-dried ACC was stored at 20 (± 1) °C and 25 (± 4) % RH (lab atmosphere) in 0.04 dm³ glass vials under different conditions. For open conditions, under constant exchange with the lab atmosphere, vials without caps were used. For a reduced exchange, the vials were closed with semi gastight polypropylene caps, in the following called semi-tight conditions. To avoid exchange with the lab atmosphere at all, a gastight Teflon cap was used.

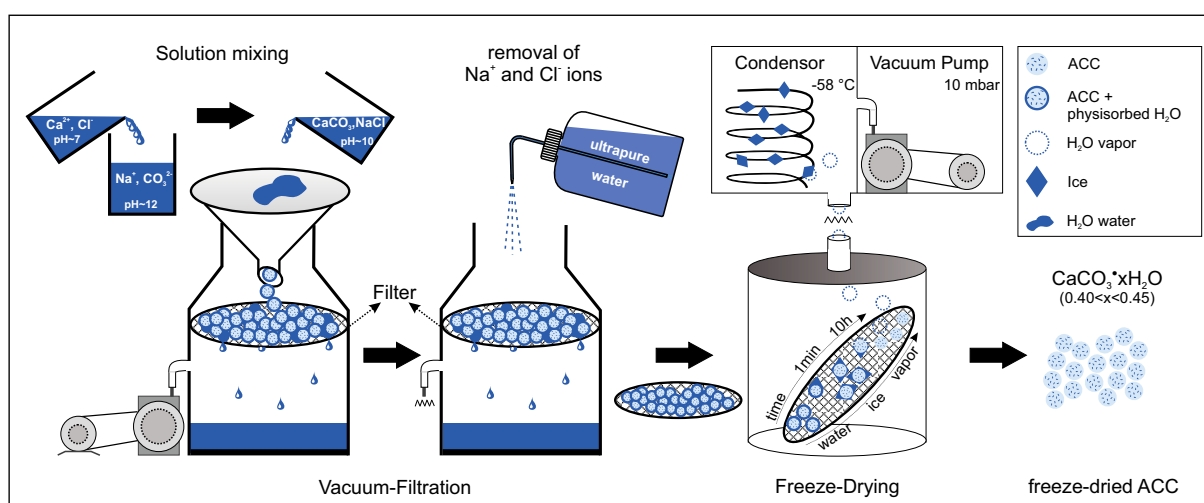
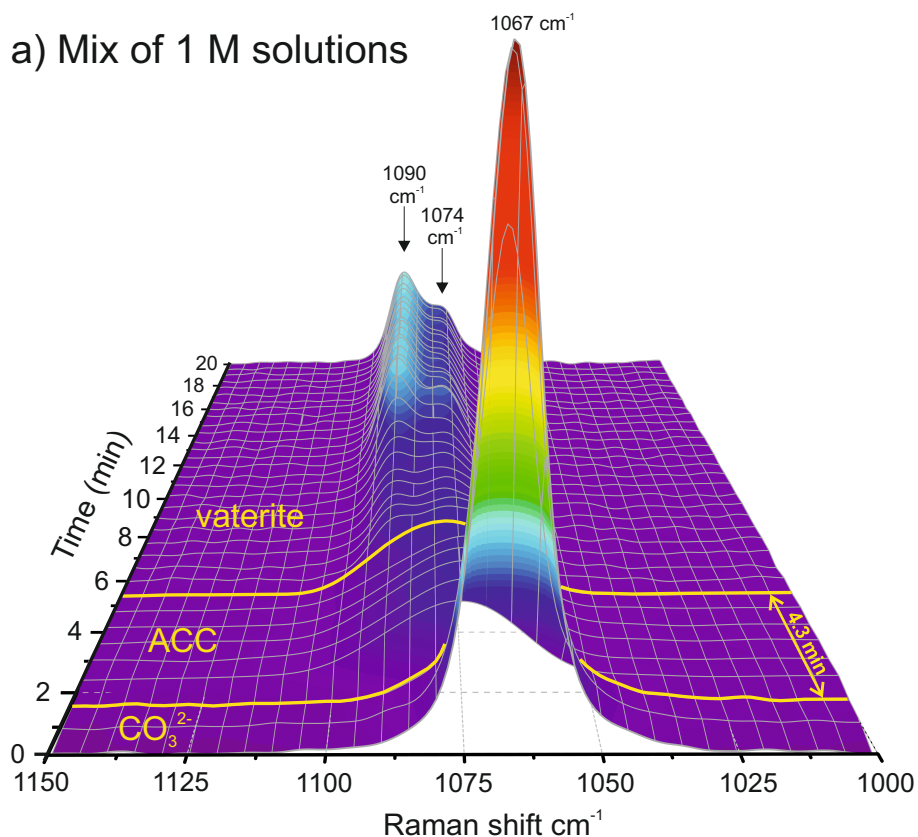


Figure 1.1. Experimental set-up exemplifying synthesis route for partially-dehydrated additive-free ACC.

1.2.2 Methods

For sublimation of physisorbed water, a Virtis Benchtop 3 dm³ freeze-dryer (-58 °C condenser temperature, 10 mbar partial vacuum) was used. The structural composition of the freeze-dried precipitates were analysed by Fourier Transform Infrared Spectroscopy (FT-IR) using a PerkinElmer Frontier FT-IR in ATR-mode in the 650 - 4 000 cm⁻¹ range at a 4 cm⁻¹ resolution, and by powder X-ray diffraction (PXRD) performed on a PANalytical X'Pert Pro diffractometer, equipped with a Co-target and a solid state real time multiple strip (RTMS) detector (measurement parameters: 40 kV, 40 mA, 0.008° step, 40 s per step, 20-60° 2θ). For qualitative characterisation of crystalline products the crystal structure database from ICSD was used. Quantitative results were obtained by Rietveld-analysis in combination with an internal standard for determination of crystallinity. The precipitates were heated in a PerkinElmer STA8000 simultaneous thermal analyser (from 25 – 1 000 °C, 10 °C min⁻¹, 0.03 dm³ min⁻¹ 99.999% N₂) coupled with the above FT-IR for evolved gas analysis to study H₂O-content and crystallization temperature. *In-situ* monitoring of the dissolved inorganic carbon and reaction products during synthesis was realised with a Raman RXN2 analyser (Kaiser Optical Systems) equipped with a Kaiser MR Probe head (quarter-inch immersion optic) running with a 785 nm laser. The spectra were collected in a 35 s interval with a resolution of 1 cm⁻¹. The precipitates were imaged by secondary electrons using a ZEISS DSM 982 Gemini scanning electron microscope (SEM) equipped with a field emission gun operated at 5 kV using gold-coated samples. For transmission electron microscopy (TEM) images and selected area electron diffraction (SAED) patterns, the reaction products were placed on holey carbon grids and measured on a FEI Tecnai 12 microscope operating at 120 kV and equipped with an EDAX Sapphire Si(Li) detector. Brunauer-Emmett-Teller (BET) surface area measurements were carried out by nitrogen adsorption conducted without pre-treatment at room temperature on a Micromeritics TriStar II 320 V1.01. Monitoring relative humidity (RH) of the lab atmosphere and of the sample compartment was realised by using a Voltcraft DL-121TH data-logger and by using a MSL Hygrochron iButton logger with reported accuracies of for a single measurement of ± 3% and ± 5% respectively.

a) Mix of 1 M solutions



b) Mix of 0.25 M solutions

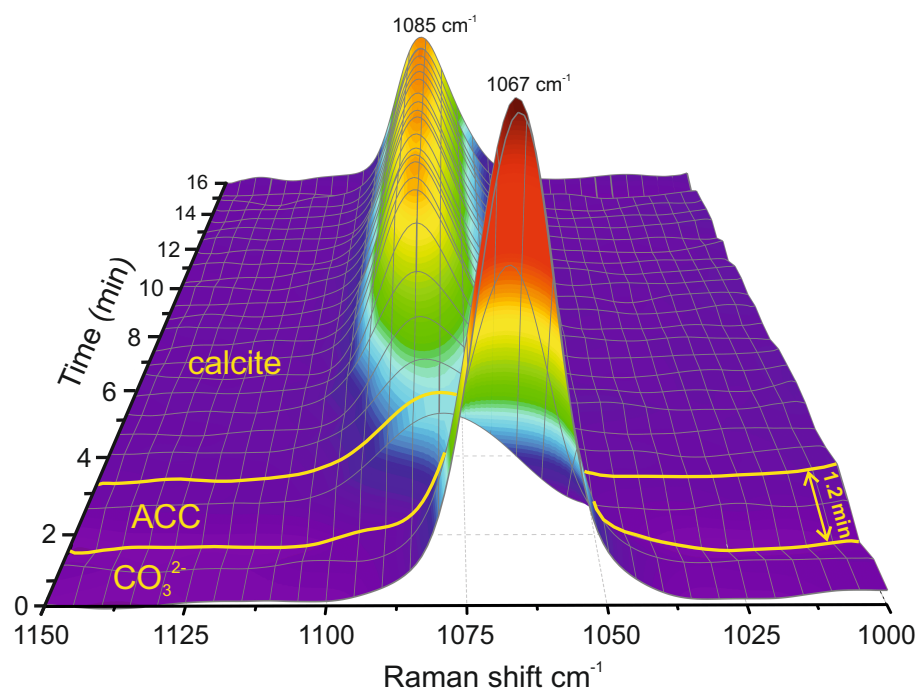


Figure 1.2. Reactive solution monitoring by *in-situ* Raman probe analysis during two syntheses runs. After mixing the Ca^{2+} - into the CO_3^{2-} -bearing solution at a reaction time of 1.5 min, the symmetric stretch band at 1067 cm^{-1} , corresponding to dissolved CO_3^{2-} -ions, decreased and a broad adsorption band with a maximum at 1080 cm^{-1} arose, indicating ACC formation. (a) For mixing 1 M solutions, ACC transformation into vaterite occurs after 4.3 min, (b) while mixing 0.25 M solutions results in transformation of ACC into calcite after 1.2 min of reaction time. It has to be mentioned that for the latter we do not exclude the intermediate formation of vaterite prior to calcite formation as e.g. reported by [Bots et al. \(2012\)](#), but vaterite was not detected within the 30 s integration time of the *in-situ* Raman analyses.

1.3 Results and discussion

1.3.1 *In-situ* monitoring of ACC (trans)formation

During synthesis of ACC the reaction time plays a crucial role with respect to the metastability of ACC in aqueous solution. When the Ca^{2+} - and CO_3^{2-} -bearing solutions were mixed, instantaneous precipitation occurred and *in-situ* Raman probe analysis indicated the formation of ACC as initial reaction product, which was valid for all experimental runs independent of the concentration used. Figure 1.2 shows the initial occurrence of dissolved CO_3^{2-} ions by the presence of the symmetric stretch band of the carbonate molecule at $1\,067\text{ cm}^{-1}$ (Geisler et al., 2012). This band decreased as the Ca^{2+} -rich solution was introduced after 1.5 min, and a broad vibration band from $1\,050 - 1\,110\text{ cm}^{-1}$ arose with a peak maximum at about $1\,080\text{ cm}^{-1}$ corresponding to ACC (Wang et al., 2012). The subsequent transformation of ACC into calcite ($1\,085\text{ cm}^{-1}$) (Wang et al., 2012) and/or vaterite (bands at $1\,074\text{ cm}^{-1}$ and $1\,090\text{ cm}^{-1}$) (Gabielli et al., 2000) occurred by using 0.25 M and 1 M solutions after 1.2 min and 4.3 min, respectively (Figure 1.2a and b). This result verifies the spontaneous formation of ACC and allows validating the kinetically limited time frame for separation of ACC from aqueous solution. Although this observation would encourage using higher concentrations for synthesis, the removal of Na^+ and Cl^- ions by washing with ultrapure H_2O was difficult to obtain at elevated concentrations of 1 M compared to 0.25 M due to the high viscosity. Therefore, we chose concentrations of 0.25 M for both stock solutions as being, according to our experience, the most effective way to synthesize reproducibly solely “additive free” ACC.

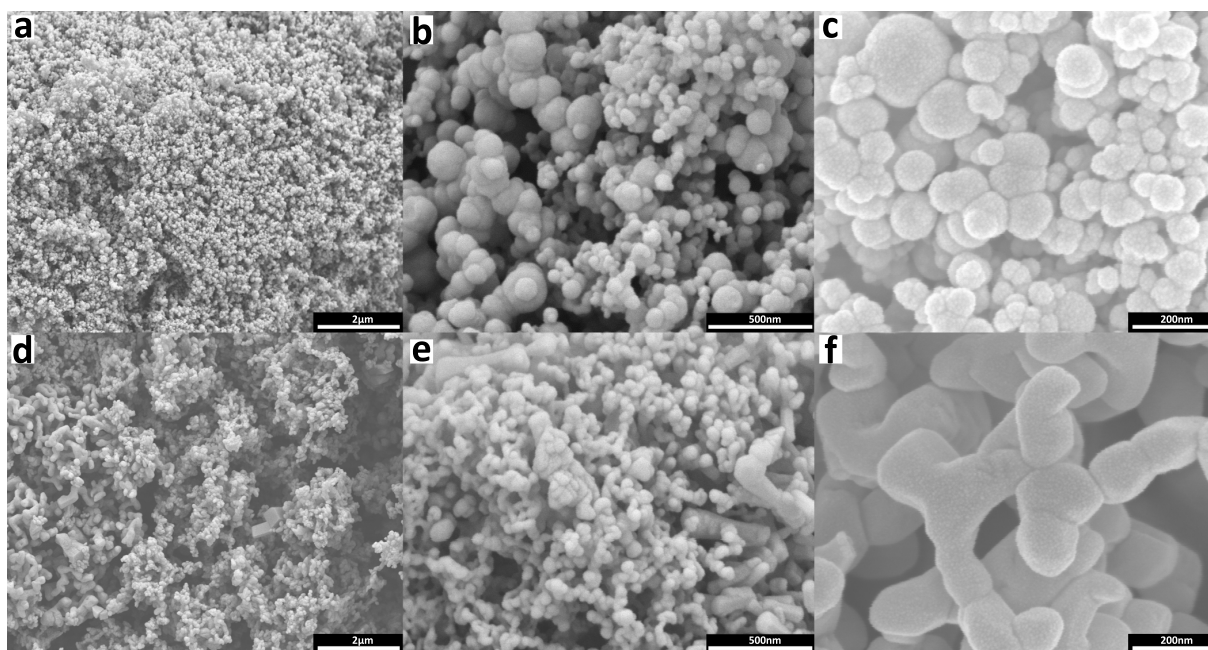


Figure 1.3. SEM images of synthesized ACC (a-c) consisting of spheroidal and aggregated nanoparticles with rough surfaces and of the final fully transformed samples (d-f) displaying slightly larger nanometre particles with poorly developed crystal faces.

1.3.2 Characterization of synthesized ACC

Reaction products from the mixing of 0.25 M solutions containing CaCl_2 and Na_2CO_3 were separated from the solution via filtration and washed within 1 min and immediately freeze-dried to obtain an ACC standard material and to avoid its potential transformation (see [Figure 1.2b](#)). SEM of the reaction products show spheroidal particles with a size range of 30-200 nm with a mean particle size of about 90 nm ([Figure 1.3a-c](#)). TEM analysis of the precipitated nanoparticles indicate no discrete structural ordering, showing instead selected area diffraction (SAED) patterns with diffuse diffraction rings only ([Figure 1.4](#)). The formation of an amorphous calcium carbonate phase is also evidenced from PXRD patterns displaying a broad hump with no discrete peaks ([Figure 1.5](#)). In accordance, the infrared spectra of all synthesis products display characteristic bands for ACC ([Figure S1.1](#)) ([Andersen and Brecevic, 1991](#)). BET surface area measurements result in $41.9 (\pm 1.5) \text{ m}^2 \text{ g}^{-1}$ as determined for three independent samples.

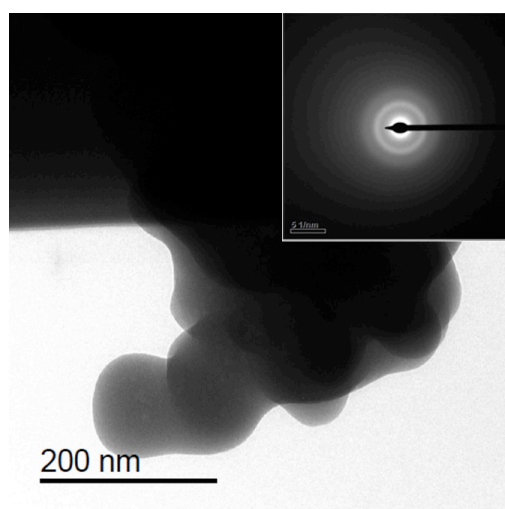


Figure 1.4. TEM image of freeze-dried ACC with selected area diffraction pattern showing diffuse rings only.

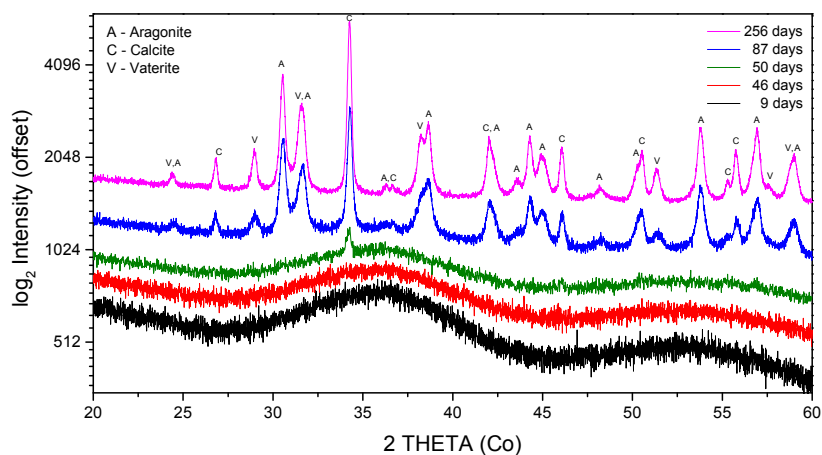


Figure 1.5. Stack plot of PXRD patterns of a synthesised ACC sample throughout storage time under semi-tight conditions showing the transformation of ACC into crystalline calcium carbonate polymorphs.

Thermal analyses of the precipitates, immediately after freeze-drying, show as a first endothermic event a continuous weight loss of about $7.0 (\pm 0.2)$ wt% over the temperature range up to $340 (\pm 3)$ °C (Table 1.1 and Figure S1.2). At this temperature an exothermic event occurs without change in weight. Subsequently, a second endothermic event related to a weight loss of about $40 (\pm 2)$ wt% is visible at an onset temperature of ~ 665 °C. The simultaneously monitored gas FT-IR absorption spectra show characteristic absorption bands for water over the range up to the first exothermic event at ~ 340 °C, and at the endothermic second event, starting at ~ 665 °C, a gas absorption spectrum of CO₂ indicates calcination (Figure S1.3). The determined H₂O-content measured by thermal analyses directly after freeze-drying yields in the chemical formula of CaCO₃•(0.42 ± 0.01)H₂O for the obtained ACC. This is in good agreement with the results of Schmidt et al.(2014), who reported remaining water-contents of 0.4 mol H₂O pfu (per formula unit) after losing, as they termed it, the fluid-like mobile H₂O. Other studies attributed the latter loss to physisorbed water due to its weak bonding and easy removal at low temperatures, leaving entrapped the more rigid and structural-bound H₂O (Michel et al., 2008; Ihli et al., 2014; Radha and Navrotsky, 2015). The exothermic event at ~ 340 °C, without any change of weight, indicates a solid-state transformation of ACC to calcite as no remaining water is available (Radha et al., 2010).

Here we want to emphasize that variable H₂O-contents are described for the composition of ACC, which were attributed, among others, to the different synthesis routines or to different properties (Addadi et al., 2003; Raiteri and Gale, 2010; Ihli et al., 2013). However, comparing several studies, where additive-free ACC was desorbed and thermogravimetry data can be interpreted accordingly, show that in each case about 0.4 mol H₂O pfu remained after losing the physisorbed H₂O (Faatz et al., 2005; Günther et al., 2005; Fernandez-Martinez et al., 2013; Schmidt et al., 2014; Rodriguez-Navarro et al., 2015). This suggests, despite different synthesis methods and observed initial water-contents, that the amount of structural-bound H₂O of ACC is the same and that the reported differences solely originated from different proportions of physisorbed H₂O. This might be explained by differences in preparation techniques, e.g. the efficiency of the filtration and washing procedure, respectively might stem from different ACC surface areas in respect to distinct particle size distributions (Raiteri and Gale, 2010; Ihli et al., 2013).

Table 1.1. H₂O-content of synthesized ACC from thermogravimetric measurements throughout storage time in relation to observed metastabilities and storage conditions. *Note:* The reported loss on ignition (LOI) at 350 °C was corrected for the anhydrous crystalline content present; *re-freeze-dried samples.

Samples	storage (days)	LOI at 350°C (wt%)	CaCO ₃ • xH ₂ O	physisorbed H ₂ O (mol pfu)	crystallinity (wt%)
FD-ACC-open 1	0	6.827	0.41		amorphous
	1	8.834	0.54	0.13	amorphous
	2	9.238	0.57	0.16	amorphous
	3	9.650	0.59	0.19	amorphous
	4	10.524	0.65	0.25	1-3 wt% crystalline
FD-ACC-open 2	0	7.118	0.43		amorphous
	5	10.410	0.65	0.22	1-3 wt% crystalline
FD-ACC-open 3	0	7.306	0.44		amorphous
	4	10.798	0.67	0.23	1-3 wt% crystalline
	4*	6.978	0.42		1-3 wt% crystalline
FD-ACC-semi-tight 1	0	6.984	0.42		amorphous
	48	11.032	0.69	0.27	1-3 wt% crystalline
	48*	7.093	0.42		1-3 wt% crystalline
FD-ACC-semi-tight 2	0	7.145	0.43		amorphous
	32	10.130	0.63		amorphous
	32*	6.913	0.41		amorphous
	37	11.319	0.71	0.28	1-3 wt% crystalline
FD-ACC-semi-tight 3	0	7.110	0.43		amorphous
	51	10.511	0.65	0.23	1-3 wt% crystalline
FD-ACC-gastight	0	6.904	0.41		amorphous
	150	8.171	0.49	0.08	amorphous
FD-ACC-desiccator	0	6.904	0.41		amorphous
	150	7.189	0.43	0.02	amorphous

1.3.3 Metastability and (re)hydration of ACC

Regular analysis by FTIR, PXRD, SEM and TG showed that in constant exchange with the lab atmosphere (25 ± 4% RH) crystallization of ACC was initiated after 4-5 days for open conditions and after 37-51 days for semi-tight conditions with a reduced exchange. As shown in [Table 1.1](#) and [Figure 1.6](#), thermogravimetry revealed that the H₂O content of freeze-dried ACC increased during storage time, and independently of storage conditions crystallization was initiated as soon as 10.8 (± 0.4) wt% H₂O, corresponding to CaCO₃•(0.67 ± 0.03)H₂O, was reached. In comparison with the initial physisorbed water-free ACC stoichiometry of 0.42 (± 0.01) mol H₂O pfu, transformation occurred after the uptake of 0.25 (± 0.03) mol H₂O pfu. Considering the uptake as physisorbed surface H₂O on ACC particles, a simplified approximation suggests a ~1.2 nm thin H₂O layer or ~4 monolayers of physisorbed H₂O for a mean particle size of 90 nm and a density of 1.9 kg dm⁻³ (for calculation details see [Table S1.1](#)) ([Bolze et al., 2004](#); [Faatz et al., 2005](#)). Monitoring the evolution of RH in the enclosed

sample compartments, shows in the case of the semi-tight conditions that the initial RH of 25 (± 4) % decreased after 2 h to a minimum of approximately 10 (± 5) %. Subsequently, the RH again reached the value of the external atmosphere until transformation, when the former structural-bound water is liberated and the RH increases abruptly to 65 (± 4) % (see [Figure 1.6](#)). Together with the TG-data, we can picture that the uptake of H₂O by ACC, immediately after its synthesis causes a corresponding decrease of RH in the semi-tight vial. The RH then equilibrates with the external atmosphere as a matter of H₂O transfer into the vial, which depends on gas permeability of the cap and the gradient between the RH of the reaction chamber and the external atmosphere. An analogous initial evolution of RH was observed in the reaction chamber of the gastight vial, where RH decreased due to the H₂O uptake of ACC to 6 (± 5) %, but in contrast to the semi-tight conditions no equilibration with the atmosphere is possible and the RH remained at this low level until the end of the experiment at 150 days (see [Figure 1.6](#)). Subsequent PXRD measurement of the latter ACC showed no transformation to crystalline CaCO₃ and the TG-results suggest an uptake of 0.08 mol H₂O pfu throughout the 150 days, which is assumed to originate from the RH decrease in the vial (see [Table 1.1](#)). This matches with the results we obtained when placing a subsample from the same ACC batch in a desiccator with silica gel, where an uptake of 0.02 mol H₂O pfu was detected after 150 days (see [Table 1.1](#)).

The availability of H₂O is clearly the rate limiting parameter for the metastability of ACC in air. Under “restricted” H₂O supply (e.g. semi-tight conditions), the metastability increases, whereas given “unlimited” availability of H₂O the metastability of ACC reduces significantly. In any case, under open or semi-tight conditions, the uptake of the same critical amount of H₂O is observed prior to and in parallel with initial crystallization. Thus, keeping the uptake of H₂O on ACC particles, with ~90 nm in size, below the observed critical amount of 0.25 (± 0.03) mol of physisorbed H₂O pfu, the ACC metastability can be extended significantly or as yet indefinitely, as transformation was not observed in the gastight vial or in a desiccator within the time frame of the present study of about 150 days. A finding, which quantitatively explains reported metastabilities of ACC of at least 3 months when kept in a container with silica gel ([Rodriguez-Navarro et al., 2015](#)). In addition, re-freeze-drying a “matured” ACC sample containing 0.63 mol H₂O pfu, which is already close to the critical water uptake level of 0.67 (± 0.03) mol pfu, resulted again in an initial H₂O-content of about 0.41 mol pfu and exhibited, accordingly, prolonged metastability (see [Table 1.1](#) and [Figure 1.6](#)). Hence, we suggest that a sufficient layer of H₂O covering the surface of ACC particles is initiating crystallization via a partial dissolution and re-precipitation process. Although there is no

evidence that ACC fully dissolves, aqueous diffusional transport of calcium and carbonate ions within the H₂O layer can be reasonable suggested as the driving force for transformation of ACC in air. Accordingly, the ACC transformation occurs in the sense of an interface-coupled dissolution/re-precipitation, reflecting the interplay between availability of H₂O and time frame for reaching a critical physisorption level of H₂O, which ultimately triggers the ACC transformation process. In contrast ion diffusion by considering solid-state transformation would take too long at ambient temperatures to be realistic for the time spans observed for ACC transformation (Rodriguez-Navarro et al., 2015). However details on ion diffusion characteristics and kinetics during ACC transformation cannot be resolved from the present experimental approach and requires further investigation.

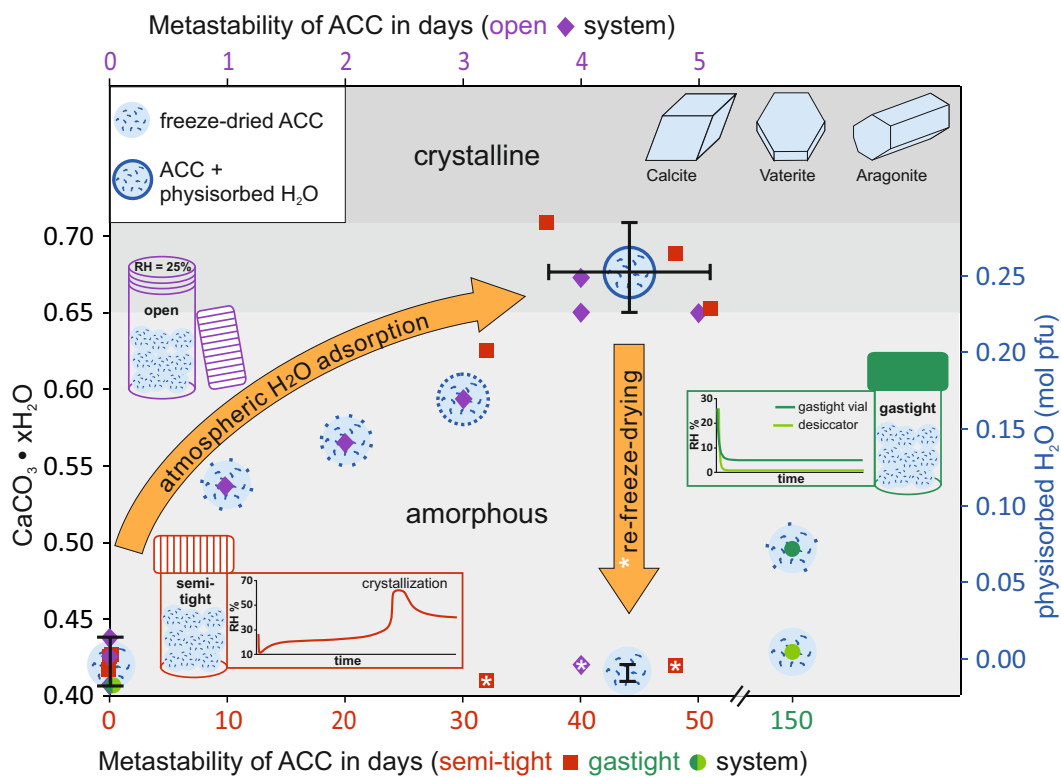


Figure 1.6. Schematic diagram illustrating the H₂O physisorption process by plotting measured H₂O-contents of ACC vs. observed ACC metastabilities from Table 1.1. The H₂O content can be followed by x total (left y -axis) and net physisorbed (right y -axis) H₂O pfu. Atmospheric H₂O becomes physisorbed on ACC particles until a critical level of 0.25 (\pm 0.03) mol of physisorbed H₂O pfu of ACC has been reached, which ultimately triggers ACC transformation. At open conditions, transformation of ACC was observed after a reaction time of 4-5 days (\blacklozenge open system; x -axis at the top). ACC at semi-tight conditions - reduced H₂O exchange with the atmosphere - showed compared to the open system prolonged metastability of up to 51 days (\blacksquare semi-tight system; x -axis below). ACC kept under gastight conditions - no exchange with the external atmosphere - did not show transformation of ACC even after 150 days (\bullet gastight system; x -axis below). Secondary removal of physisorbed H₂O by re-freeze-drying mature ACC samples results in ongoing metastability of ACC (vertical arrow). Inserted figures display the typical evolution of the measured relative humidity (RH in %) as a function of reaction time. At open conditions, RH is constant throughout physisorption of H₂O on ACC (RH = 25 %). At gas-tight conditions, RH is reduced to a minimum due to physisorption of the vial's H₂O on ACC. In contrast, at semi-tight conditions RH increases again by approaching the RH of the external atmosphere. At the above given critical level of 0.25 (\pm 0.03) mol of physisorbed H₂O pfu of ACC its transformation to crystalline anhydrous CaCO₃ is promoted, which is accompanied by the liberation of physisorbed and formerly structural-bound H₂O and can be seen by reaching a maximum RH value of about 65%.

Since crystallization occurs progressively, the critical uptake of $0.25 (\pm 0.03)$ mol H₂O pfu may not be used unequivocally as a constraint to estimate the required amount of H₂O for commencing surface dissolution and re-precipitation. We suppose that the progressive crystallization is governed by spatial differences in H₂O availability depending on micro-environmental conditions, gaseous H₂O diffusion rates and individual particle sizes. This may lead to areas, which show promoted crystallization, whereas other parts of the sample still remain in its amorphous state. Dehydration of ACC prior to crystallization into an intermediate anhydrous ACC phase, as reported by others (Rodriguez-Blanco et al., 2011; Bots et al., 2012; Ihli et al., 2014), was not detected in the present study. Instead, we observed an ongoing uptake of H₂O on ACC without any sign of ordering. Only when the critical uptake of $0.25 (\pm 0.03)$ mol H₂O pfu was reached, dehydration was detected originating from the liberation of structurally bound H₂O during the crystallization to anhydrous CaCO₃ polymorphs (e.g. see RH maximum at semi-tight conditions in Figure 1.6).

1.3.4 Crystallization of CaCO₃ polymorphs from ACC transformation

Transformation of freeze-dried ACC, from the first sign thereof to the complete crystallization to anhydrous CaCO₃ polymorphs, took several days for samples in an open system and at least a month for samples in the semi-tight system (Table 1.1). Figure 1.4 shows exemplarily PXRD-patterns of an ACC sample with the development of a first small (1 0 4) peak of calcite in a predominantly amorphous powder after 50 days of storage in the semi-tight system. After 87 days ACC was still detectable by the amorphous hump in the PXRD pattern, whereas calcite, vaterite and aragonite are indicated by broad peaks. Continuous crystallization until 256 days led to well-developed peaks of calcite, vaterite and aragonite in the PXRD patterns, indicating an increased state of atomic order and an entire transformation of ACC to a mixture of the three anhydrous CaCO₃ polymorphs. SEM images of the crystallized samples (Figure 1.3d-f) show single particles, which do resemble the crystalline polymorphs, but the overall appearance, even after 300 days, remains akin to the amorphous compound in respect to particle sizes and shapes (Figure 1.3 and S1.4). Idiomorphic crystals of rhombohedral calcite and needle-like aragonite are scarce. Some agglomerated particles tend to form larger crystals, but for the majority the growth and development of crystal faces is retarded.

In our experiments ACC mostly transforms into calcite and vaterite at different proportions, whereas in some cases aragonite was additionally formed. Different proportions of calcite and vaterite from ACC transformation are often reported. They could be explained e.g. by the development of proto-structures in ACC originating from the changing pH conditions during

synthesis, which drops from about pH 12 at the very beginning to about pH 10 at the end of precipitation (Gebauer et al., 2008; Rodriguez-Blanco et al., 2012). Although aragonite is rarely observed when mixing CaCl_2 - with Na_2CO_3 -solutions without additives (Nielsen et al., 2014), variations in pH could lead to the formation of proto-aragonite structures in ACC as well. However, placing different amounts of subsamples of the identical ACC product in separate vials (0.04 dm^3) at semi-tight conditions resulted in crystallization of different proportions of anhydrous CaCO_3 polymorphs (Figure S1.5). As these three experiments only differ in respect to their sample amount vs. air volume of the compartment, we propose that the availability of H_2O in the whole system plays a decisive role in the formation of individual CaCO_3 polymorphs. In general, samples stored at semi-tight compared to open conditions, show on average less calcite and more vaterite and on occasion aragonite, which was never detected in the open system.

Since we are observing three crystalline calcium carbonate polymorphs at different proportions from an identical ACC depending on physicochemical conditions, it seems unlikely that the herein synthesized ACC carries an inherent proto-crystalline structure, in contrast to that previously proposed for ACC synthesized at lower pH and concentration (Gebauer et al., 2008; Gebauer et al., 2010). Farhadi Khouzani et al. (2015) recently reported, that ACC synthesized in isopropanol instead of water, show no proto-structural features related to any crystalline polymorph. They concluded that using alcohol is comparable to high supersaturation in aqueous fluids, where no distinct pre-nucleation clusters could have been detected so far and that water is necessary for developing distinct proto-structures. Xu et al. (2008), dispersed ACC into anhydrous ethanol and different volumes of water and observed different polymorph proportions. They concluded, when the amount of water was low, the transformation rate is reduced and the metastable intermediate phases, such as vaterite and aragonite, can be observed. Furthermore, Baltrusaitis and Grassian (2009), pointed out from AFM-studies, that the physisorption of H_2O on the (1 0 -1 4) plane forms an amorphous hydrate layer, which acts as substrate for vaterite formation. Assuming an interface-coupled surface dissolution process, the restricted H_2O availability at semi-tight conditions can generate highly supersaturated particle surface solutions with respect to the metastable intermediate phases (Putnis, 2014). Since the observed physisorption process in air is slow compared to instant and unlimited water access in an aqueous solution, reaction kinetics at limited H_2O availability respectively at low humidities in air are considered to be slow as well. The proposed slow reaction kinetics could therefore explain the finding of more than one metastable CaCO_3 polymorph next to calcite. Polymorphism of CaCO_3 was also

suggested to be correlated with particle sizes from the originating ACC (Zou et al., 2015), but again, as we observe different polymorph developments from an identical ACC sample, which was randomly split, this might not apply to our transformation in air. However, further detailed experimental investigations are needed (i) to draw unequivocal conclusions on the relationship between the H₂O availability and the development of individual crystalline polymorphs from ACC transformation and (ii) to being able to control rather than observe CaCO₃ polymorph formation from ACC.

1.4 Conclusions

The removal of physisorbed water from ACC particles retards its transformation to anhydrous crystalline CaCO₃ polymorphs in air. This slow transformation, in comparison to that in aqueous solution enables to relate and quantify metastabilities of ACC and its subsequent transformation with the uptake of H₂O. It was found, that the metastability of ACC is controlled by the availability of H₂O during storage time and that crystallization is triggered only after the uptake of a critical value of 0.25 (\pm 0.03) mol H₂O pfu corresponding to the conceptual formation of a ~1.2 nm thin physisorbed H₂O layer on 90 nm sized ACC particles. The physisorbed H₂O is considered as the driving force for reorganization of ACC into anhydrous CaCO₃ structures via partial dissolution and precipitation, and thus the critical parameter for ACC transformation kinetics in air. Uptake of H₂O below the critical value, results in ACC persisting in its metastable amorphous form. In consensus, re-freeze-drying a matured ACC sample and thus removing again the loosely bound, physisorbed H₂O, prolonged the metastability and prevented transformation. Our observation on the transformation of ACC revealed differences in polymorph developments, namely the occurrence of calcite, vaterite and aragonite at different proportions, in respect to H₂O availability. Thus, it seems unlikely that the herein synthesized ACC carries an inherent proto-crystalline structure, indicating that physicochemical boundary conditions are decisive for the reaction kinetics and paths of ACC transformation.

1.5 Supporting Information

Table S1.1. Critical H₂O uptake level to initiate crystallization calculated as physisorbed layers on the surface of synthesised ACC particles. Mean particle sizes of ACC are approximated from SEM images. Reported are results accounting for the uncertainty of the critical H₂O uptake of 0.25 (± 0.03) mol. *Note:* ACC density of 1.9 kg/dm³ was chosen according to [Faatz et al. \(2005\)](#), for ACC with 0.5 mol H₂O pfu, being close to our reported value after freeze-drying. For ACC, alternative density values from 2.18 to 2.7 kg/dm³ are reported ([Fernandez-Martinez et al., 2013](#); [Saharay et al., 2013](#)), which changes the critical number of ACC covering H₂O layers from around 4 to 5. The thickness of one H₂O monolayer was taken from [Beruto and Botter \(2000\)](#).

Description	Value	Unit	Comment
volume of 90 nm spherical ACC particle	381 704	nm ³	$(4/3) * \Pi * r^3$
mass of 90 nm ACC particle	7.25E-16	g	*ACC density 1.9 kg/dm ³
mol of 90 nm ACC particle	6.75E-18	mol	/107.5 g MW of freeze-dried ACC
mean critical H₂O uptake of ACC pfu	0.25 ± 0.03	mol	
H ₂ O uptake on 90 nm ACC particle	1.69E-18	mol	*mol of 90 nm ACC particle
	30 358.74	nm ³	*18 g MW of H ₂ O
volume of ACC particle + H ₂ O uptake	412 062.25	nm ³	
radius of 90 nm particle + H ₂ O uptake	46.16	nm	$\left(\frac{Volume}{(4/3) * \Pi}\right)^{\frac{1}{3}}$
thick H₂O layer around 90 nm particle	1.16 ± 0.14	nm	
H₂O monolayers on 90 nm ACC particle	3.75 ± 0.44	layers	/0.31 nm one H ₂ O monolayer

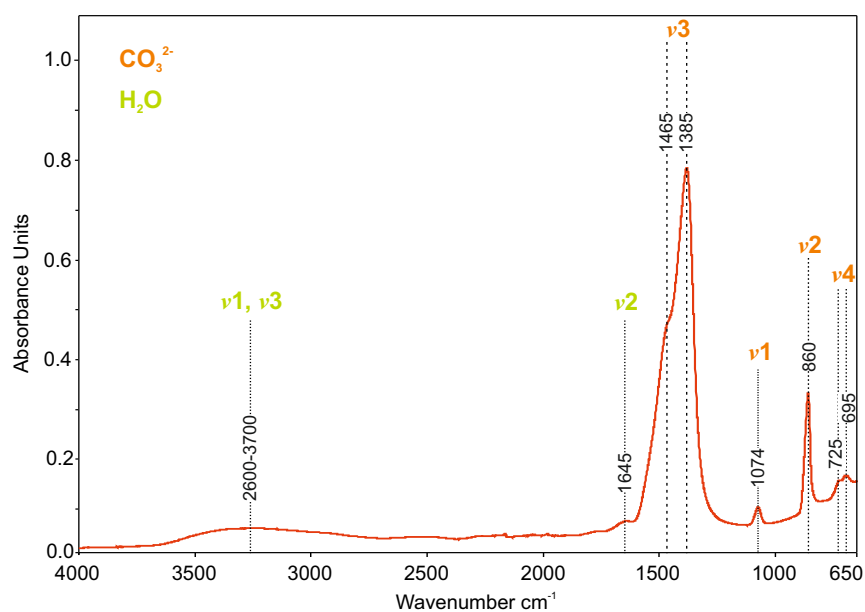


Figure S1.1. FT-IR pattern of ACC directly after freeze-drying, highlighting the molecular bending and stretching vibrations of the carbonate and H₂O molecule. The molecular vibrations of the carbonate ion exhibit broad split ν_4 deformation bands at ~ 695 and ~ 725 cm⁻¹, ν_2 bands at ~ 860 cm⁻¹, ν_1 stretching vibrations at ~ 1074 cm⁻¹, split ν_3 bands at ~ 1385 and ~ 1465 cm⁻¹ and attributed to water ν_2 bending vibrations at ~ 1645 cm⁻¹ as well as broad superimposed ν_1 and ν_3 bands from 2600 to 3700 cm⁻¹. The main differences between ACC and crystalline polymorphs of calcium carbonate can be observed in the bending vibrations as the ν_4 bands of the latter are sharp and discrete and the ν_2 bands are shifted either to lower wavenumbers around 854 cm⁻¹ for aragonite or to higher wavenumbers around 873 cm⁻¹ for calcite, vaterite and monohydrocalcite (Andersen and Brecevic, 1991; Coleyshaw et al., 2003).

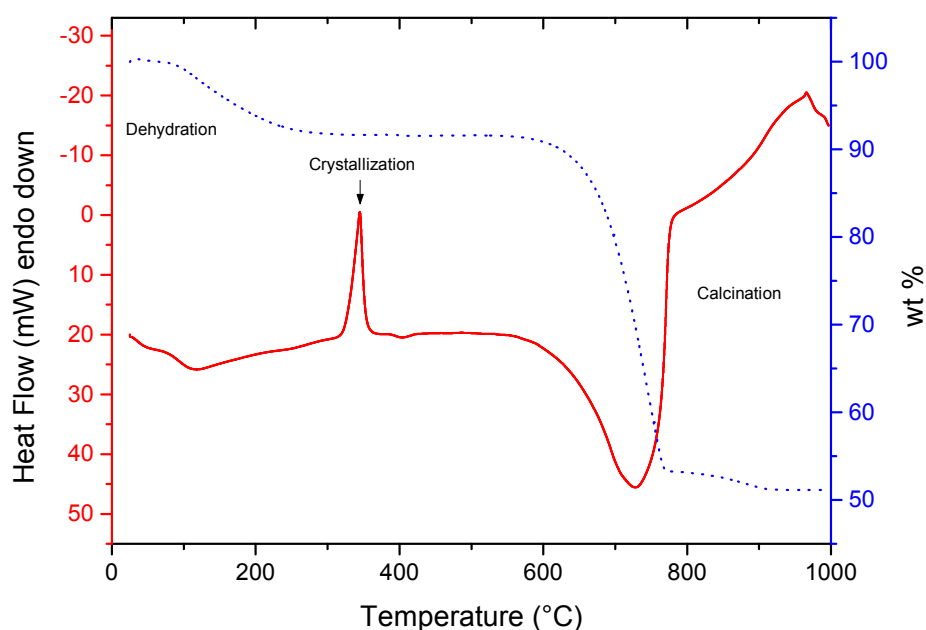


Figure S1.2. Typical result from thermal analysis synthesized after freeze-drying (sample FD-ACC-open 3). The endothermic weight loss between 25 °C and 340 ± 3 °C is ascribed to dehydration of ACC (see Figure S1.3 for analyses of liberated gas), followed by exothermic crystallization at $340 (\pm 3)$ °C and subsequent calcination above 665 °C. Dashed blue line denotes weight loss in wt%. Solid red line shows heat flow in milliwatts.

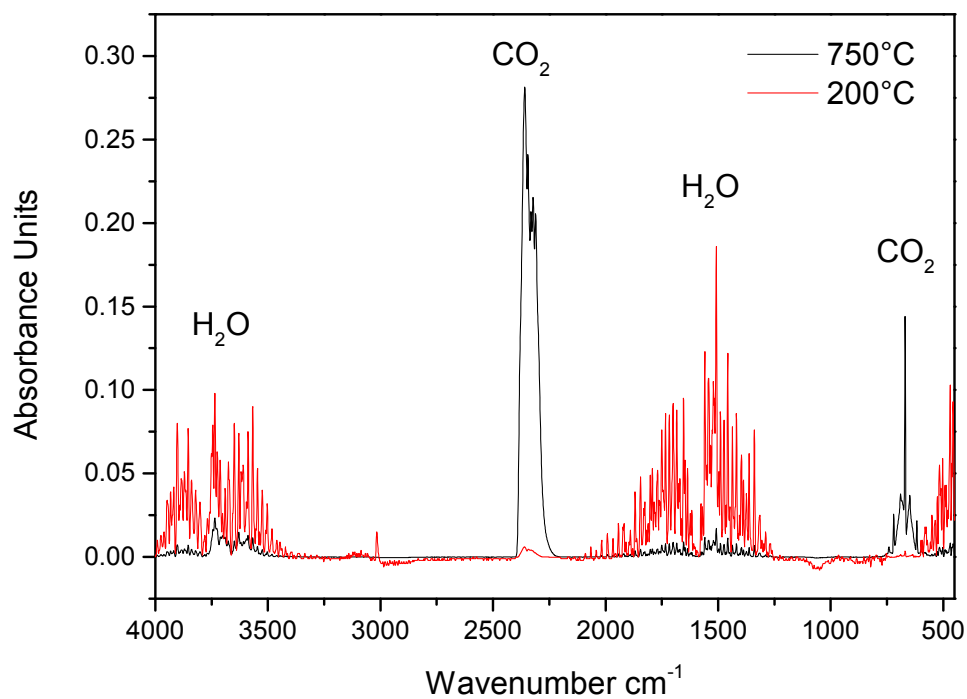


Figure S1.3. Gas FT-IR absorption spectra measured during thermal analysis (see [Figure S1.2](#)) at 200 °C and 750 °C, which clearly indicates H₂O release from the solid and CO₂ liberation caused by calcination, respectively.

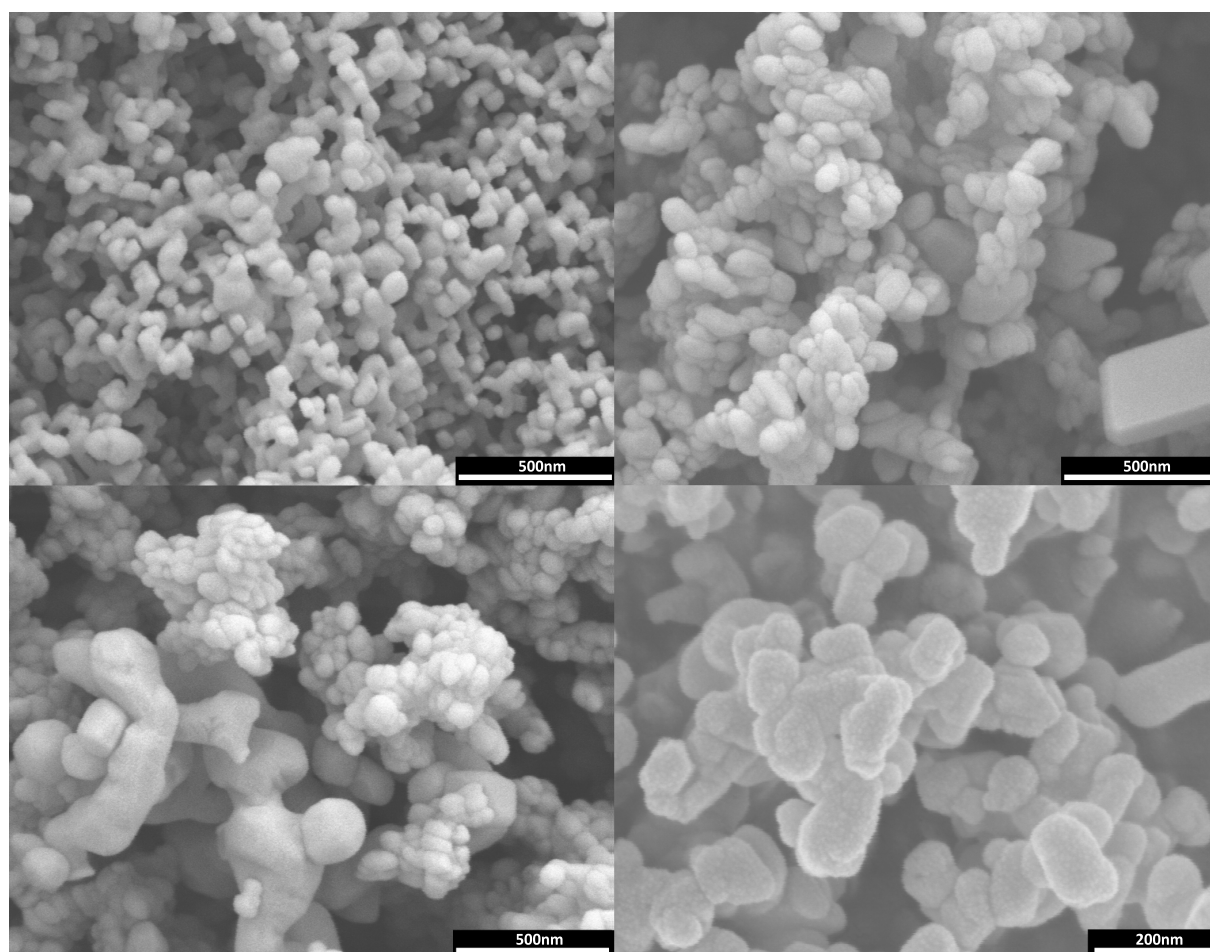


Figure S1.4. Additional SEM images of fully transformed ACC samples from [Table 1.1](#).

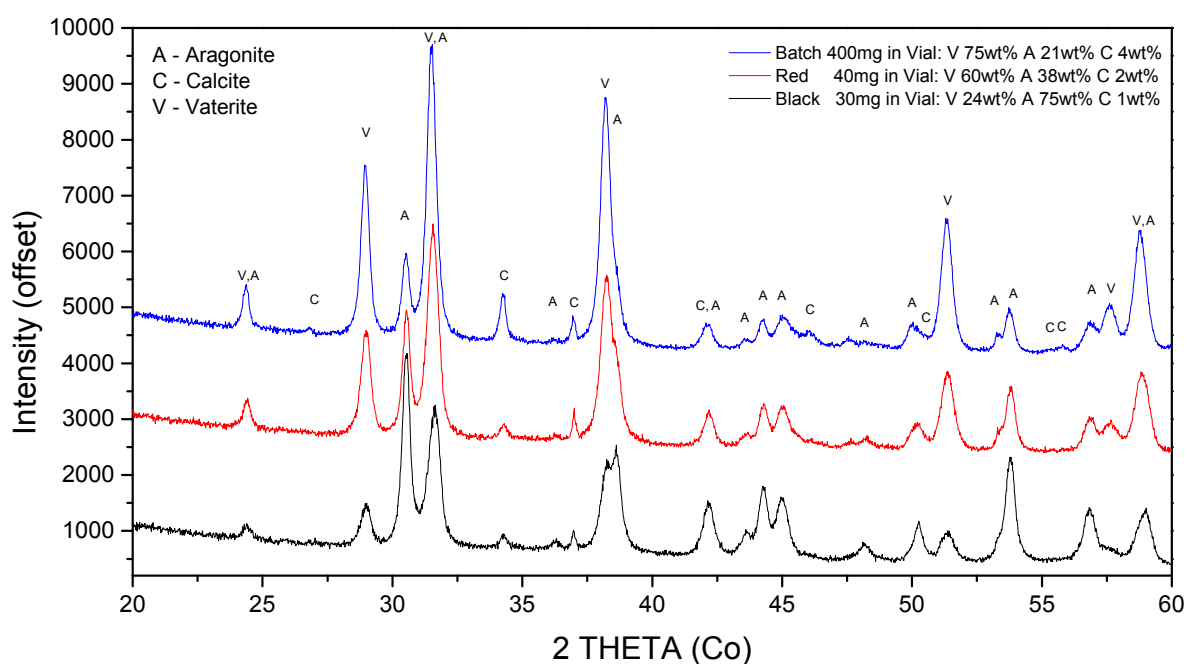


Figure S1.5. PXRD patterns of a fully transformed ACC sample stored in three vials under semi-tight conditions, varying only in the sample amount (400, 40, 30 mg) vs. air volume of the vial (0.04 dm³). Although the same synthesized ACC is used in all three experiments, results show different proportions of calcium carbonate polymorphs.

1.6 References

- Addadi L., Raz S. and Weiner S. (2003) Taking Advantage of Disorder: Amorphous Calcium Carbonate and Its Roles in Biomineralization. *Adv. Mater.* **15**, 959–970.
- Aizenberg J., Lambert G., Weiner S. and Addadi L. (2002) Factors involved in the formation of amorphous and crystalline calcium carbonate: a study of an ascidian skeleton. *J. Am. Chem. Soc.* **124**, 32–39.
- Aizenberg J., Muller D. A., Grazul J. L. and Hamann D. R. (2003) Direct fabrication of large micropatterned single crystals. *Science* **299**, 1205–1208.
- Andersen F. and Brecevic L. (1991) Infrared spectra of amorphous and crystalline calcium carbonate. *Acta Chem. Scand* **45**, 1018–1024.
- Baltrusaitis J. and Grassian V. H. (2009) Calcite surface in humid environments. *Surf. Sci.* **603**, L99–L104.
- Beniash E., Addadi L. and Weiner S. (1999) Cellular Control Over Spicule Formation in Sea Urchin Embryos: A Structural Approach. *J. Struct. Biol.* **125**, 50–62.
- Beruto D. T. and Botter R. (2000) Liquid-like H₂O adsorption layers to catalyze the Ca(OH)₂/CO₂ solid–gas reaction and to form a non-protective solid product layer at

- 20°C. *J. Eur. Ceram. Soc.* **20**, 497–503.
- Bolze J., Pontoni D., Ballauff M., Narayanan T. and Cölfen H. (2004) Time-resolved SAXS study of the effect of a double hydrophilic block-copolymer on the formation of CaCO₃ from a supersaturated salt solution. *J. Colloid Interface Sci.* **277**, 84–94.
- Bots P., Benning L. G., Rodriguez-Blanco J.-D., Roncal-Herrero T. and Shaw S. (2012) Mechanistic Insights into the Crystallization of Amorphous Calcium Carbonate (ACC). *Cryst. Growth Des.* **12**, 3806–3814.
- Brečević L. and Nielsen A. E. (1989) Solubility of amorphous calcium carbonate. *J. Cryst. Growth* **98**, 504–510.
- Clarkson J. R., Price T. J. and Adams C. J. (1992) Role of metastable phases in the spontaneous precipitation of calcium carbonate. *J. Chem. Soc. Faraday Trans.* **88**, 243.
- Coleyshaw E. E., Crump G. and Griffith W. P. (2003) Vibrational spectra of the hydrated carbonate minerals ikaite, monohydrocalcite, lansfordite and nesquehonite. *Spectrochim. Acta Part A Mol. Biomol. Spectrosc.* **59**, 2231–2239.
- Devol R. T., Sun C. Y., Marcus M. A., Coppersmith S. N., Myneni S. C. B. and Gilbert P. U. P. A. (2015) Nanoscale Transforming Mineral Phases in Fresh Nacre. *J. Am. Chem. Soc.* **137**, 13325–13333.
- Faatz M., Cheng W., Wegner G., Fytas G., Penciu R. S. and Economou E. N. (2005) Mechanical Strength of Amorphous CaCO₃ Colloidal Spheres. *Langmuir* **21**, 6666–6668.
- Farhadi Khouzani M., Chevrier D. M., Güttlein P., Hauser K., Zhang P., Hedin N. and Gebauer D. (2015) Disordered amorphous calcium carbonate from direct precipitation. *CrystEngComm* **17**, 4842–4849.
- Fernandez-Martinez A., Kalkan B., Clark S. M. and Waychunas G. a. (2013) Pressure-induced polyamorphism and formation of “aragonitic” amorphous calcium carbonate. *Angew. Chemie - Int. Ed.* **52**, 8354–8357.
- Gabrielli C., Jaouhari R., Joiret S. and Maurin G. (2000) In situ Raman spectroscopy applied to electrochemical scaling. Determination of the structure of vaterite. *J. Raman Spectrosc.* **31**, 497–501.
- Gal A., Habraken W., Gur D., Fratzl P., Weiner S. and Addadi L. (2013) Calcite Crystal Growth by a Solid-State Transformation of Stabilized Amorphous Calcium Carbonate Nanospheres in a Hydrogel. *Angew. Chemie Int. Ed.* **52**, 4867–4870.
- Gal A., Weiner S. and Addadi L. (2010) The stabilizing effect of silicate on biogenic and synthetic amorphous calcium carbonate. *J. Am. Chem. Soc.* **132**, 13208–11.
- Gebauer D., Gunawidjaja P. N., Ko J. Y. P., Bacsik Z., Aziz B., Liu L., Hu Y., Bergström L.,

- Tai C., Sham T.-K., Edén M. and Hedin N. (2010) Proto-Calcite and Proto-Vaterite in Amorphous Calcium Carbonates. *Angew. Chemie Int. Ed.* **49**, 8889–8891.
- Gebauer D., Völkel A. and Cölfen H. (2008) Stable prenucleation calcium carbonate clusters. *Science* **322**, 1819–1822.
- Geisler T., Perdikouri C., Kasiopas A. and Dietzel M. (2012) Real-time monitoring of the overall exchange of oxygen isotopes between aqueous and H₂O by Raman spectroscopy. *Geochim. Cosmochim. Acta* **90**, 1–11.
- Günther C., Becker A., Wolf G. and Epple M. (2005) In vitro Synthesis and Structural Characterization of Amorphous Calcium Carbonate. *Zeitschrift für Anorg. und Allg. Chemie* **631**, 2830–2835.
- Habraken W. J. E. M., Masic A., Bertinetti L., Al-Sawalmih A., Glazer L., Bentov S., Fratzl P., Sagi A., Aichmayer B. and Berman A. (2015) Layered growth of crayfish gastrolith: About the stability of amorphous calcium carbonate and role of additives. *J. Struct. Biol.* **189**, 28–36.
- Ihli J., Kulak A. N. and Meldrum F. C. (2013) Freeze-drying yields stable and pure amorphous calcium carbonate (ACC). *Chem. Commun.* **49**, 3134.
- Ihli J., Wong W. C., Noel E. H., Kim Y.-Y., Kulak A. N., Christenson H. K., Duer M. J. and Meldrum F. C. (2014) Dehydration and crystallization of amorphous calcium carbonate in solution and in air. *Nat. Commun.* **5**, 3169.
- Lee H. S., Ha T. H. and Kim K. (2005) Fabrication of unusually stable amorphous calcium carbonate in an ethanol medium. *Mater. Chem. Phys.* **93**, 376–382.
- Lee K., Wagermaier W., Masic A., Kommareddy K. P., Bennet M., Manjubala I., Lee S.-W., Park S. B., Cölfen H. and Fratzl P. (2012) Self-assembly of amorphous calcium carbonate microlens arrays. *Nat. Commun.* **3**, 725.
- Levi-Kalisman Y., Raz S., Weiner S., Addadi L. and Sagi I. (2002) Structural Differences Between Biogenic Amorphous Calcium Carbonate Phases Using X-ray Absorption Spectroscopy. *Adv. Funct. Mater.* **12**, 43.
- Meiron O. E., Bar-David E., Aflalo E. D., Shechter A., Stepensky D., Berman A. and Sagi A. (2011) Solubility and bioavailability of stabilized amorphous calcium carbonate. *J. Bone Miner. Res.* **26**, 364–72.
- Michel F. M., MacDonald J., Feng J., Phillips B. L., Ehm L., Tarabrella C., Parise J. B. and Reeder R. J. (2008) Structural characteristics of synthetic amorphous calcium carbonate. *Chem. Mater.* **20**, 4720–4728.
- Nielsen M. H., Aloni S. and De Yoreo J. J. (2014) In situ TEM imaging of CaCO₃ nucleation

- reveals coexistence of direct and indirect pathways. *Science* **345**, 1158–1162.
- Politi Y., Arad T., Klein E., Weiner S. and Addadi L. (2004) Sea urchin spine calcite forms via a transient amorphous calcium carbonate phase. *Science* **306**, 1161–1164.
- Putnis A. (2014) Why Mineral Interfaces Matter. *Science* **343**, 1441–1442.
- Radha A. V, Forbes T. Z., Killian C. E., Gilbert P. U. P. A. and Navrotsky A. (2010) Transformation and crystallization energetics of synthetic and biogenic amorphous calcium carbonate. *Proc. Natl. Acad. Sci. U. S. A.* **107**, 16438–43.
- Radha A. V and Navrotsky A. (2015) Direct Experimental Measurement of Water Interaction Energetics in Amorphous Carbonates MCO_3 (M = Ca, Mn, and Mg) and Implications for Carbonate Crystal Growth. *Cryst. Growth Des.* **15**, 70–78.
- Raiteri P. and Gale J. D. (2010) Water is the key to nonclassical nucleation of amorphous calcium carbonate. *J. Am. Chem. Soc.* **132**, 17623–34.
- Raz S., Hamilton P. C., Wilt F. H., Weiner S. and Addadi L. (2003) The Transient Phase of Amorphous Calcium Carbonate in Sea Urchin Larval Spicules: The Involvement of Proteins and Magnesium Ions in Its Formation and Stabilization. *Adv. Funct. Mater.* **13**, 480–486.
- Rodriguez-Blanco J. D., Shaw S. and Benning L. G. (2008) How to make “stable” ACC: protocol and preliminary structural characterization. *Mineral. Mag.* **72**, 283–286.
- Rodriguez-Blanco J. D., Shaw S. and Benning L. G. (2011) The kinetics and mechanisms of amorphous calcium carbonate (ACC) crystallization to calcite, via vaterite. *Nanoscale* **3**, 265–71.
- Rodriguez-Blanco J. D., Shaw S., Bots P., Roncal-Herrero T. and Benning L. G. (2012) The role of pH and Mg on the stability and crystallization of amorphous calcium carbonate. *J. Alloys Compd.* **536**, S477–S479.
- Rodriguez-Navarro C., Burgos Cara A., Elert K., Putnis C. V. and Ruiz-Agudo E. (2016) Direct Nanoscale Imaging Reveals the Growth of Calcite Crystals via Amorphous Nanoparticles. *Cryst. Growth Des.* **16**, 1850–1860.
- Rodriguez-Navarro C., Kudłacz K., Cizer Ö. and Ruiz-Agudo E. (2015) Formation of amorphous calcium carbonate and its transformation into mesostructured calcite. *CrystEngComm* **17**, 58–72.
- Saharay M., Yazaydin A. O. and Kirkpatrick R. J. (2013) Dehydration-Induced Amorphous Phases of Calcium Carbonate. *J. Phys. Chem. B* **117**, 3328–3336.
- Schmidt M. P., Illott A. J., Phillips B. L. and Reeder R. J. (2014) Structural Changes upon Dehydration of Amorphous Calcium Carbonate. *Cryst. Growth Des.* **14**, 938–951.

- Wang D., Hamm L. M., Bodnar R. J. and Dove P. M. (2012) Raman spectroscopic characterization of the magnesium content in amorphous calcium carbonates. *J. Raman Spectrosc.* **43**, 543–548.
- Xiao J. and Yang S. (2011) Unveiling the critical process in which organic molecules control the polymorphism of magnesium-containing calcium carbonate: the early nucleation of amorphous precursors or the subsequent amorphous to crystalline transformations? *CrystEngComm* **13**, 6223.
- Xu X.-R., Cai A.-H., Liu R., Pan H.-H., Tang R.-K. and Cho K. (2008) The roles of water and polyelectrolytes in the phase transformation of amorphous calcium carbonate. *J. Cryst. Growth* **310**, 3779–3787.
- Xu X., Han J. T., Kim D. H. and Cho K. (2006) Two modes of transformation of amorphous calcium carbonate films in air. *J. Phys. Chem. B* **110**, 2764–2770.
- Zhao Y., Luo Z., Li M., Qu Q., Ma X., Yu S. and Zhao Y. (2015) A Preloaded Amorphous Calcium Carbonate/Doxorubicin@Silica Nanoreactor for pH-Responsive Delivery of an Anticancer Drug. *Angew. Chemie Int. Ed.* **54**, 919–922.
- Zou Z., Bertinetti L., Politi Y., Jensen A. C. S., Weiner S., Addadi L., Fratzl P. and Habraken W. J. E. M. (2015) Opposite Particle Size Effect on Amorphous Calcium Carbonate Crystallization in Water and during Heating in Air. *Chem. Mater.* **27**, 4237–4246.

Chapter 2

Influence of solution chemistry on metastability and transformation of amorphous calcium carbonate

ABSTRACT: In natural aquatic environments amorphous calcium carbonate (ACC) shows remarkable metastabilities, which are assumed to arise from the incorporation of foreign cations as well as organic ligands. In addition, these incorporated substances are considered to be eminent in the control of the transformation behaviour of ACC and finally occurring CaCO₃ polymorphs. In contrast, the distinct influence of aqueous solution compositions on the transformation mechanisms and kinetics of ACC is still less explored. Here, we present experimental results on the metastability and transformation behaviour of an additive-free ACC exposed to variable MgCl₂ containing solutions using *in-situ* Raman spectroscopy. Our results suggest that in aqueous medium the transformation mechanisms and kinetics of ACC are strongly controlled by the chemical composition of the fluid phase. The dispersed ACC immediately transformed in *pure* water, exhibited prolonged metastability at elevated MgCl₂ concentrations in solution of up to 696 min. During the prolonged lifetime, ACC incorporated up to 4 mol% of Mg from the reactive solutions in the course of dissolution and re-precipitation. Depending on the concentrations of aqueous MgCl₂, the transformation pathway of the dispersed ACC changed from forming Mg-calcite and vaterite to precipitating aragonite with the intermediate formation of nesquehonite and monohydrocalcite. The observed distinct mineral phase formation suggests that the metastability of additive-free ACC, and its overall transformation behaviour, is strongly controlled by the fluid composition, where the Mg content and/or pre-structuring of ACC seems to be non-relevant.

2.1 Introduction

Amorphous calcium carbonate (ACC) is nowadays considered to be an important precursor for calcium carbonate based skeletons (Addadi et al., 2003). It was first described as metastable intermediate in sea urchin larvae utilizing the amorphous phase during spiculogenesis to form single crystal calcite spicules (Beniash et al., 1997). Since then, ACC has been recognized as a widespread precursor in biomineralization for anhydrous CaCO₃-

based skeletons found, for example, in larvae of bivalves (Weiss et al., 2002), in ascidians (Aizenberg et al., 2002), in crustaceans (Raz et al., 2002), in seabream (Foran et al., 2013) and in the calcareous corpuscles of a tapeworm together with monohydrocalcite [CaCO₃•H₂O], suggesting the latter might act as a possible precursor for the calcium carbonate monohydrate as well (Señorale-Pose et al., 2008). In a non-marine environment, ACC has been recently documented in drip water of speleothems from a Hungarian cave (Demény et al., 2016) and in hot spring deposits from China (Jones and Peng, 2012), possibly associated with microbial activity. It was furthermore found as the dominant phase of intracellular formed Ca-carbonates in cyanobacteria, which play a major role in the carbon cycle by using photosynthesis to turn CO₂ into organic carbon and carbonates (Couradeau et al., 2012; Benzerara et al., 2014).

Biogenic ACC does not occur as pure calcium carbonate hydrate, but contains a range of substituting inorganic ions and organic ligands, which are thought to enhance the metastability of the amorphous phase in aqueous media and prevent its otherwise immediate transformation into a crystalline calcium carbonate polymorph (Raz et al., 2000; Levi-Kalishman et al., 2002; Addadi et al., 2003; Habraken et al., 2015). Studies trying to elucidate the interrelationship of these additives with ACC have strongly focused on magnesium, as it is ubiquitous in carbonate precipitating environments and frequently incorporated as a minor or even major element in crystalline carbonates (e.g. Liu et al., 2013; Blue and Dove, 2015; Rodriguez-Blanco et al., 2015; Purgstaller et al., 2016). In this respect, it was ascertained in laboratory experiments that Mg retards the transformation of ACC in solution as well as in air (Loste et al., 2003; Ajikumar et al., 2005; Radha et al., 2012; Rodriguez-Blanco et al., 2012). It was suggested that the higher dehydration energy of the Mg²⁺ ion compared to the Ca²⁺ ion is responsible for the enhanced metastability (Di Tommaso and de Leeuw, 2010). Furthermore, it was speculated that the Mg content in ACC alters the protocrystalline structure and governs the subsequent crystalline polymorph development (Blue et al., 2017). Recently, studies emerged that take into account, besides the solid Mg content, the influence of Mg concentration in the reactive aqueous solution as a possible decisive parameter for ACC metastability and prospective phase evolution (Blue et al., 2017; Purgstaller et al., 2017). Evidence was found that polymorph development is controlled to a large extent by the reactive solution chemistry, triggering monohydrocalcite or aragonite formation instead of calcite and vaterite when the activity ratio $a\text{Mg}^{2+}/a\text{Ca}^{2+}$ is high in solution. However, in all these experiments Mg/Ca-rich solutions were mixed with carbonate-bearing ones, synthesizing as well as aging Mg-ACC in the same solution for studying crystallization

behaviour. These results concordantly show the importance of $a\text{Mg}^{2+}/a\text{Ca}^{2+}$ in solution on the transformation of ACC, but make it difficult to differentiate unequivocally the influence of solution chemistry and the incipient Mg content of ACC on observed metastabilities and subsequent phase evolutions. Surprisingly, information about the distinct influence of solution chemistry on metastability and transformation development of additive-free ACC is scarce. The most common approach is the one step synthesis of ACC from an Mg/Ca-rich solution and the crystallization therein. The choice of using the Mg-ACC phase to study the effect of solution chemistry can surely be attributed to the highly challenging synthesis of additive-free ACC and its high instability compared to Mg stabilized ACC. To our knowledge, there is only one study synthesising additive-free ACC as a first step prior to the second separate step of dispersing and monitoring transformation behaviour of the ACC in Mg containing solutions (Zhang et al., 2012). Unfortunately, ion concentrations of solutions as well as sampled solids were not measured by Zhang et al. (2012) and the additive-free ACC was aged in Mg/Ca containing ethanol/water mixtures, which aggravates interpretation of the experiments with respect to the influence of solution chemistry.

This study aims to investigate the distinct influence of magnesium in aqueous solution on the metastability and transformation of ACC. Therefore, the synthesis process of additive-free ACC was decoupled from the aging of the amorphous phase in solution. ACC was synthesised and subsequently re-dispersed as a second step into MgCl_2 solution of different concentrations. The phase evolution was monitored with *in-situ* Raman spectroscopy and fluid and solid samples were taken regularly for analyses to decipher the impact of solution chemistry on the amorphous phase transformation reaction mechanisms and kinetics.

2.2 Experimental

2.2.1 ACC synthesis

ACC was synthesized after the method described in Konrad et al. (2016). Briefly, calcium and carbonate bearing solutions, each of 0.25 M, were prepared with Milli-Q water (18.2 M Ω cm) using calcium chloride dehydrate (> 99%, p.a., ACS, Carl Roth) and sodium carbonate (> 99.5%, p.a., ACS, Carl Roth), respectively. The solutions were rapidly mixed and vacuum-filtered through a membrane cellulose acetate filter (0.2 μm pore size and 10 cm diameter). The obtained filter cake was washed with ultrapure water and transferred into a Virtis Benchtop 3 dm³ freeze dryer (-58 °C condenser temperature and 10 mbar partial vacuum) in order to sublime the non-structurally bound H₂O. The obtained ACC standard material has the composition $\text{CaCO}_3 \cdot (0.42 \pm 0.01)\text{H}_2\text{O}$ and consists of spherical particles with a diameter

range of 30-200 nm and an averaged mean particle size of about 90 nm (see [Konrad et al. \(2016\)](#)). In order to prevent transformation in air, the physisorbed water-free powder was stored under gastight conditions and the synthesis protocol was repeated several times until 15 g were produced.

2.2.2 Experimental Setup

0.5 mol dm⁻³ of synthesized ACC were dispersed into stirring lab reactors containing 0.03 dm³ solutions ranging from *pure* water (Milli-Q, 18.2 MΩ cm) to 1 mol dm⁻³ of MgCl₂ in concentration. The solutions were prepared by using Milli-Q water and different amounts of magnesium chloride hexahydrate (> 99%, p.a., ACS, Carl Roth). The dispersed ACC was monitored by *in-situ* Raman spectroscopy recording the molecular vibrations of the carbonate molecule and by pH. Samples of the suspension were taken by using a pipette whenever a change in the *in-situ* spectra were observable, obtaining the first sample after 15 s of reaction time starting with the dispersion of ACC into the solutions. The samples were pipetted into a suction filtration unit through a membrane cellulose acetate filter (0.2 μm pore size) and the separated reaction products analysed by infrared spectroscopy - within 60 s after separation from the reactive solution - for verification of the phases determined in solution by *in-situ* Raman spectroscopy.

2.2.3 Methods

The *in-situ* Raman spectra were collected with a Raman RXN2 analyzer (Kaiser Optical Systems) equipped with a Kaiser MR Probe head (quarter-inch immersion optic), running with a 785 nm laser, following the molecular vibrations of the dissolved inorganic carbon (DIC) and carbonate bearing reaction products. Spectra were integrated for 30 s for a better signal-to-noise ratio following a 5 s pause in between, thereby collecting spectra every 35 s. pH was tracked during the experiment with a Schott BlueLine 28 combined electrode placed in solution and calibrated against NIST standard buffers at pH 4.01, 7.00 and 10.00. Subsamples of separated solids and solutions were digested in 6% HNO₃ for analyses of ion concentrations with inductively coupled plasma optical emission spectroscopy (ICP-OES) on a Perkin Elmer Optima 8300 DV with an analytical error for Ca and Mg < ± 3%. Solutions were additionally measured for total alkalinity on a Schott TitroLine alpha plus titrator using a 0.01 M HCl solution. Phase characterisation of the separated solids was conducted immediately after filtration by Fourier transform infrared spectroscopy (FTIR) in attenuated total reflection (ATR) mode from 650 – 4 000 cm⁻¹ at a resolution of 4 cm⁻¹, and, after drying

under laboratory atmosphere, by powder X-ray diffraction (PXRD) performed on a PANalytical X'Pert Pro diffractometer, equipped with a Co target and a solid-state real time multiple strip (RTMS) detector (measurement parameters: 40 kV, 40 mA, 0.008° step, 40 s/step and 4-80° 2θ). Phase identification and quantification from PXRD patterns was accomplished by using the inorganic crystal structure database (ICSD) and by Rietveld analysis, respectively. Secondary electron images of the reaction products were obtained using a ZEISS DSM 982 Gemini scanning electron microscope (SEM) equipped with a field emission electron gun operated at 5 kV, for which the sampled materials were coated with gold/palladium. Speciation calculations and saturation indices (SI) with respect to the obtained reaction products were carried out with PHREEQC software using the MINTEQv4 database as well as the Pitzer model for the 1 M MgCl₂ solution (Parkhurst and Appelo, 2013) modified by the inclusion of the solubility products for ACC (Brečević and Nielsen, 1989), nesquehonite (Wang and Li, 2012), monohydrocalcite (Kralj and Brečević, 1995), vaterite (Plummer and Busenberg, 1982) and brucite (Pokrovsky and Schott, 2004).

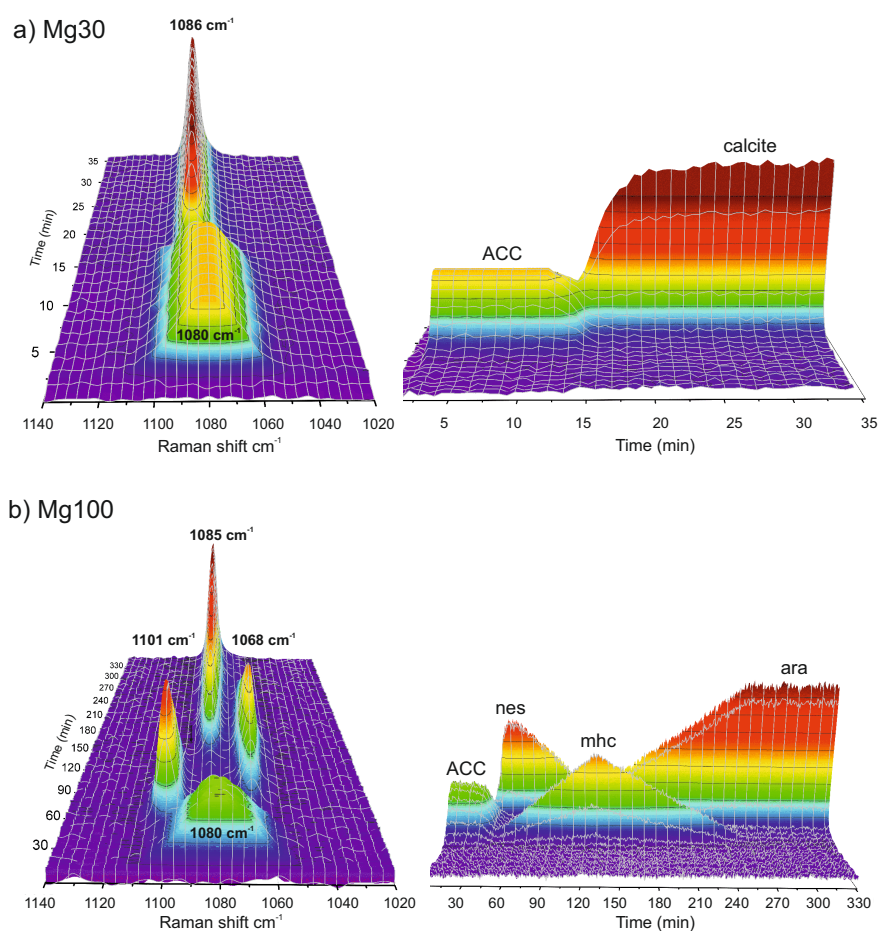


Figure 2.1. In-situ Raman spectroscopy measurements reveal solution dependent formation and transformation behaviour of ACC when dispersed in pure water and MgCl₂ solutions of different concentration. In MgCl₂ solutions ≤ 0.03 mol dm⁻³ ACC transforms into calcite and vaterite (a), while in solutions containing ≥ 0.055 mol dm⁻³ of MgCl₂ suspended ACC transforms to aragonite via intermediate nesquehonite and monohydrocalcite (b).

Table 2.1. Time of sampling, pH, alkalinity, and chemical composition of fluid and solid as well as mineralogical phase analysis from *in-situ* Raman and FTIR spectroscopy of the conducted experiments. The samples are labelled MgN, where N refers to the approximate targeted concentration of Mg (mmol) in the stock solution. cc: calcite, vat: vaterite, nes: nesquehonite, mhc: monohydrocalcite, ara: aragonite.

samples	time (min)	pH	alkalinity mmol dm ⁻³	fluid mmol dm ⁻³		solid mol%		<i>in-situ</i> Raman	FTIR
				Ca	Mg	Ca	Mg		
Mg0_stock		6.9							
Mg0_1	0.3	10.4	4.5	4.3	0.2	100.0	0.0	cc, vat	cc, vat
Mg0_2	4.6	10.2	8.7	0.3	0.1	100.0	0.0	cc, vat	cc, vat
Mg0_3	13.2	10.3	9.3	0.1	0.0	100.0	0.0	cc, vat	cc, vat
Mg0_4	23.0	10.4	9.3	0.1	0.0	100.0	0.0	cc, vat	cc, vat
Mg10_stock		6.6			9.8				
Mg10_1	0.3	10.2	6.5	4.0	6.2	99.2	0.8	ACC	ACC
Mg10_2	2.2	10.1	6.9	5.2	6.1	99.2	0.8	cc, vat	cc, vat
Mg10_3	20.5	8.2	3.2	3.4	1.7	98.4	1.6	cc, vat	cc, vat
Mg30_stock		6.3			28.3				
Mg30_1	0.3	10.1	9.6	7.0	22.3	98.7	1.3	ACC	ACC
Mg30_2	2.0	10.1	8.1	6.8	19.5	98.2	1.8	ACC	ACC
Mg30_3	6.7	10.0	7.2	7.5	21.1	98.5	1.5	ACC	ACC
Mg30_4	11.6	9.8	6.1	7.7	17.6	97.8	2.2	ACC	cc, vat
Mg30_5	32.9	7.6	1.5	10.3	9.7	96.3	3.7	cc	cc, vat
Mg55_stock		5.9			51.7				
Mg55_1	0.3	10.0	11.5	7.9	39.5	97.5	2.5	ACC	ACC
Mg55_2	8.2	9.8	11.1	9.7	40.9	97.8	2.2	ACC	ACC
Mg55_3	14.6	9.8	10.1	8.9	37.7	97.0	3.0	ACC	ACC
Mg55_4	25.0	9.9	9.9	7.8	40.0	97.6	2.4	ACC, nes	ACC, nes
Mg55_5	36.4	10.0	7.7	2.9	31.9	95.9	4.1	nes, mhc	nes, mhc
Mg55_6	63.8	10.0	7.8	2.5	42.4	98.1	1.9	nes, mhc, ara	nes, mhc, ara
Mg100_stock		5.6			94.0				
Mg100_1	0.3	9.8	14.8	11.9	76.9	96.5	3.5	ACC	ACC
Mg100_2	8.4	9.7	15.0	12.5	73.9	95.8	4.2	ACC	ACC
Mg100_3	18.6	9.7	15.1	12.9	74.3	95.8	4.2	ACC	ACC
Mg100_4	28.7	9.7	13.3	11.4	69.5	94.8	5.2	ACC, nes	ACC, nes
Mg100_5	38.7	9.7	13.0	10.9	76.6	96.5	3.5	ACC, nes	ACC, nes, mhc
Mg100_6	58.8	9.5	10.4	4.1	81.3	97.4	2.6	nes, mhc	nes, mhc
Mg100_7	84.9	9.3	10.3	3.7	84.2	98.0	2.0	nes, mhc	nes, mhc
Mg100_8	137.5	8.8	6.1	3.1	82.0	97.6	2.4	mhc, ara	mhc, ara
Mg100_9	330.6	9.1	4.8	1.7	85.2	98.2	1.8	ara	ara
Mg1000_stock		5.2			1100.0				
Mg1000_1	0.3	8.9	78.7	51.7	1075.5	94.9	5.1	ACC	ACC
Mg1000_2	27.5	8.8	83.1	58.9	1079.2	95.6	4.4	ACC	ACC
Mg1000_3	49.0	8.7	82.0	59.3	1083.1	96.5	3.5	ACC	ACC
Mg1000_4	77.5	8.7	67.2	63.3	1074.7	94.7	5.3	ACC	ACC
Mg1000_5	670.0	8.5	78.9	65.3	1079.7	95.8	4.2	ACC	ACC
Mg1000_6	2394.0	8.5	25.0	13.6	1057.6	91.5	8.5	-	nes, mhc
Mg1000_7	12430.0	8.5	13.8	6.0	1099.9	100.0	0.0	-	ara

2.3 Results

2.3.1 Solid phase behaviour in solution

From the *in-situ* Raman measurements we see that ACC powder dispersed into *pure* water (zero Mg concentration, labelled Mg0) shows the direct formation of calcite and vaterite, indicated by the characteristic Raman shifts of the carbonate molecule for calcite at 1 086 (ν_1 band) and 712 cm^{-1} (ν_4 band) and for vaterite at 1 074 as well as 1 090 cm^{-1} (split ν_1 bands) (Gabrielli et al., 2000) (Table 2.1). This was confirmed by the FTIR-spectra obtained from the sampled separated solids, displaying ν_4 deformation bands at 710 and 741 cm^{-1} for calcite and vaterite, respectively (Andersen and Brecevic, 1991). Calcite and vaterite were obtained as well as final reaction products in the experiments where ACC was suspended into 0.01 (exp. Mg10) and 0.03 M (exp. Mg30) solutions of MgCl_2 . However, as initial phase ACC was detected in the *in-situ* Raman spectra (Figure 2.1a), forming a broad ν_1 band at 1 080 cm^{-1} (Wang et al., 2012) and confirmed by FTIR measurements of the solids, characterised by the ν_4 deformation band at 860 cm^{-1} (Figure 2.2a) (Becker et al., 2003).

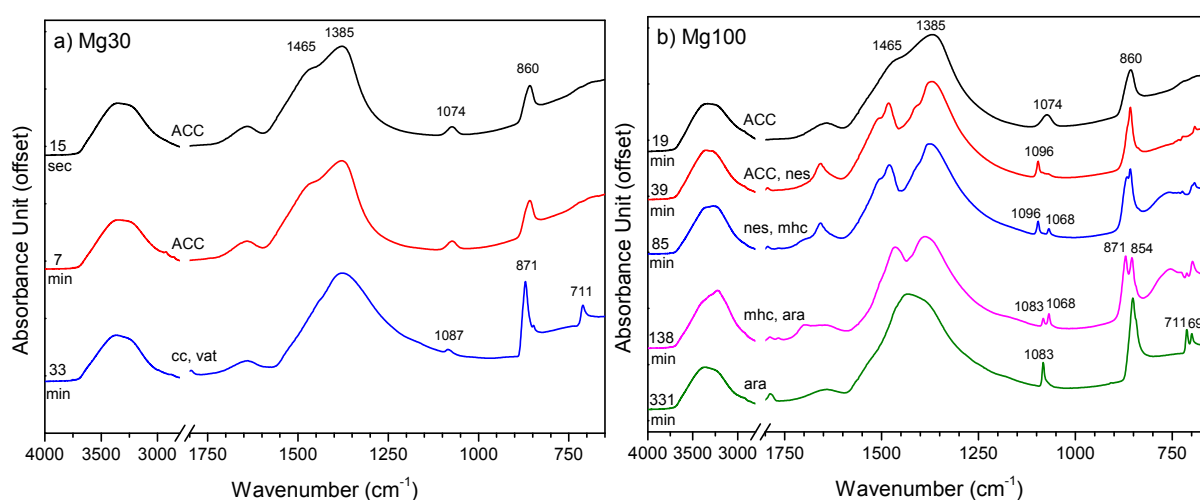


Figure 2.2. Immediate measurements of sampled and separated solids with FTIR (still wet), verify observations made by *in-situ* Raman technique. Exemplarily, the solution dependent phase development of ACC dispersed into (a) 0.03 M (exp. Mg30) and (b) 0.1 M (exp. Mg100) MgCl_2 solution is shown.

The suspension of ACC into the yet higher concentrated MgCl_2 solutions, ranging from 0.055 to 1 M (exp. Mg55, Mg100 and Mg1000), shows an increasing persistence of the amorphous phase at the beginning of each experiment of up to a minimum metastability of 696 min in the 1 M MgCl_2 solution (Table 2.1 and Figure 2.3). Subsequently, the formation of nesquehonite [$\text{MgCO}_3 \cdot 3\text{H}_2\text{O}$] and monohydrocalcite can be observed in these solutions (Figures 2.1b and 2.2b), indicated by the ν_1 bands in the *in-situ* Raman spectra at 1 101 cm^{-1} (Edwards et al., 2005; Bonales et al., 2013) and 1 068 cm^{-1} (Coleyshaw et al., 2003), respectively, and from FTIR by the ν_1 bands at 1 096 cm^{-1} for nesquehonite (White, 1971; Frost and Palmer, 2011)

and $1\,068\text{ cm}^{-1}$ for monohydrocalcite (Neumann and Epple, 2007). Eventually, aragonite was formed as final reaction product after nesquehonite and monohydrocalcite dissolved again in the higher MgCl_2 concentration experiments, which was indicated by the Raman shifts measured in suspension at $1\,085$ (ν_1 band) and 205 cm^{-1} (lattice mode) (Gabielli et al., 2000), and confirmed with FTIR spectra from the sampled solids forming a ν_2 band at 854 and a split ν_4 band at 698 and 711 cm^{-1} (Table 2.1 and Figure 2.2b) (Andersen and Brecevic, 1991). Secondary electron images of the *pure* water experiment show euhedral calcite rhombohedra of $\sim 2\text{-}5\text{ }\mu\text{m}$ in size and vaterite spheres of $\sim 2\text{-}8\text{ }\mu\text{m}$ in diameter composed of ~ 100 nm particles (Figure 2.4a). Experiments up to 0.03 mol dm^{-3} of MgCl_2 in solution display rhombohedral calcite crystals of $\sim 1\text{-}2\text{ }\mu\text{m}$ in size forming $\sim 10\text{ }\mu\text{m}$ elongated aggregates as well as vaterite spheres of about $\sim 4\text{-}6\text{ }\mu\text{m}$ in diameter composed of $\sim 60\text{-}90$ nm sized crystals (Figure 2.4b). Nesquehonite crystals forming euhedral needles of $\sim 1\text{-}2\text{ }\mu\text{m}$ in length were observed from ACC transformed in MgCl_2 solutions $\geq 0.055\text{ mol dm}^{-3}$ (Figure 2.4c) as well as the formation of aragonite as final reaction product (Figure 2.4d), indicated by $\sim 200\text{-}300$ nm crystals aggregating into $\sim 2\text{ }\mu\text{m}$ sized rods. Monohydrocalcite, although confirmed by spectroscopy at the time of sampling, was never observed in SEM images after drying under air exposure.

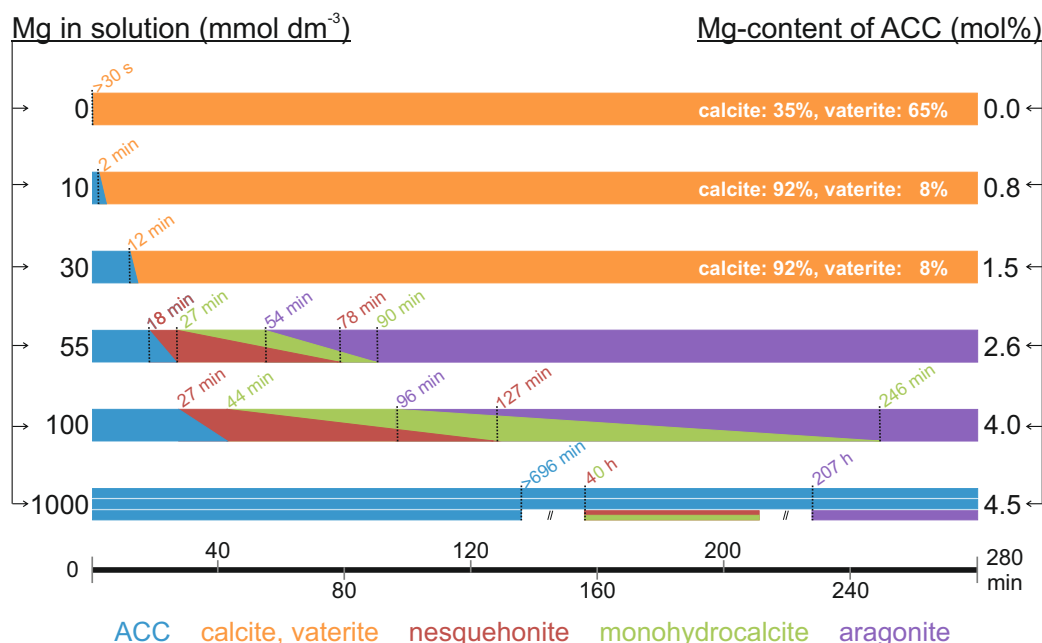


Figure 2.3. Phase evolution of conducted experiments and their respected occurrence in solution as observed from mineralogical *in-* and *ex-situ* analyses. The given Mg content of ACC for each experiment shows the average amount of Mg incorporated (± 0.4 mol%) from samples where ACC was occurring as single phase, and was determined by chemical digestion of sampled solids and subsequent ICP-OES analyses. Quantification of the final reaction products was obtained by XRD and Rietveld refinement (see Table S2.1). *Note:* In the experiment Mg1000, the in-situ Raman monitoring stopped after 696 min. Further analyses was conducted ex-situ by FTIR.

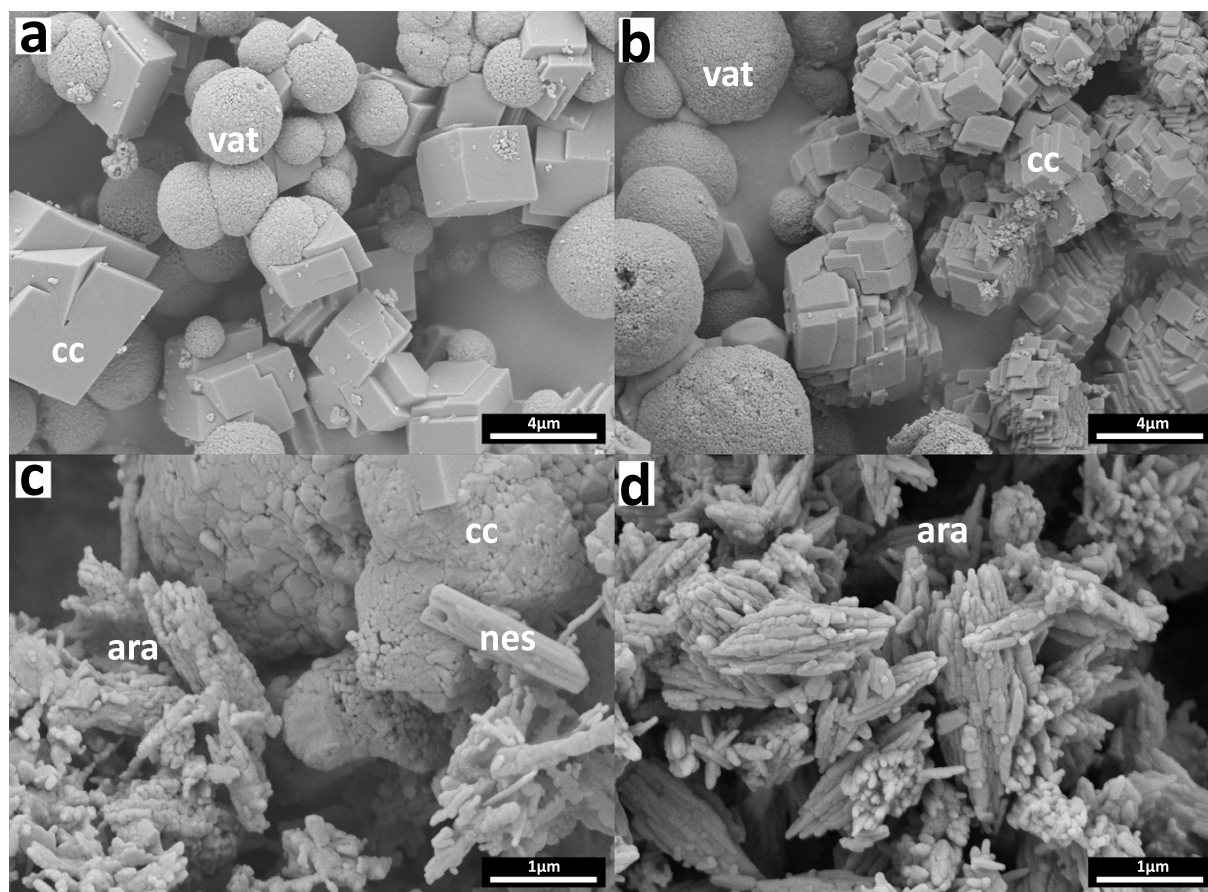


Figure 2.4. SEM images of sampled solids, dried under air exposure, show euhedral calcite and vaterite spheres composed of nanoparticles in the experiment with *pure* water (exp. Mg0) (a) and rhombohedral calcite with slightly rounded corners forming elongated aggregates as well as vaterite spheres in experiment Mg10 (b). In the experiment Mg100, the intermediate nesquehonite can be found in SEM images along with aragonite and calcite (c) and as final reaction product aragonite is observed (d). *Note:* the calcite and aragonite displayed in image (c) originate from ACC and monohydrocalcite, which transformed under air exposure after sampling.

2.3.2 Evolution of solid and solution chemistry

After the dispersion of ACC an instant rise of pH is observed and the introduced alkalinity and Ca^{2+} ions show that more ACC is being dissolved in higher concentrated MgCl_2 solutions (Table 2.1). At the onset of experiments about 1% of the 0.5 mol of ACC was dissolved in *pure* water and in the 0.01 M MgCl_2 solution, which increased to 10% in the 1 M MgCl_2 solution. All reaction products from initially Mg-free ACC dispersed into MgCl_2 rich solutions incorporated Mg into their structure with bulk amounts ranging on average from 1 mol% in the experiment Mg10 to 4.5 mol% in the experiment Mg1000. The highest Mg content of the reaction products was observed in a sample containing nesquehonite and monohydrocalcite with 8.5 mol% from the experiment Mg1000, while the uptake of Mg from metastable ACC in solution never exceeded 5.3 mol% (Table 2.1).

Table 2.2. Aqueous speciation (a : activity of given species) and saturation states (SI: saturation index) from sampled solutions calculated with PHREEQC software using the MINTEQA4 and Pitzer database (exp. Mg1000) as a function of experimental time. Missing solubility products in the databases for SI value calculations were used from Brečević and Nielsen (1989) for ACC, Wang and Li (2012) for nesquehonite, Kralj and Brečević (1995) for monohydrocalcite, Plummer and Busenberg (1982) for vaterite, and from Pokrovsky and Schott (2004) for brucite, respectively. mhc: monohydrocalcite, vat: vaterite, ara: aragonite, cc: calcite, nes: nesquehonite, bru: brucite.

samples	time (min)	$a \text{Ca}^{2+}$	$a \text{Mg}^{2+}$	$a \text{CO}_3^{2-}$	$\frac{a \text{Mg}^{2+}}{a \text{Ca}^{2+}}$	$\frac{a \text{MgCO}_3^{\circ}}{a \text{CO}_3^{2-}}$	SI _{ACC}	SI _{mhc}	SI _{vat}	SI _{ara}	SI _{cc}	SI _{nes}	SI _{bru}
Mg0_1	0.3	1.77E-03	-	3.81E-04	-	-	0.22	0.88	1.83	2.13	2.31	-	-
Mg0_2	4.6	7.46E-05	-	1.34E-03	-	-	-0.61	0.05	1.01	1.30	1.48	-	-
Mg0_3	13.2	2.29E-05	-	1.56E-03	-	-	-1.05	-0.40	0.56	0.85	1.03	-	-
Mg0_4	23.0	2.31E-05	-	1.49E-03	-	-	-1.07	-0.41	0.54	0.84	1.02	-	-
Mg10_1	0.3	1.58E-03	2.71E-03	4.03E-04	1.7	2.3	0.20	0.85	1.81	2.10	2.28	-0.69	0.18
Mg10_2	2.2	2.02E-03	2.62E-03	3.87E-04	1.3	2.2	0.29	0.94	1.90	2.19	2.37	-0.72	0.02
Mg10_3	20.5	1.56E-03	7.96E-04	1.92E-05	0.5	0.7	-1.13	-0.47	0.48	0.78	0.96	-2.54	-4.21
Mg30_1	0.3	2.30E-03	7.82E-03	3.20E-04	3.4	6.5	0.26	0.92	1.87	2.17	2.35	-0.33	0.48
Mg30_2	2.0	2.34E-03	7.10E-03	2.82E-04	3.0	5.9	0.21	0.87	1.83	2.12	2.30	-0.43	0.36
Mg30_3	6.7	2.58E-03	7.61E-03	2.29E-04	2.9	6.3	0.17	0.82	1.78	2.07	2.25	-0.49	0.29
Mg30_4	11.6	2.75E-03	6.59E-03	1.94E-04	2.4	5.5	0.12	0.78	1.73	2.03	2.21	-0.62	-0.26
Mg30_5	32.9	4.02E-03	3.80E-03	1.98E-06	0.9	3.2	-1.71	-1.05	-0.09	0.20	0.38	-2.85	-4.82
Mg55_1	0.3	2.34E-03	1.23E-02	2.88E-04	5.3	10.3	0.22	0.88	1.83	2.13	2.31	-0.18	0.48
Mg55_2	8.2	2.86E-03	1.27E-02	2.57E-04	4.4	10.6	0.26	0.92	1.87	2.17	2.35	-0.22	0.19
Mg55_3	14.6	2.69E-03	1.20E-02	2.43E-04	4.5	10.0	0.21	0.87	1.82	2.12	2.30	-0.27	0.08
Mg55_4	25.0	2.31E-03	1.24E-02	2.38E-04	5.4	10.3	0.13	0.79	1.75	2.04	2.22	-0.26	0.20
Mg55_5	36.4	9.11E-04	1.05E-02	2.38E-04	11.5	8.7	-0.27	0.39	1.34	1.64	1.82	-0.33	0.44
Mg55_6	63.8	7.45E-04	1.31E-02	2.05E-04	17.5	10.9	-0.42	0.23	1.19	1.48	1.66	-0.30	0.48
Mg100_1	0.3	3.16E-03	2.13E-02	2.40E-04	6.7	17.7	0.27	0.93	1.88	2.18	2.36	-0.03	0.33
Mg100_2	8.4	3.32E-03	2.05E-02	2.43E-04	6.2	17.1	0.30	0.96	1.91	2.21	2.39	-0.03	0.11
Mg100_3	18.6	3.42E-03	2.06E-02	2.41E-04	6.0	17.2	0.31	0.97	1.92	2.22	2.40	-0.04	0.02
Mg100_4	28.7	3.08E-03	1.96E-02	2.22E-04	6.4	16.3	0.23	0.89	1.84	2.14	2.32	-0.09	-0.01
Mg100_5	38.7	2.91E-03	2.12E-02	2.07E-04	7.3	17.7	0.17	0.83	1.78	2.08	2.26	-0.09	0.05
Mg100_6	58.8	1.11E-03	2.27E-02	1.66E-04	20.5	18.9	-0.34	0.31	1.27	1.56	1.74	-0.16	-0.16
Mg100_7	84.9	1.00E-03	2.35E-02	1.44E-04	23.5	19.6	-0.45	0.21	1.17	1.46	1.64	-0.20	-0.65
Mg100_8	137.5	8.72E-04	2.35E-02	5.75E-05	26.9	19.5	-0.91	-0.25	0.71	1.00	1.18	-0.60	-1.55
Mg100_9	330.6	4.79E-04	2.43E-02	5.99E-05	50.7	20.2	-1.15	-0.49	0.46	0.76	0.94	-0.57	-0.93
Mg1000_1	0.3	2.05E-02	5.13E-01	4.37E-05	25.0	552.6	0.34	0.99	1.95	2.16	2.45	0.54	-0.03
Mg1000_2	27.5	2.27E-02	4.97E-01	4.71E-05	21.9	560.8	0.41	1.07	2.03	2.24	2.52	0.56	-0.23
Mg1000_3	49.0	2.43E-02	5.33E-01	4.30E-05	22.0	567.7	0.40	1.06	2.02	2.23	2.51	0.55	-0.42
Mg1000_4	77.5	2.52E-02	5.16E-01	3.63E-05	20.5	569.2	0.35	1.00	1.96	2.17	2.46	0.46	-0.42
Mg1000_5	670.0	2.72E-02	5.43E-01	3.93E-05	19.9	572.0	0.42	1.08	2.03	2.25	2.53	0.52	-0.82
Mg1000_6	2394.0	6.71E-03	6.49E-01	1.08E-05	96.7	550.0	-0.75	-0.09	0.87	1.08	1.36	0.03	-0.84
Mg1000_7	12430.0	2.68E-03	6.09E-01	6.32E-06	226.8	620.7	-1.38	-0.73	0.23	0.44	0.73	-0.23	-0.79

The calculated SIs of the precipitating reaction products reveal that at the onset of the experiments (first sample after 15 s) all reactive solutions were slightly (super)saturated with respect to ACC (SI = 0.25 +/- 0.05), including the *pure* water experiment Mg0 with no sign of ACC detected by the *in-situ* Raman measurements (Table 2.2). After transformation of ACC into a crystalline phase, accompanied with the undersaturation of ACC, reaction products of experimental solutions containing up to 0.03 mol dm⁻³ of MgCl₂ show the formation of calcite and vaterite despite supersaturation of monohydrocalcite. The latter was observed to

precipitate together with nesquehonite from reactive solutions with $\geq 0.055 \text{ mol dm}^{-3} \text{ MgCl}_2$ concentration with nesquehonite approaching saturation. Aragonite is being formed as final reaction product from the highly Mg-rich solutions after monohydrocalcite reaches undersaturation (Table 2.2). Note, although supersaturated at initial stages and alkaline pH conditions, brucite $[\text{Mg}(\text{OH})_2]$ was never detected by mineralogical analyses, e.g. by its characteristic OH-stretching band at $3\,700 \text{ cm}^{-1}$ in infrared spectroscopy (Figure 2.2) (Frost and Klopogge, 1999).

2.4 Discussion

2.4.1 Retardation of ACC transformation in aqueous MgCl_2 solutions

Information about re-introducing ACC into solution is scarce, but commonly it is assumed that additive-free ACC transforms immediately after the dispersion in water (Zhang et al., 2012). This behaviour was confirmed by experiment Mg0, where ACC was introduced into pure water and immediately transformed to calcite and vaterite within the *in-situ* Raman time resolution of 35 s with no detection of the amorphous phase (Table 2.1 and Figure 2.3). Nonetheless, this behaviour changed when ACC was introduced into MgCl_2 containing solutions with an increasing persistence of up to at least 696 min in the 1 M MgCl_2 solution (exp. Mg1000), when *in-situ* monitoring was stopped (Figure 2.3). The dispersed ACC dissolved in the MgCl_2 -rich solutions until nearly saturation with respect to ACC was reached. Simultaneously Mg containing ACC was formed. This is inferred by the Mg-content of the sampled solids and from the still present band positions in Raman and FTIR spectroscopy characteristic for ACC as well as from the absence of a $3\,700 \text{ cm}^{-1}$ band in FTIR indicating brucite (Figure 2.2). Although the Mg^{2+} activity, $a\text{Mg}^{2+}$, in the experimental solutions was up to 25 times higher than $a\text{Ca}^{2+}$ throughout transformation (exp. Mg1000), the ACC incorporated only 1-4 mol% of Mg in the bulk (Tables 2.1 and 2.2). The increasing persistence of ACC in solution might be attributed to the Mg incorporation and, indeed, many studies have found a relationship between enhanced metastability and solid Mg content (Loste et al., 2003; Rodriguez-Blanco et al., 2014; Blue et al., 2017 and therein). However, none of these experiments clearly discriminated between the influences of Mg incorporated in ACC versus aqueous species of Mg in the solution in which the ACC was aged. This can lead to inconsistencies in terms of obtained results regarding ACC metastability and the developing CaCO_3 polymorphs, as Blue et al. (2017) pointed out.

Table 2.3. Experimental time for sampling, pH and calculated activity fractions (PHREEQC) of the dissolved inorganic carbon (DIC) species of sampled solutions.

samples	time (min)	pH	activity fractions of DIC species [%]					
			αCO_3^{2-}	αHCO_3^-	αCaCO_3^0	αCaHCO_3^-	αMgCO_3^0	αMgHCO_3^-
Mg0_1	0.3	10.4	21.1	17.5	59.2	0.6	1.6	0.0
Mg0_2	4.6	10.2	41.6	52.3	4.9	0.1	1.1	0.0
Mg0_3	13.2	10.3	49.2	49.0	1.8	0.0	0.0	0.0
Mg0_4	23.0	10.4	51.4	46.7	1.9	0.0	0.0	0.0
Mg10_1	0.3	10.2	13.7	19.8	34.4	0.6	31.0	0.5
Mg10_2	2.2	10.1	12.2	20.7	39.2	0.8	26.6	0.6
Mg10_3	20.5	8.2	0.8	93.4	1.9	2.7	0.5	0.8
Mg30_1	0.3	10.1	7.6	13.2	27.9	0.6	49.6	1.1
Mg30_2	2.0	10.1	7.9	14.9	29.1	0.6	46.4	1.1
Mg30_3	6.7	10.0	7.2	15.4	29.6	0.7	45.8	1.2
Mg30_4	11.6	9.8	6.7	24.7	29.1	1.3	36.6	1.7
Mg30_5	32.9	7.6	0.2	88.2	1.0	6.6	0.5	3.4
Mg55_1	0.3	10.0	5.7	12.5	21.2	0.5	58.6	1.6
Mg55_2	8.2	9.8	5.1	15.6	23.0	0.8	53.5	2.0
Mg55_3	14.6	9.8	5.2	17.6	22.2	0.9	51.9	2.2
Mg55_4	25.0	9.9	5.4	16.3	19.8	0.7	55.8	2.1
Mg55_5	36.4	10.0	7.4	15.5	10.7	0.3	64.5	1.7
Mg55_6	63.8	10.0	6.4	14.3	7.6	0.2	69.6	1.9
Mg100_1	0.3	9.8	3.6	12.1	17.9	0.7	63.2	2.6
Mg100_2	8.4	9.7	3.5	14.8	18.3	0.9	59.4	3.1
Mg100_3	18.6	9.7	3.4	16.1	18.3	1.0	57.8	3.4
Mg100_4	28.7	9.7	3.5	16.9	17.3	1.0	57.8	3.4
Mg100_5	38.7	9.7	3.4	16.0	15.8	0.9	60.5	3.5
Mg100_6	58.8	9.5	3.4	21.0	6.0	0.4	64.3	4.9
Mg100_7	84.9	9.3	2.8	30.5	4.4	0.6	54.5	7.3
Mg100_8	137.5	8.8	1.6	50.9	2.3	0.8	32.2	12.2
Mg100_9	330.6	9.1	2.4	37.3	1.8	0.3	48.8	9.3
Mg1000_1	0.3	8.9	0.2	4.7	-	-	95.1	-
Mg1000_2	27.5	8.8	0.2	5.8	-	-	94.0	-
Mg1000_3	49.0	8.7	0.2	7.1	-	-	92.7	-
Mg1000_4	77.5	8.7	0.2	7.1	-	-	92.7	-
Mg1000_5	670.0	8.5	0.2	10.8	-	-	89.1	-
Mg1000_6	2394.0	8.5	0.2	11.1	-	-	88.7	-
Mg1000_7	12430.0	8.5	0.1	10.0	-	-	89.9	-

The limited Mg content in Mg-ACC obtained during aging additive-free ACC in greatly varying MgCl₂ containing solutions in this study indicates that the aqueous chemistry has to be considered as one of the major parameters for the retardation of ACC transformation. For instance, the average amount of Mg in ACC of experiments conducted in 0.1 and 1 mol dm⁻³ MgCl₂ in solution is 4 mol% (exp. Mg100) and 4.5 mol% (exp. Mg1000), respectively. Although the amount of Mg in ACC differs by only 0.5 mol%, the lifetime of the ACC was

extended about 25 times, from 27 min to at least 696 min, suggesting that reaction kinetics is predominately governed by the chemical composition of the aqueous solution (Figure 2.3). In the experiments of Purgstaller et al. (2017) it was shown that Mg-ACC with 10 mol% Mg in its structure persisted 24 min longer in a solution with an ion activity ratio $a\text{Mg}^{2+}/a\text{Ca}^{2+}$ of 12, transforming into monohydrocalcite, as in a solution with an ion activity ratio of 5, when transforming into Mg-Calcite. It was concluded that the prevailing $a\text{Mg}^{2+}/a\text{Ca}^{2+}$ ratio, and as a consequence the retarded formation of monohydrocalcite and Mg-calcite, respectively, determines the persistence of Mg-ACC. Blue et al. (2017) obtained similar results where Mg-ACC persisted longest at an $a\text{Mg}^{2+}/a\text{Ca}^{2+}$ ratio > 4 and/or an $a\text{CO}_3^{2-}/a\text{Ca}^{2+}$ ratio > 1 with the subsequent formation of monohydrocalcite, than in low Mg/Ca solutions where Mg-calcite was obtained.

Although we find a correlation of prolonged metastability of ACC at elevated $a\text{Mg}^{2+}/a\text{Ca}^{2+}$ ratios, we suggest that in these studies having conditions of alkaline pH, the retarded crystallization process lies in the increasing complexation of the carbonate molecule in more concentrated MgCl_2 solutions, notably the strong complexation with Mg^{2+} to form MgCO_3° . Indeed, calculating the individual proportions of carbonate species from fluid chemistry (Table 2.3) reveals that as long as ACC is present in solution CaCO_3° and MgCO_3° are the dominating carbonate aquocomplexes - the latter MgCO_3° accounting already for 31% in the experiment Mg10 with CaCO_3° being 34%. Beginning with the experiment Mg30, MgCO_3° is the dominant species with 50% rising to 95% in the experiment Mg1000 (Table 2.3). During the period while ACC is present, the proportions of CO_3^{2-} , while still accounting for 21% in the Mg-free experiment Mg0, decreased to 14% in the experiment Mg10 and finally to 0.2% in the experiment Mg1000. Therefore, we suggest that the availability of CO_3^{2-} in respect to the complexation potential governs the metastability of ACC in this study. The pH of the experiments - ranging from 8.9 to 10.4 after ACC dispersion - was not controlled, and the initial value was governed by the concentration of MgCl_2 in the solution, ranging from 5.2 to 6.9 (Table 2.1). This admittedly could have an influence on the overall reaction kinetics. However, with respect to ACC metastability, the effects are negligible in this case as the lower pH is a consequence of the increased MgCl_2 concentrations in solution. Therefore, the dominant carbonate species remains MgCO_3° instead of HCO_3^- , as can be observed from the proportions of the carbonate species (Table 2.3). HCO_3^- remains unchanged or decreases despite lower pH conditions with increasing MgCl_2 in solution, that is to say as long as ACC or nesquehonite are present. HCO_3^- becomes only dominant in the last stages when the final reaction product(s) of calcite and vaterite or aragonite forms. The addition of MgCl_2 in

solution resulted in considerable dissolution of ACC of up to 10% in the experiment Mg1000, which can be observed by the increase of Ca and alkalinity in the liquid phase (Table 2.1). However, at the same time, the supersaturation with respect to ACC only slightly increased for all experiments. While Ca^{2+} accumulated in the liquid phase, CO_3^{2-} decreased mainly in favour of MgCO_3° . The extended dissolution of ACC with MgCl_2 in the liquid phase corroborates the importance of MgCO_3° as a governing parameter for the phase evolution in these experiments (Ruiz-Agudo et al., 2009). As carbonate is complexed with Mg, the solubility of ACC would decrease and eventually become undersaturated. In order to prevent this, more ACC, and therefore more carbonate, has to be dissolved to maintain saturation state.

2.4.2 Distinct carbonate mineral formation controlled by aqueous MgCl_2 content

Additive-free ACC dispersed in *pure* water transformed immediately into vaterite and calcite (Table 2.1 and Figure 2.3), suggesting that the reaction kinetics are extreme fast, where calcite formation proceeds via the vaterite intermediate at high precipitation rates (Ogino et al., 1987; Bots et al., 2012; Rodriguez-Blanco et al., 2012). This transformation behaviour is also found in the experiments Mg10 and Mg30, but protracted and with predominantly calcite and less vaterite, which can be attributed to the instability of the vaterite structure in the presence of Mg in the system (Figure 2.3 and Table S2.1) (Rodriguez-Blanco et al., 2012). The time span where crystallization occurred, however, is almost equal for the experiments Mg10 and Mg30, 2.5 min from the start of ACC decline to the last signs of the amorphous phase. This suggests that Mg at these concentration levels does not significantly inhibit calcite precipitation kinetics once proper nuclei sizes are reached. From the experiment Mg55 onwards to higher Mg concentrations, transformation behaviour changes and nesquehonite starts to crystallize prior to, or in parallel with, the formation of monohydrocalcite at the onset of ACC decline (Figures 2.1b and 2.3). The formation of a hydrous magnesium carbonate phase together with monohydrocalcite is a common observation in natural settings and was also reported from laboratory studies (Nishiyama et al., 2013; Rodriguez-Blanco et al., 2014). In the latter, the formation of monohydrocalcite from a Mg-ACC precursor was studied and as by-product hydromagnesite obtained. As nesquehonite is metastable and is known to convert readily into hydromagnesite, the results of the laboratory studies infer a possible transformation during aging from nesquehonite (Hopkinson et al., 2008). Indeed, calculated saturation states in these studies imply that reactive solutions were approaching saturation or were slightly

supersaturated with respect to nesquehonite, as is the case in our study for the highly concentrated MgCl₂ solutions (Table 2.2).

The formation of brucite, although supersaturated from the beginning for most experiments in this study (Table 2.2), was never detected. An *in-situ* Raman spectroscopy study reported that aging of amorphous magnesium carbonate at 25 °C in solution directly formed nesquehonite as transient phase before transformation via dissolution and re-precipitation of dypingite was observed (Montes-Hernandez and Renard, 2016). Further, in the course of synthesizing Mg-ACC, the joint formation of brucite was reported to appear only at pH conditions > 10.8 (Blue and Dove, 2015). The highest pH observed in this study for a Mg containing solution was 10.2 in the experiment Mg10 (Table 2.1). In the low MgCl₂ solutions, the pH is higher compared to the high concentrated MgCl₂ solutions, as the stock solutions were less acidic, leading to higher supersaturations with respect to brucite (Table 2.2). Additionally, as more ACC is dissolved in the more concentrated MgCl₂ solutions, the alkalinity in solution increases, despite the lower pH conditions due to complexation. Therefore, it appears that the pH is not high enough and the increasing alkalinity conditions in the more concentrated MgCl₂ solutions, results in the preferred formation of nesquehonite rather than brucite. This is consistent with brucite carbonation studies, where lower pH and elevated HCO₃⁻ concentrations enhances brucite dissolution, leading to the formation of hydrous Mg carbonates (Hövelmann et al., 2012; Qafoku et al., 2015) and with the finding that nesquehonite forms abiotically in alkaline wetlands up to a pH of 10.3 with no indication of brucite formation (Power et al., 2007).

With the last signs of ACC in the experiments Mg55 onwards, nesquehonite reaches its highest intensity in the *in-situ* Raman pattern (Figure 2.1b and 2.3) and decreases upon monohydrocalcite commencing crystallization. Nishiyama et al. (2013) suggested that the formation of monohydrocalcite requires the paragenesis of hydrous magnesium carbonates. Monohydrocalcite then grows until aragonite formation is observed, which increases in line with the decline of monohydrocalcite to become the final reaction product (Figure 2.3). Transformation of metastable monohydrocalcite into aragonite is well documented to occur in solutions containing high Mg concentrations, and is explained by the inhibition of calcite formation due to aqueous Mg²⁺ ions (Loste et al., 2003; Rodriguez-Blanco et al., 2014; Blue et al., 2017; Purgstaller et al., 2017).

The initial formation of intermediate monohydrocalcite from Mg-ACC, instead of Mg-calcite and vaterite, was previously attributed to the Mg content of the given ACC (Rodriguez-Blanco et al., 2014). The study suggests that in solution pure ACC transforms into vaterite,

ACC with 10 mol% Mg into calcite, with 30 mol% into monohydrocalcite and with 50 mol% into protodolomite. However, as reported, recent studies show that solution chemistry is rather decisive for the polymorph development, in which Mg-ACC with 10 mol% Mg transforms either into Mg-calcite or monohydrocalcite depending on the physicochemical solution conditions (Blue et al., 2017; Purgstaller et al., 2017). The reactive solution conditions in this study agree well with the above-mentioned results in terms of an $a\text{Mg}^{2+}/a\text{Ca}^{2+}$ ratio being > 5 (Table 2.2). This corroborates the governing role of solution chemistry in particular, as in this study the initial amorphous precursor was Mg-free.

The low amounts of Mg being incorporated during dissolution and re-precipitation into ACC are unlikely to influence polymorphism to any great extent. For example, the averaged Mg content between the experiment Mg30, precipitating calcite and vaterite, and the experiment Mg55, obtaining monohydrocalcite and nesquehonite, differs only by 1 mol%. In this regard, Nishiyama et al. (2013) obtained either monohydrocalcite or combined calcite and vaterite from the same initial Mg/Ca ratio in solution each at different alkalinity. Although the authors ascribe the difference in obtained carbonate minerals to the higher $a\text{CO}_3^{2-}/a\text{Ca}^{2+}$ ratio, the reacted solution chemistry resulting in monohydrocalcite had also a high $a\text{Mg}^{2+}/a\text{Ca}^{2+}$ ratio, in contrast to the reacted solutions from which calcite and vaterite was obtained. In all experiments of Nishiyama et al. (2013), calcite and vaterite were obtained from solutions with a low Mg/Ca ratio and vice versa for monohydrocalcite, which supports aqueous chemistry as being the governing factor for the proceeding evolution of ACC rather than initial Mg content of the amorphous precursor. Therefore, our results contrast with the notion of a protocrystalline predetermination (Gebauer et al., 2008; Gebauer et al., 2010) for additive-free ACC, as distinct polymorph pathways were observed from the same educt exposed to varying solution chemistries. Thus, the chemical composition of the reactive solution via dissolution and re-precipitation determine the distinct carbonate mineral formation from ACC.

2.4.3 Conceptual transformation mechanisms of ACC into different crystalline polymorphs

The immediate transformation of ACC in the experiment Mg0 shows that activation energy for the transformation into crystalline products can be overcome simply by dispersing the amorphous phase into water. In contrast, in the experiments Mg10-Mg1000 transformation was progressively inhibited with increasing MgCl_2 in solution (Figure 2.3). However, a conclusive answer to what the underlying process is to accomplish such retardation is difficult to deduce from the present study, as it cannot be unequivocally clarified whether Mg is

incorporated homogeneously in ACC or enriched in the outer layers, but there are evidences for the latter. During the transformation of ACC into nesquehonite in the high MgCl_2 -rich experimental solutions ($\geq \text{Mg55}$), judging from the *in-situ* Raman and FTIR spectra, it appears that at some point nesquehonite is the sole phase in solution with no indication of ACC or monohydrocalcite (Table 2.1 and Figure 2.1b). However, Mg concentrations in the reactive solutions are too low to precipitate solely hydrous magnesium carbonates given that 0.5 mol dm^{-3} of ACC was dispersed. In FTIR and Raman spectroscopy, amorphous materials have, in general, lower intensity bands than crystalline products. Due to their non-ordered atomic structure, a broad rather than a narrow intense band is observed (Purgstaller et al., 2017). The high intensity of nesquehonite, therefore, could obscure the continual presence of ACC and explain the apparent exclusive formation of nesquehonite. On the other hand, a closer look at the continuously recorded Raman spectra of the experiments Mg10 and Mg30, with calcite and vaterite as reaction products, reveals the short existence of a nesquehonite band during the transformation of ACC (Figure S2.1). Although not verified with FTIR, as no sample was taken at that time, this could infer that, in general, Mg adsorbs on ACC particles building an Mg-rich layer around the surface, hence explaining the apparent exclusive occurrence of nesquehonite since Raman, or infrared reflection, spectroscopy mainly irradiates the outer layer only. When synthesizing monohydrocalcite via Mg-ACC from artificial seawater, Dejehet et al. (1999) observed spherulites which had a 5 times higher Mg concentration on the surface than in the bulk when measured with an electron microprobe. They concluded that Mg forms a protective layer stabilizing the spherulites. This conclusion can be found in other studies as well, ascertaining high Mg amounts in monohydrocalcite to be partly present as amorphous or hydrated magnesium carbonate phases surrounding monohydrocalcite (R. Liu et al., 2013; Nishiyama et al., 2013; Wang et al., 2015).

Assuming that ACC particles are covered by a Mg-rich layer, metastability and phase evolution of ACC could result from the lower availability of CO_3^{2-} and the increasing adsorption of Mg on the amorphous phase with higher MgCl_2 concentrations in the reactive solutions. The lower availability of CO_3^{2-} from 21% in the experiment Mg0 to 0.2% in the experiment Mg1000 would restrict further formation of carbonate phases and so inhibit crystallization (Table 2.3). In addition, the predominant neutral MgCO_3° ion pair, when considered to be directly incorporated on the surface of particles as suggested in other studies (Ruiz-Agudo et al., 2009; Mavromatis et al., 2017), could create a protective hydrous magnesium carbonate layer, thereby forming nesquehonite at the surface. In the low Mg experiments ($\leq \text{Mg30}$) the hydrous magnesium carbonates are undersaturated (Table 2.2),

thereby explaining the short existence of a nesquehonite band due to the subsequent fast dissolution. In combination with the low $a\text{Mg}^{2+}/a\text{Ca}^{2+}$ ratio < 4 in solution, Mg-calcite and vaterite are formed, which is consistent with the results of other studies (Blue et al., 2017; Purgstaller et al., 2017). In the experiments $\geq \text{Mg}55$, nesquehonite approaches saturation and goes on to become supersaturated such that the Mg phase can act as a protective layer. The subsequent formation of monohydrocalcite might then be explained by the requirement of a hydrous magnesium carbonate paragenesis as Nishiyama et al. (2013) suggested, or by the higher $a\text{Mg}^{2+}/a\text{Ca}^{2+}$ ratio of the solution being > 5 inhibiting the formation of calcite (Blue et al., 2017; Purgstaller et al., 2017).

2.5 Conclusions

The dispersion of 0.5 mol dm^{-3} of additive-free ACC into *pure* water and at different concentration levels of aqueous MgCl_2 ranging from 0.010 to 1 M, allowed us to study the influence of fluid chemistry on the phase development of ACC. It was found that while ACC dispersed in *pure* water transforms immediately into crystalline calcium carbonate, its transformation is retarded with increasing MgCl_2 in solution for up to ≥ 696 min. During ACCs metastable occurrence, it incorporated about 1-4 mol% of Mg instead of Ca in the bulk. Crystallization in MgCl_2 solutions ≤ 0.03 M resulted in the formation of Mg-calcite and vaterite, with the amount of the latter decreasing at elevated Mg concentration levels in the fluid phase. Experimental solutions ≥ 0.055 M of MgCl_2 resulted in the intermediate formation of nesquehonite and monohydrocalcite before transforming into the final reaction product aragonite. The distinct phase evolutions observed are a strong argument against protocrystalline predetermination of ACC, as from the same ACC batch different calcium carbonate minerals developed depending on the chemical composition of the solution. Since dispersion of ACC creates a highly alkaline solution, the retardation of ACC transformation is assumed to be caused by strong aquocomplex formation of the dissolved carbonate molecule with Mg^{2+} ions. The formation of MgCO_3° accounts for up to 95% of the dissolved inorganic carbon in the 1 M MgCl_2 solution, thereby decreasing the concentration of the free CO_3^{2-} species for carbonate mineral precipitation tremendously, which as a consequence retards mineral formation.

2.6 Supporting Information

Table S2.1. PXRD measurements, and subsequent quantification with Rietveld refinement of the final reaction products in solution show that vaterite was predominantly formed in the *pure* water experiment Mg0, while at low Mg^{2+} concentration in the reactive solutions, exp. Mg10 and 30, calcite is dominant and vaterite below 10 wt% is observed. From exp. Mg55 onwards in increasing $MgCl_2$ concentration, aragonite is the only phase detected in the final reaction product.

Experiments	PXRD of final reaction product		
	calcite	vaterite	aragonite
Mg0	35.3	64.7	0.0
Mg10	92.5	7.5	0.0
Mg30	92.1	7.9	0.0
Mg55	0.0	0.0	100.0
Mg100	0.0	0.0	100.0
Mg1000	0.0	0.0	100.0

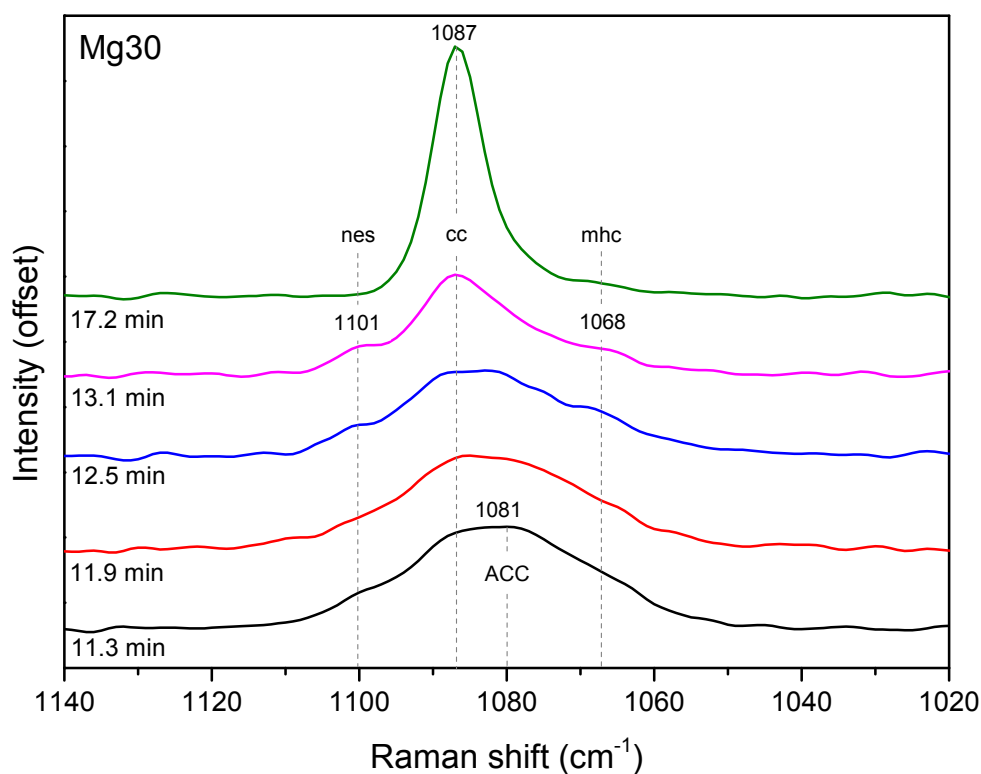


Figure S2.1. *In-situ* Raman spectra reveal hints of a short period of nesquehonite and maybe monohydrocalcite occurrence prior to the transformation of ACC into Mg-calcite and vaterite in the low $MgCl_2$ experiments (< 0.055 M), indicating a possible $MgCO_3$ -rich surface layer covering ACC particles.

2.7 References

- Addadi L., Raz S. and Weiner S. (2003) Taking Advantage of Disorder: Amorphous Calcium Carbonate and Its Roles in Biomineralization. *Adv. Mater.* **15**, 959–970.
- Aizenberg J., Lambert G., Weiner S. and Addadi L. (2002) Factors involved in the formation of amorphous and crystalline calcium carbonate: a study of an ascidian skeleton. *J. Am. Chem. Soc.* **124**, 32–39.
- Ajikumar P. K., Wong L. G., Subramanyam G., Lakshminarayanan R. and Valiyaveetil S. (2005) Synthesis and Characterization of Monodispersed Spheres of Amorphous Calcium Carbonate and Calcite Spherules. *Cryst. Growth Des.* **5**, 1129–1134.
- Andersen F. and Brecevic L. (1991) Infrared spectra of amorphous and crystalline calcium carbonate. *Acta Chem. Scand* **45**, 1018–1024.
- Becker A., Bismayer U., Epple M., Fabritius H., Hasse B., Shi J. and Ziegler A. (2003) Structural characterisation of X-ray amorphous calcium carbonate (ACC) in sternal deposits of the crustacea *Porcellio scaber*. *Dalt. Trans.*, 551–555.
- Beniash E., Aizenberg J., Addadi L. and Weiner S. (1997) Amorphous calcium carbonate transforms into calcite during sea urchin larval spicule growth. *Proc. R. Soc. B Biol. Sci.* **264**, 461–465.
- Benzerara K., Skouri-Panet F., Li J., Ferard C., Gugger M., Laurent T., Couradeau E., Ragon M., Cosmidis J., Menguy N., Margaret-Oliver I., Tavera R., Lopez-Garcia P. and Moreira D. (2014) Intracellular Ca-carbonate biomineralization is widespread in cyanobacteria. *Proc. Natl. Acad. Sci.*, 1–6.
- Blue C. R. and Dove P. M. (2015) Chemical controls on the magnesium content of amorphous calcium carbonate. *Geochim. Cosmochim. Acta* **148**, 23–33.
- Blue C. R., Giuffre A., Mergelsberg S., Han N., De Yoreo J. J. and Dove P. M. (2017) Chemical and physical controls on the transformation of amorphous calcium carbonate into crystalline CaCO₃ polymorphs. *Geochim. Cosmochim. Acta* **196**, 179–196.
- Bonales L. J., Muñoz-Iglesias V., Santamaría-Pérez D., Caceres M., Fernandez-Remolar D. and Prieto-Ballesteros O. (2013) Quantitative Raman spectroscopy as a tool to study the kinetics and formation mechanism of carbonates. *Spectrochim. Acta. A. Mol. Biomol. Spectrosc.* **116**, 26–30.
- Bots P., Benning L. G., Rodriguez-Blanco J.-D., Roncal-Herrero T. and Shaw S. (2012) Mechanistic Insights into the Crystallization of Amorphous Calcium Carbonate (ACC). *Cryst. Growth Des.* **12**, 3806–3814.
- Brečević L. and Nielsen A. E. (1989) Solubility of amorphous calcium carbonate. *J. Cryst.*

- Growth* **98**, 504–510.
- Coleyshaw E. E., Crump G. and Griffith W. P. (2003) Vibrational spectra of the hydrated carbonate minerals ikaite, monohydrocalcite, lansfordite and nesquehonite. *Spectrochim. Acta Part A Mol. Biomol. Spectrosc.* **59**, 2231–2239.
- Couradeau E., Benzerara K., Gerard E., Moreira D., Bernard S., Brown G. E. and Lopez-Garcia P. (2012) An Early-Branching Microbialite Cyanobacterium Forms Intracellular Carbonates. *Science (80-.)*. **336**, 459–462.
- Dejehet F., Idrissi S. and Debuyst R. (1999) Magnesium and occluded water in calcium carbonate monohydrate. *J. Chim. Phys.* **96**, 741–753.
- Demény A., Németh P., Czuppon G., Leél-Össy S., Szabó M., Judik K., Németh T. and Stieber J. (2016) Formation of amorphous calcium carbonate in caves and its implications for speleothem research. *Sci. Rep.* **6**, 39602.
- Edwards H. G. M., Villar S. E. J., Jehlicka J. and Munshi T. (2005) FT–Raman spectroscopic study of calcium-rich and magnesium-rich carbonate minerals. *Spectrochim. Acta Part A Mol. Biomol. Spectrosc.* **61**, 2273–2280.
- Foran E., Weiner S. and Fine M. (2013) Biogenic fish-gut calcium carbonate is a stable amorphous phase in the gilt-head seabream, *Sparus aurata*. *Sci. Rep.* **3**, 1700.
- Frost R. L. and Klopogge J. T. (1999) Infrared emission spectroscopic study of brucite. *Spectrochim. Acta - Part A Mol. Biomol. Spectrosc.* **55**, 2195–2205.
- Frost R. L. and Palmer S. J. (2011) Infrared and infrared emission spectroscopy of nesquehonite $\text{Mg}(\text{OH})(\text{HCO}_3) \cdot 2\text{H}_2\text{O}$ -implications for the formula of nesquehonite. *Spectrochim. Acta. A. Mol. Biomol. Spectrosc.* **78**, 1255–60.
- Gabrielli C., Jaouhari R., Joiret S. and Maurin G. (2000) In situ Raman spectroscopy applied to electrochemical scaling. Determination of the structure of vaterite. *J. Raman Spectrosc.* **31**, 497–501.
- Gebauer D., Gunawidjaja P. N., Ko J. Y. P., Bacsik Z., Aziz B., Liu L., Hu Y., Bergström L., Tai C., Sham T.-K., Edén M. and Hedin N. (2010) Proto-Calcite and Proto-Vaterite in Amorphous Calcium Carbonates. *Angew. Chemie Int. Ed.* **49**, 8889–8891.
- Gebauer D., Völkel A. and Cölfen H. (2008) Stable prenucleation calcium carbonate clusters. *Science* **322**, 1819–1822.
- Habraken W. J. E. M., Masic A., Bertinetti L., Al-Sawalmih A., Glazer L., Bentov S., Fratzi P., Sagi A., Aichmayer B. and Berman A. (2015) Layered growth of crayfish gastrolith: About the stability of amorphous calcium carbonate and role of additives. *J. Struct. Biol.* **189**, 28–36.

- Hopkinson L., Rutt K. . and Cressey G. (2008) The transformation of nesquehonite to hydromagnesite in the system CaO-MgO-H₂O-CO₂: an experimental spectroscopic study. *J. Geol.* **116**, 387–400.
- Hövelmann J., Putnis C. V, Ruiz-Agudo E. and Austrheim H. (2012) Direct Nanoscale Observations of CO₂ Sequestration during Brucite [Mg(OH)₂] Dissolution. *Environ. Sci. Technol.* **46**, 5253–5260.
- Jones B. and Peng X. (2012) Amorphous calcium carbonate associated with biofilms in hot spring deposits. *Sediment. Geol.* **269–270**, 58–68.
- Konrad F., Gallien F., Gerard D. E. and Dietzel M. (2016) Transformation of Amorphous Calcium Carbonate in Air. *Cryst. Growth Des.* **16**, 6310–6317.
- Kralj D. and Brečević L. (1995) Dissolution kinetics and solubility of calcium carbonate monohydrate. *Colloids Surfaces A Physicochem. Eng. Asp.* **96**, 287–293.
- Levi-Kalisman Y., Raz S., Weiner S., Addadi L. and Sagi I. (2002) Structural Differences Between Biogenic Amorphous Calcium Carbonate Phases Using X-ray Absorption Spectroscopy. *Adv. Funct. Mater.* **12**, 43.
- Liu R., Liu F., Zhao S., Su Y., Wang D. and Shen Q. (2013) Crystallization and oriented attachment of monohydrocalcite and its crystalline phase transformation. *CrystEngComm* **15**, 509–515.
- Liu Y.-Y., Jiang J., Gao M.-R., Yu B., Mao L.-B. and Yu S.-H. (2013) Phase Transformation of Magnesium Amorphous Calcium Carbonate (Mg-ACC) in a Binary Solution of Ethanol and Water. *Cryst. Growth Des.* **13**, 59–65.
- Loste E., Wilson R. M., Seshadri R. and Meldrum F. C. (2003) The role of magnesium in stabilising amorphous calcium carbonate and controlling calcite morphologies. *J. Cryst. Growth* **254**, 206–218.
- Mavromatis V., Purgstaller B., Dietzel M., Buhl D., Immenhauser A. and Schott J. (2017) Impact of amorphous precursor phases on magnesium isotope signatures of Mg-calcite. *Earth Planet. Sci. Lett.* **1**, 1–10.
- Montes-Hernandez G. and Renard F. (2016) Time-Resolved in Situ Raman Spectroscopy of the Nucleation and Growth of Siderite, Magnesite, and Calcite and Their Precursors. *Cryst. Growth Des.* **16**, 7218–7230.
- Neumann M. and Epple M. (2007) Monohydrocalcite and Its Relationship to Hydrated Amorphous Calcium Carbonate in Biominerals. *Eur. J. Inorg. Chem.* **2007**, 1953–1957.
- Nishiyama R., Munemoto T. and Fukushi K. (2013) Formation condition of monohydrocalcite from CaCl₂-MgCl₂-Na₂CO₃ solutions. *Geochim. Cosmochim. Acta*

100, 217–231.

- Ogino T., Suzuki T. and Sawada K. (1987) The formation and transformation mechanism of calcium carbonate in water. *Geochim. Cosmochim. Acta* **51**, 2757–2767.
- Parkhurst D. L. and Appelo C. A. J. (2013) Description of input and examples for PHREEQC version 3--A computer program for speciation, batch- reaction, one-dimensional transport, and inverse geochemical calculations: U.S. Geological Survey Techniques and Methods, book 6, chap. A43, 497 p.
- Plummer L. N. and Busenberg E. (1982) The solubilities of calcite, aragonite and vaterite in CO₂-H₂O solutions between 0 and 90°C, and an evaluation of the aqueous model for the system CaCO₃-CO₂-H₂O. *Geochim. Cosmochim. Acta* **46**, 1011–1040.
- Pokrovsky O. S. and Schott J. (2004) Experimental study of brucite dissolution and precipitation in aqueous solutions: surface speciation and chemical affinity control. *Geochim. Cosmochim. Acta* **68**, 31–45.
- Power I. M., Wilson S. A., Thom J. M., Dipple G. M. and Southam G. (2007) Biologically induced mineralization of dypingite by cyanobacteria from an alkaline wetland near Atlin, British Columbia, Canada. *Geochem. Trans.* **8**, 13.
- Purgstaller B., Konrad F., Dietzel M., Immenhauser A. and Mavromatis V. (2017) Control of Mg²⁺/Ca²⁺ Activity Ratio on the Formation of Crystalline Carbonate Minerals via an Amorphous Precursor. *Cryst. Growth Des.* **17**, 1069–1078.
- Purgstaller B., Mavromatis V., Immenhauser A. and Dietzel M. (2016) Transformation of Mg-bearing amorphous calcium carbonate to Mg-calcite – In situ monitoring. *Geochim. Cosmochim. Acta* **174**, 180–195.
- Qafoku O., Dixon D. A., Rosso K. M., Schaefer H. T., Bowden M. E., Arey B. W. and Felmy A. R. (2015) Dynamics of Magnesite Formation at Low Temperature and High pCO₂ in Aqueous Solution. *Environ. Sci. Technol.* **49**, 10736–10744.
- Radha A. V., Fernandez-Martinez A., Hu Y., Jun Y., Waychunas G. A. and Navrotsky A. (2012) Energetic and structural studies of amorphous Ca_{1-x}Mg_xCO₃·nH₂O (0 ≤ x ≤ 1). *Geochim. Cosmochim. Acta* **90**, 83–95.
- Raz S., Testeniere O., Hecker A. and Weiner S. (2002) Stable Amorphous Calcium Carbonate Is the Main Component of the Calcium Storage Structures of the Crustacean *Orchestia cavimana*. *Biol. Bull.*, 269–274.
- Raz S., Weiner S. and Addadi L. (2000) Formation of High-Magnesian Calcites via an Amorphous Precursor Phase: Possible Biological Implications. *Adv. Mater.* **12**, 38–42.
- Rodriguez-Blanco J. D., Shaw S. and Benning L. G. (2015) A route for the direct

- crystallization of dolomite. *Am. Mineral.* **100**, 1172–1181.
- Rodríguez-Blanco J. D., Shaw S., Bots P., Roncal-Herrero T. and Benning L. G. (2014) The role of Mg in the crystallization of monohydrocalcite. *Geochim. Cosmochim. Acta* **127**, 204–220.
- Rodríguez-Blanco J. D., Shaw S., Bots P., Roncal-Herrero T. and Benning L. G. (2012) The role of pH and Mg on the stability and crystallization of amorphous calcium carbonate. *J. Alloys Compd.* **536**, S477–S479.
- Ruiz-Agudo E., Putnis C. V., Jiménez-López C. and Rodríguez-Navarro C. (2009) An atomic force microscopy study of calcite dissolution in saline solutions: The role of magnesium ions. *Geochim. Cosmochim. Acta* **73**, 3201–3217.
- Señorale-Pose M., Chalar C., Dauphin Y., Massard P., Pradel P. and Marín M. (2008) Monohydrocalcite in calcareous corpuscles of *Mesocestoides corti*. *Exp. Parasitol.* **118**, 54–58.
- Di Tommaso D. and de Leeuw N. H. (2010) Structure and dynamics of the hydrated magnesium ion and of the solvated magnesium carbonates: insights from first principles simulations. *Phys. Chem. Chem. Phys.* **12**, 894–901.
- Wang D., Hamm L. M., Bodnar R. J. and Dove P. M. (2012) Raman spectroscopic characterization of the magnesium content in amorphous calcium carbonates. *J. Raman Spectrosc.* **43**, 543–548.
- Wang D. and Li Z. (2012) Chemical Modeling of Nesquehonite Solubility in Li + Na + K + NH₄⁺ Mg⁺ Cl⁺ H₂O System with a Speciation-based Approach. *Chinese J. Chem. Eng.* **20**, 267–276.
- Wang Y.-Y., Yao Q.-Z., Zhou G.-T. and Fu S.-Q. (2015) Transformation of amorphous calcium carbonate into monohydrocalcite in aqueous solution: a biomimetic mineralization study. *Eur. J. Mineral.* **27**, 717–729.
- Weiss I. M., Tuross N., Addadi L. and Weiner S. (2002) Mollusc larval shell formation: amorphous calcium carbonate is a precursor phase for aragonite. *J. Exp. Zool.* **293**, 478–491.
- White W. B. (1971) Infrared characterization of water and hydroxyl ion in the basic magnesium carbonate minerals. *Am. Mineral.* **56**, 46–53.
- Zhang Z., Xie Y., Xu X., Pan H. and Tang R. (2012) Transformation of amorphous calcium carbonate into aragonite. *J. Cryst. Growth* **343**, 62–67.

Chapter 3

Ikaite formation from ACC up to 18 °C questions its use as an indicator of low temperature conditions

ABSTRACT: Ikaite, $\text{CaCO}_3 \cdot 6\text{H}_2\text{O}$, is documented to precipitate from aqueous solution at low temperatures up to 9 °C. It forms unique pyramidal crystals, which can be preserved after its transformation into calcite as pseudomorphs. These pseudomorphs after ikaite are thus used as a (paleo)climate proxy for near freezing water conditions. However, as the preservation of the temperature sensitive mineral is difficult to achieve and experimental studies are sparse, data about the physicochemical (trans)formation conditions of ikaite are lacking. To date, it is not known whether ikaite can be formed directly from CaCO_3^0 aqueous complexes or via transformation of an amorphous calcium carbonate (ACC) precursor. Furthermore, studies report different upper temperature limits of stability. Here, we investigate ikaite formation via an ACC precursor in the temperature range between 6 and 25 °C in Mg containing solutions. It was found that the formation of ikaite from an amorphous precursor is a viable pathway and that ikaite can be formed up to 18 °C in aqueous solutions containing Mg. These findings have to be considered with respect to the mechanisms of ikaite formation and might have severe implications regarding the use of ikaite occurrence as a reliable indicator of low temperature environments.

3.1 Introduction

In natural environments, the mineral ikaite is reported to precipitate as a stable calcium carbonate phase under cold water conditions of up to 7-9 °C (Pauly, 1963; Marland, 1975; Buchardt et al., 1997; Selleck et al., 2007; Field et al., 2017). Bischoff, Fitzpatrick, et al. (1993) found that ikaite shows retrograde solubility as a function of temperature contrarily to the usual solubility behaviour of carbonate minerals. As a consequence, exposing the mineral to a warmer environment, e.g. to ambient temperatures, leads to elevated dissolution rates of ikaite and subsequent recrystallization as anhydrous CaCO_3 (Sánchez-Pastor et al., 2016). The crystal morphologies thereby are considered to be preserved, if the elevated transition

temperature is close to ikaite's formation temperature (Larsen, 1994), which can then be observed as glendonite, thinolite, jarrowite and more, all attributed to be pseudomorphs after ikaite (Shearman and Smith, 1985; Huggett et al., 2005). Glendonites have already been described as rarely appearing calcite pseudomorphs since the nineteenth century (Dana, 1849). Yet, the search for the parent mineral was over not before 1982, when Suess et al. (1982) recognized that ikaite shares similar crystal morphologies with glendonites and after transformation shows calcite pseudomorphs of the latter.

The environmental conditions in which ikaite has been found, beside low prevailing temperatures, are commonly associated with high alkalinity and in most cases elevated phosphate concentrations. The latter, although a known inhibitor of anhydrous calcium carbonate formation, apparently does not retard the formation of ikaite (Bischoff, Stine, et al., 1993; Hu et al., 2014). These formation environments are met at high latitudes, e.g. at the type-locality for ikaite the Ikka-Fjord in Greenland (Pauly, 1963) or in the sea-ice at polar regions, presumably influencing the global carbon cycle (Dieckmann et al., 2008; Dieckmann et al., 2010; Rysgaard et al., 2013; Geilfus et al., 2016). Natural ikaite is also found in saline lakes and spring waters formed seasonally during winter (Council and Bennett, 1993; Ito, 1996; Last et al., 2013; Oehlerich et al., 2013). In an industrial environment, it was first described from a water treatment plant (Slack, 1980) and recently also found in anthropogenically influenced hyperalkaline speleothems (Field et al., 2017) as well as in a man-made river bed (Boch et al., 2015), in all cases related to low temperature conditions. The apparent upper temperature range of about 9° C found for ikaite formation in nature and above all its transformation into calcite pseudomorphs after ikaite is the reason why it is considered as a valuable paleo-temperature proxy, indicating a change from colder to warmer temperature conditions and used as such for climate studies of the past (Shearman and Smith, 1985; Swainson and Hammond, 2001; Spielhagen and Tripathi, 2009; Lu et al., 2012). On the other hand, experimental protocols on obtaining and stabilizing calcium carbonate hexahydrate at ambient conditions using various additives go way back with studies synthesizing the latter, e.g. in saccharose (Mackenzie, 1923) or in the presence of polymeric metaphosphates (Brooks et al., 1950; Dickens and Brown, 1970).

Temperature limitations for ikaite stability as suggested by the formation conditions found in natural environments are dissonant with laboratory studies obtaining calcium carbonate hexahydrate at ambient temperatures. The extended temperature stability of ikaite observed from laboratory studies might be due to additives being used therein not found in nature or due to concentrations levels of the latter not applicable for natural environments. However, if

ikaite can be formed at significantly higher temperatures than previously thought, this would have severe implications on its use as a (paleo)climate proxy. Furthermore, the formation pathway of ikaite is still under discussion, with studies suggesting ikaite being formed directly from CaCO_3^0 aqueous complexes (e.g. [Buchardt et al., 2001](#)) and a recent study indicating its crystallization via an amorphous calcium carbonate (ACC) precursor (e.g. [Purgstaller, 2017](#)). Here, we present laboratory experiments dispersing amorphous calcium carbonate (ACC) into Mg-rich solutions at cold to ambient temperatures ($6 \leq T(^{\circ}\text{C}) \leq 25$) using *in-situ* Raman spectroscopy for monitoring and try to elucidate (i) if ACC can act as a precursor for ikaite formation and (ii) if ikaite can only be formed at proposed cold temperature levels.

3.2 Experimental

3.2.1 Synthesis of ACC

ACC formation followed the protocol described earlier in [Konrad et al. \(2016\)](#). In brief, calcium- and carbonate-rich stock solutions of equimolar concentrations (0.25 M) were rapidly and vigorously mixed and immediately vacuum-filtered using a membrane cellulose acetate filter (0.2 μm pore size with 10 cm in diameter), washed with ultrapure water and transferred into a Virtis Benchtop 3 dm³ freeze dryer (-58 $^{\circ}\text{C}$ condenser temperature and 10 mbar partial vacuum) in order to sublime the non-structurally bound H₂O. This was repeated several times until the necessary amounts of about 10 g of ACC for the conducted experiments were reached. This physisorbed water-free ACC has the composition $\text{CaCO}_3 \cdot (0.42 \pm 0.01)\text{H}_2\text{O}$ and consists of spherical particles ranging between 30 and 200 nm in diameter with an averaged mean particle size of about 90 nm (see [Konrad et al. \(2016\)](#)). In order to prevent transformation in air, the ACC powder was stored under gastight conditions until use.

3.2.2 Experimental Setup

To monitor the impact of temperature on the ACC transformation behaviour a 0.03 M magnesium stock solution was prepared using Milli-Q water and magnesium chloride hexahydrate (> 99%, p.a., ACS, Carl Roth), in which 0.5 mol dm⁻³ of synthesized ACC were dispersed in a stirring lab reactor containing 0.03 dm³ of the magnesium-rich solution, while keeping the temperature at 6, 12, 18 and 25 $^{\circ}\text{C}$, respectively. Temperature control was realized with an EasyMax 102 workstation (Mettler Toledo) equipped with a solid state thermostat keeping temperature fluctuations under ± 0.1 $^{\circ}\text{C}$. The evolution of ACC in suspension was followed by tracking the pH and by monitoring the vibrational behaviour of the carbonate molecule with *in-situ* Raman spectroscopy. Using a pipette adjusted to 1 cm³,

the first samples were always taken after 15 s of reaction time, the latter starting with the dispersion of ACC into the Mg-solution. Thereafter, sampling took place continuously and whenever a change was observable in the *in-situ* Raman spectra. The samples were transferred from the pipette directly into a suction filtration unit. By using a membrane cellulose acetate filter (0.2 μm pore size), the reaction products were separated from solution and immediately analysed by ATR-FTIR spectroscopy to verify the phase composition seen in suspension by *in-situ* Raman spectroscopy. An additional experiment was conducted, monitoring *in-situ* the mixing of a CaCl_2 solution into a Na_2CO_3 solution of equimolar concentrations (1 M) at 6 °C.

3.2.3 Methods

During experiments the pH was tracked with a Schott BlueLine 28 combined electrode, calibrated against NIST standard buffers at pH 4.01, 7.00 and 10.00. *In-situ* observations of the dissolved inorganic carbon and carbonate bearing reaction products were realized with a Raman RXN2 analyzer (Kaiser Optical Systems) equipped with a Kaiser MR Probe head (quarter-inch immersion optic) running with a 785 nm laser. The spectra were collected every 35 s with a resolution of 1 cm^{-1} , integrating the Raman signal for 30 s to obtain a better signal-to-noise ratio and a 5 s delay in between measurements. Subsamples of separated solids and solutions were digested in 6% HNO_3 for analyses of ion concentrations with inductively coupled plasma optical emission spectroscopy (ICP-OES) on a Perkin Elmer Optima 8300 DV with an analytical error for Ca and Mg $< \pm 3\%$. Total alkalinity measurements of the sampled solutions were conducted on a Schott TitroLine alpha plus titrator using a 0.01 M HCl solution. For phase characterisation, the obtained solids were analysed by Fourier transform infrared spectroscopy (FTIR) in attenuated total reflection (ATR) mode from 650 to $4\,000\text{ cm}^{-1}$ at a resolution of 4 cm^{-1} and by powder X-ray diffraction (PXRD) performed on a PANalytical X'Pert Pro diffractometer, equipped with a Co target and a solid-state real time multiple strip (RTMS) detector (measurement parameters: 40 kV, 40 mA, 0.008° step, 40 s/step and $4\text{-}80^\circ\ 2\theta$). Phase identification and quantification from PXRD pattern was accomplished by using the inorganic crystal structure database (ICSD) and by Rietveld analysis, respectively. Subsamples of the reaction products were coated with gold/palladium and imaged by secondary electrons using a ZEISS DSM 982 Gemini scanning electron microscope (SEM) equipped with a field emission gun operated at 5 kV. Speciation calculations were performed with PHREEQC software using the MINTEQA4 database ([Parkhurst and Appelo, 2013](#)).

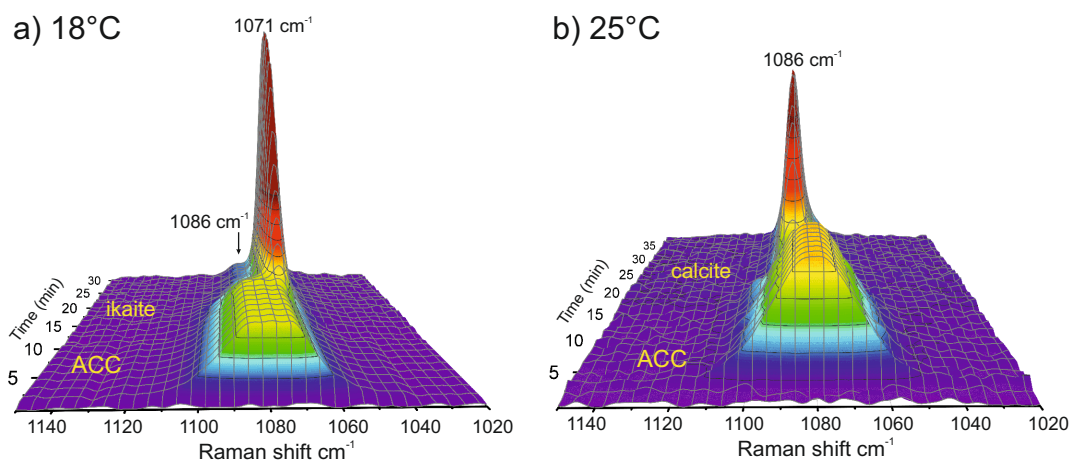


Figure 3.1. The evolution of ACC in Mg-rich solutions at different temperatures from *in-situ* Raman spectroscopy measurements display from 6-18 °C the transformation of ACC into ikaite (a), while at 25 °C calcite is formed (b).

3.3 Results

3.3.1 Phase evolution at distinct temperatures

Dispersing additive-free ACC into 0.03 M MgCl₂-solutions (pH ~6.9 at 25 °C) displayed a broad Raman band with a maximum at 1 080 cm⁻¹ in the *in-situ* Raman analyses in all experiments (Figure 3.1). This symmetric stretch band of the carbonate molecule and the absence of any other lattice modes indicate that ACC is present in solution as initial phase (Wang et al., 2012), its sole occurrence ranging between 2 min at 6 °C and 12 min at 25 °C (Table 3.1). The subsequent transformation of ACC in solution resulted in a narrowing and shift of the carbonate ν₁-band to 1 071 cm⁻¹ in experiments conducted at 6, 12 and 18 °C, while at 25 °C the band shifted to 1 086 cm⁻¹. Comparing the absorption bands with literature values, indicate the formation of ikaite (Tlili et al., 2001; Hu et al., 2014) in the temperature range between 6 and 18 °C and the formation of calcite (Gabielli et al., 2000; Wang et al., 2012) at 25 °C. There is indication that calcite might be present as minor phase during the late stages of the 18 °C experiment as a 1 086 cm⁻¹ band is arising after 26 min (Figure 3.1a). The phase determinations in solution by *in-situ* Raman spectroscopy were confirmed by FTIR measurements of separated solids (Figure 3.2 and Table 3.1). ACC was characterised by the ν₂ deformation band at 860 cm⁻¹ and by the ν₁ symmetric stretch band at 1 074 cm⁻¹ (Purgstaller et al., 2016; Konrad et al., 2016), whereas infrared spectra of ikaite displayed the ν₂ deformation band at 869 cm⁻¹ and by the ν₄ deformation band at 721 cm⁻¹ (Coleyshaw et al., 2003; Purgstaller, 2017). Additionally, a band at 667 cm⁻¹ was observed, which was ascribed as second split ν₄-band. Calcite and vaterite from the 25 °C experiment were determined by their ν₄ absorption bands at 710 and 741 cm⁻¹, respectively (Andersen and Brecevic, 1991).

Table 3.1. Time of sampling, pH, alkalinity, and chemical composition of fluid and solid as well as qualitative and quantitative phase analysis of experiments conducted. ^aNote: PXRD measurements were conducted after drying and subsequent transformation of metastable phases in air.

samples	time (min)	pH	alkalinity mmol dm ⁻³	fluid mmol dm ⁻³		solid mol%		<i>in-situ</i> Raman	FTIR	PXRD ^a wt%	
				Ca	Mg	Ca	Mg			calcite	vaterite
6 °C_1	0.3	10.4	8.7	6.6	21.8	98.7	1.3	ACC	ACC	79.6	20.4
6 °C_2	4.0	10.4	5.9	5.6	20.1	98.3	1.7	ACC, ikaite	ACC, ikaite	55.4	44.7
6 °C_3	7.3	10.4	4.1	4.5	19.3	98.2	1.8	ikaite, ACC	ikaite, ACC	71.6	28.4
6 °C_4	24.3	10.3	2.7	3.2	19.7	98.3	1.7	ikaite	ikaite	100.0	0.0
12 °C_1	0.3	10.2	8.1	5.7	19.9	98.3	1.7	ACC	ACC	85.8	14.2
12 °C_2	3.6	10.2	6.0	6.5	20.3	98.4	1.6	ACC	ACC	79.3	20.7
12 °C_3	7.4	10.2	5.4	6.2	20.1	98.3	1.7	ACC, ikaite	ACC, ikaite	79.0	21.0
12 °C_4	18.7	10.2	3.7	3.9	19.4	98.2	1.8	ikaite	ikaite	80.9	19.2
18 °C_1	0.3	10.2	9.2	5.8	19.8	98.2	1.8	ACC	ACC	90.1	9.9
18 °C_2	2.5	10.2	9.3	7.1	19.1	98.1	1.9	ACC	ACC	91.4	8.6
18 °C_3	8.9	10.1	7.7	5.9	19.0	98.0	2.0	ACC	ACC	95.9	4.1
18 °C_4	13.7	10.2	7.0	5.9	20.1	98.3	1.7	ACC, ikaite	ACC, ikaite	97.1	2.9
18 °C_5	23.7	10.2	5.2	3.7	19.8	98.3	1.7	ikaite	ikaite	100.0	0.0
25 °C_1	0.3	10.1	9.6	7.0	22.3	98.7	1.3	ACC	ACC	87.8	12.2
25 °C_2	2.0	10.1	8.1	6.8	19.5	98.2	1.8	ACC	ACC	92.9	7.1
25 °C_3	6.7	10.0	7.2	7.5	21.1	98.5	1.5	ACC	ACC	95.4	4.6
25 °C_4	11.6	9.8	6.1	7.7	17.6	97.8	2.2	ACC	calcite, vaterite	90.0	10.0
25 °C_5	32.9	7.6	1.5	10.3	9.7	96.3	3.7	calcite	calcite, vaterite	92.1	7.9

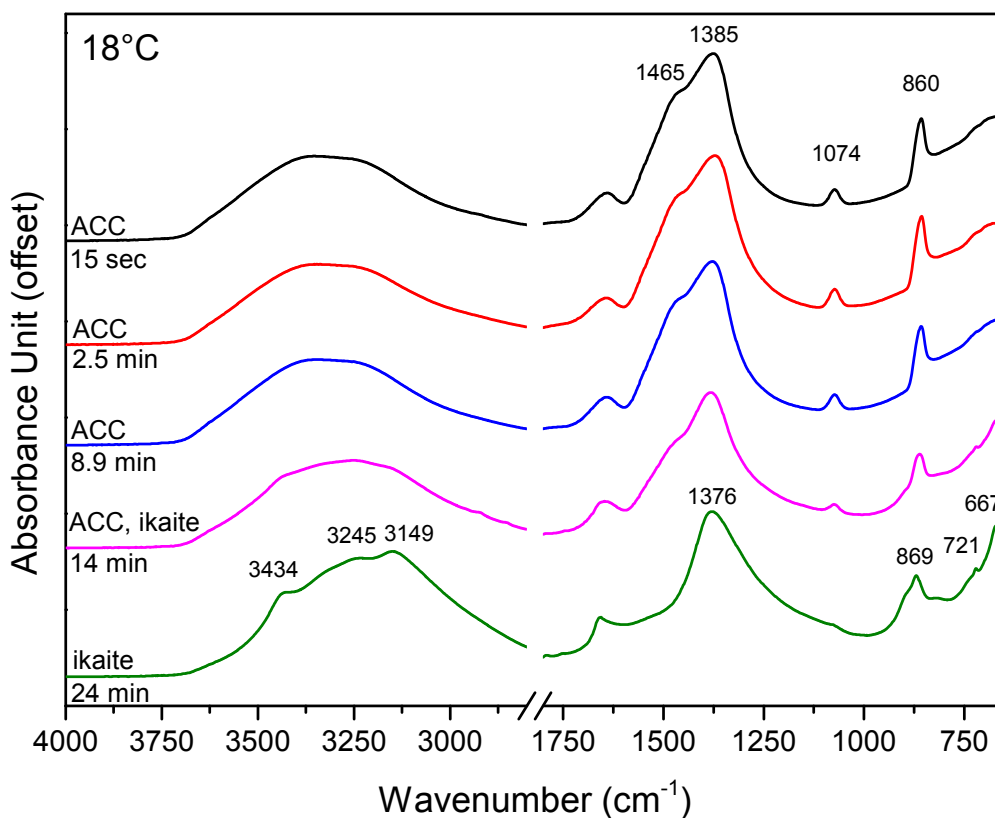


Figure 3.2. FTIR analyses of wet, formerly suspended, solids – instantaneously measured after separation from the experimental solution - verify the *in-situ* results of ikaite formation from ACC.

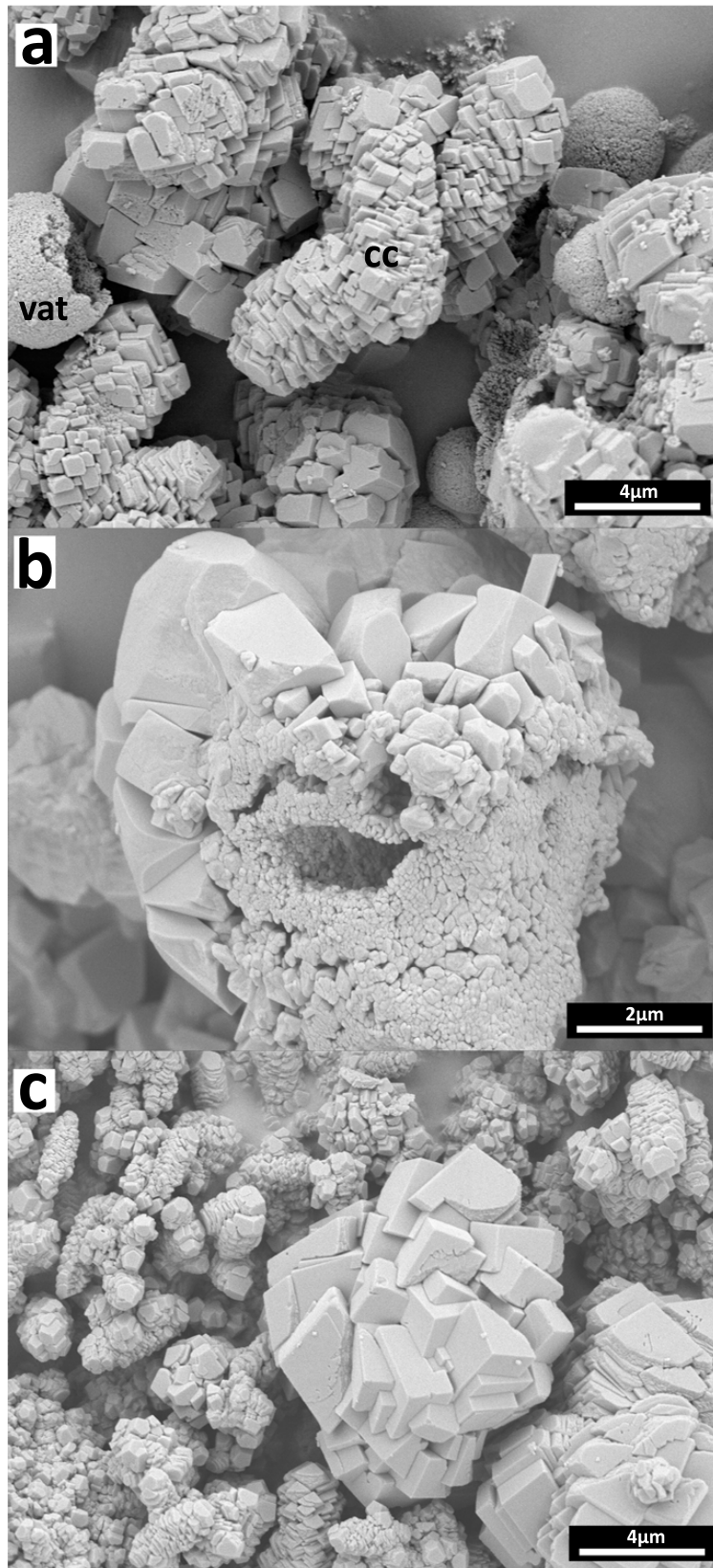


Figure 3.3. SEM images of precipitates transformed under air exposure, displaying elongated aggregates of rhombohedral calcites and spheres of vaterite after transformation from ACC (a), rhombohedral μm -sized calcites as well as hollow shapes consisting of nm-sized calcites formed from disintegration of ikaite under air (b) and again elongated calcite aggregates plus about $7 \mu\text{m}$ -sized flower-like structures of calcite rhombohedra from the transformation of ACC in solution at $25 \text{ }^\circ\text{C}$ (c). vat: vaterite; cc: calcite.

PXRD measurements show that independent of the phase present in solution and during analysis by FTIR, the subsequent drying of the samples under air-exposure resulted for all solids in calcite and with some exceptions in vaterite as minor phase (Table 3.1). All SEM images of the solids transformed from ACC display $\sim 10 \mu\text{m}$ elongated aggregates of rhombohedral calcite crystals each of $\sim 1\text{-}2 \mu\text{m}$ in diameter and spheres of $\sim 4\text{-}6 \mu\text{m}$ in diameter composed of $\sim 60\text{-}90 \text{ nm}$ crystals indicating vaterite (Figure 3.3a). After its disintegration under air exposure, ikaite is seen in SEM images displaying $2 \mu\text{m}$ sized rhombohedral shaped as well as aggregated nanometre sized calcite crystals, forming porous and hollow shapes (Figure 3.3b). The calcite and vaterite, obtained from ACC transformation in solution at $25 \text{ }^\circ\text{C}$, show rhombohedral calcites only, predominantly formed in elongated shapes with individual crystals of $\sim 0.5\text{-}1 \mu\text{m}$ in diameter and some larger flower-like structures having a diameter of $\sim 7 \mu\text{m}$ (Figure 3.3c). The mixing experiment, conducted additionally in the pure system at $6 \text{ }^\circ\text{C}$ in the absence of Mg, shows in the *in-situ* Raman measurements, after the introduction of the Ca-rich into the carbonate-rich solution, the decrease of the symmetric stretch band at 1067 cm^{-1} of dissolved CO_3^{2-} (Geisler et al., 2012) and for about 30 s the occurrence of ACC, indicated by the broad and weak 1080 cm^{-1} band prior to the appearance of the carbonate ν_1 -band of ikaite at 1071 cm^{-1} (Figure 3.4).

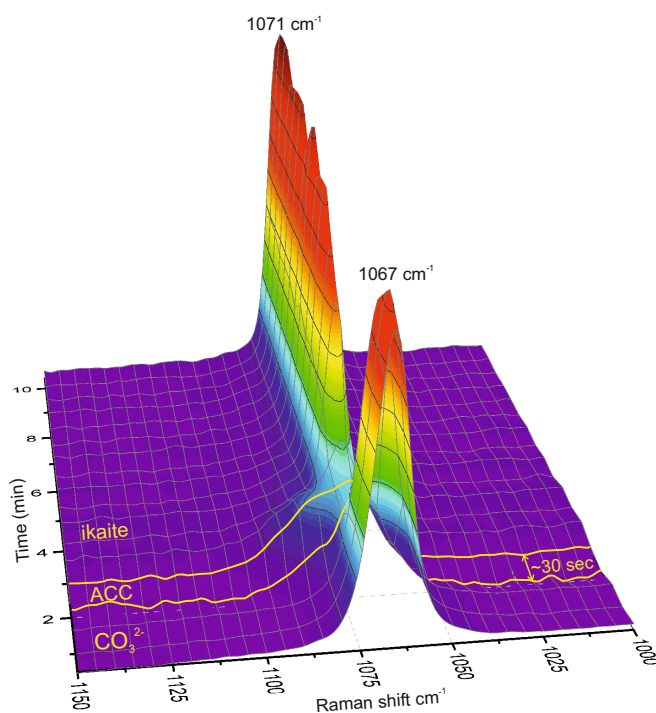


Figure 3.4. The additional mixing experiment of a Ca- into a carbonate-bearing solution at $6 \text{ }^\circ\text{C}$ reveals in the *in-situ* Raman measurements the short-term occurrence of ACC (broad band with centre at 1080 cm^{-1}) for a maximum time frame of 30 s between the decrease of dissolved CO_3^{2-} (1067 cm^{-1}) and the formation of ikaite (1071 cm^{-1}) as intermediate phase.

3.3.2 Chemical composition of solids and solution chemistry

After the dispersion of ACC into the solution, Ca^{2+} ions get introduced into the fluid, suggesting that 1.3 ± 0.1 % of the 0.5 mol dm^{-3} of ACC was dissolved (Table 3.1). The Mg concentrations dropped after the dispersion and, consequently, the compositions of the solids show that the initially Mg-free ACC incorporated between 1.3 and 2.2 mol% of Mg instead of Ca and that ikaite as well incorporated 1.74 ± 0.04 mol% of Mg, both phases showing no correlation of incorporation behaviour with the prevailing temperature. A comparably elevated incorporation of Mg can be observed in the resulting Mg-calcite from the 25 °C experiment with an Mg-content of 3.7 mol%.

Since all solids contained Mg resulting in $\text{Ca}_{(1-x)}\text{Mg}_x\text{CO}_3$ -precipitates, the ionic activity product (IAP) was calculated as

$$\text{IAP} = (a\text{Ca}^{2+})^x \cdot (a\text{Mg}^{2+})^{(1-x)} \cdot (a\text{CO}_3^{2-})$$

(Table 3.2). However, as the Mg content does not surpass 2.2 mol% in ACC, 1.8 mol% in ikaite and 3.7 mol% in calcite, the differences against calculated log IAPs without Mg are negligible (≤ 0.02) and smaller than the error produced by speciation calculations. In this respect, the solubility products from the works of Brečević and Nielsen (1989) for ACC and Bischoff, Fitzpatrick, et al. (1993) for ikaite were used for comparison with obtained solubilities and for calculations of saturation indices (SI) and in the case of calcite, solubility products from Busenberg and Plummer (1989) were used. The calculated log IAPs with respect to ACC and ikaite for all experimental solutions (at 6, 12, 18 and 25 °C) solely containing the respected phase are -5.98, -6.16 ± 0.04 , -6.12 ± 0.07 and -6.17 ± 0.05 for ACC and -6.99, -6.73 and -6.58 for ikaite (Table 3.2). Evolution of SIs for ACC and ikaite verify observations made by *in-situ* Raman spectroscopy and show that after the dispersion of ACC, and independent of the prevailing temperature, solutions are initially (super)saturated in respect to all calcium carbonate polymorphs (Table 3.2) and dependent on the temperature, the SI_{ACC} stays between 4 and 14 min near saturation conditions until ikaite, respectively Mg-calcite formation, is observed. The occurrence of ikaite and Mg-calcite was monitored for at least 10 min without change, before the experiments were terminated. The last samples taken suggest solutions being saturated with ikaite ($\text{SI}_{\text{ikaite}} = 0.10 \pm 0.05$) at 6-18 °C and slightly supersaturated with respect to calcite ($\text{SI}_{\text{calcite}} = 0.38$) at 25 °C (Table 3.2). Note, although (slightly) supersaturated at 18 and 25°C, brucite $[\text{Mg}(\text{OH})_2]$ formation was neither observed in PXRD (Table 3.1) nor in FTIR on its characteristic $3\,700 \text{ cm}^{-1}$ OH-stretching band (Figure 3.2 and see also Chapter 2).

Table 3.2. Aqueous speciation and saturation states from sampled solutions calculated by using PHREEQC software together with the MINTEQv4 database adding the solubility products of ACC and ikaite from Brečević and Nielsen (1989) and Bischoff et al. (1993), respectively. *Note:* brucite is supersaturated at 18 and 25°C, respectively. However, no formation was observed in PXRD measurements (Table 3.1) or in FTIR spectra, e.g. on the characteristic 3 700 cm⁻¹ OH-stretching band (Figure 3.3 and see also Chapter 2).

samples	time (min)	$a_{Ca^{2+}}$	$a_{Mg^{2+}}$	$a_{CO_3^{2-}}$	log IAP	$\frac{a_{Mg^{2+}}}{a_{Ca^{2+}}}$	$\frac{a_{Ca^{2+}}}{a_{CO_3^{2-}}}$	SI _{ACC}	SI _{ikaite}	SI _{vaterite}	SI _{aragonite}	SI _{calcite}	SI _{brucite}
6 °C_1	0.3	2.40E-03	8.00E-03	4.31E-04	-5.98	3.3	5.6	0.21	1.06	1.88	2.17	2.40	-0.17
6 °C_2	4.0	2.06E-03	7.66E-03	2.82E-04	-6.23	3.7	7.3	-0.04	0.81	1.63	1.92	2.15	-0.24
6 °C_3	7.3	1.61E-03	7.44E-03	1.73E-04	-6.54	4.6	9.3	-0.36	0.49	1.31	1.60	1.83	-0.32
6 °C_4	24.3	1.08E-03	7.55E-03	9.14E-05	-6.99	7.0	11.8	-0.81	0.04	0.86	1.15	1.38	-0.39
12 °C_1	0.3	2.04E-03	7.46E-03	3.63E-04	-6.12	3.7	5.6	0.14	0.76	1.78	2.07	2.28	-0.20
12 °C_2	3.6	2.40E-03	7.69E-03	2.56E-04	-6.20	3.2	9.4	0.06	0.68	1.70	1.99	2.20	-0.18
12 °C_3	7.4	2.25E-03	7.54E-03	2.21E-04	-6.29	3.4	10.2	-0.03	0.59	1.60	1.90	2.11	-0.21
12 °C_4	18.7	1.35E-03	7.33E-03	1.34E-04	-6.73	5.4	10.0	-0.47	0.15	1.16	1.46	1.67	-0.31
18 °C_1	0.3	1.96E-03	7.28E-03	3.73E-04	-6.13	3.7	5.3	0.21	0.61	1.81	2.11	2.31	0.19
18 °C_2	2.5	2.40E-03	6.98E-03	3.66E-04	-6.05	2.9	6.6	0.29	0.69	1.89	2.19	2.39	0.17
18 °C_3	8.9	2.06E-03	7.09E-03	3.09E-04	-6.19	3.4	6.7	0.15	0.55	1.75	2.05	2.25	0.18
18 °C_4	13.7	2.04E-03	7.32E-03	2.71E-04	-6.25	3.6	7.5	0.09	0.49	1.69	1.99	2.19	0.20
18 °C_5	23.7	1.25E-03	7.14E-03	2.02E-04	-6.58	5.7	6.2	-0.25	0.15	1.35	1.65	1.85	0.16
25 °C_1	0.3	2.30E-03	7.82E-03	3.20E-04	-6.13	3.4	7.2	0.26	0.45	1.87	2.17	2.35	0.48
25 °C_2	2.0	2.34E-03	7.10E-03	2.82E-04	-6.17	3.0	8.3	0.21	0.40	1.83	2.12	2.30	0.36
25 °C_3	6.7	2.58E-03	7.61E-03	2.29E-04	-6.22	2.9	11.3	0.17	0.36	1.78	2.07	2.25	0.29
25 °C_4	11.6	2.75E-03	6.59E-03	1.94E-04	-6.26	2.4	14.2	0.12	0.31	1.73	2.03	2.21	-0.26
25 °C_5	32.9	4.02E-03	3.80E-03	1.98E-06	-8.10	0.9	2026.3	-1.71	-1.51	-0.09	0.20	0.38	-4.82

3.4 Discussion

3.4.1 Ikaite formation from an amorphous calcium carbonate precursor

Evidence from aqueous fluids sampled in natural environments precipitating ikaite (Bischoff, Stine, et al., 1993; Buchardt et al., 2001), reveal the natural solutions are often supersaturated with respect to ACC, suggesting the possibility of ikaite formation from an amorphous precursor. Nonetheless, the presence of ACC in environments of ikaite formation was never observed and laboratory experiments are scarce, mainly reporting direct precipitation of ikaite (Rodríguez-Ruiz et al., 2014; Hu et al., 2014; Sánchez-Pastor et al., 2016). On the other hand, these studies were neither conducted in aqueous media nor did they prioritize the finding of ACC (Rodríguez-Ruiz et al., 2014; Hu et al., 2014; Sánchez-Pastor et al., 2016). Therefore, the experimental setups were often not designed for short-time detection of such short-lived precursors should they have been present. Other studies reported about a white paste appearing gelatinous under the microscope before ikaite crystals did evolve or about a milky solution of amorphous CaCO₃ rapidly forming prior to the appearance of ikaite crystals, when mixing collected column water with seawater from the Ikka Fjord in the laboratory, indicating a possible precursor formation beforehand, but omitted to give details of the analyses

(Mackenzie, 1923; Buchardt et al., 2001). Interestingly, Buchardt et al. (2001) argue, despite their description about a milky solution of amorphous CaCO_3 , that ikaite forms directly from CaCO_3^0 aqueous complexes as their geochemical modelling implies high CaCO_3^0 concentrations compared to Ca^{2+} ions in solution, therefore rejecting a possible transient phase between aqueous complexes and ikaite.

To our knowledge, only one study so far reports about the detection of ACC together with ikaite in precipitates collected from suspensions by FTIR (Purgstaller, 2017). However, these authors did not observe the amorphous phase in solution, which is crucial, as Tlili et al. (2001) described the dehydration process of the calcium carbonate hexahydrate proceeding via the amorphous phase and Dieckmann et al. (2010) reported the decomposition of ikaite into ACC while stored in absolute ethanol. This suggests a possible dissolution of ikaite in its own crystal water, creating a supersaturated surface solution convenient for ACC formation, when exposed to air (Putnis, 2014). Thus, to determine unequivocally the possibility of ikaite precipitation via ACC, *in-situ* observations are necessary to allocate the origin of ACC being in solution and not being formed during decomposition of ikaite in air.

Our *in-situ* Raman results as well as FTIR show that, after the dispersion of ACC into the Mg-solutions, ACC is present for several minutes depending on prevailing temperatures before a progressive transformation into ikaite is occurring (Table 3.1 and Figure 3.1), clearly demonstrating that ikaite formation via an amorphous precursor is a viable pathway. Furthermore, the presented mixing experiment of a highly concentrated CaCl_2 solution into a Na_2CO_3 solution at 6 °C in the absence of magnesium reveals that, after mixing, the first precipitate is the amorphous phase prior to the formation of ikaite (Figure 3.4). However, the presence of ikaite is limited to a maximum of 30 s. This illustrates the important role of magnesium for prolonging metastabilities of ACC (e.g. Rodriguez-Blanco et al., 2012; Purgstaller et al., 2016) and explains why in this study the occurrence of ACC is prolonged in Mg containing solutions compared to the Mg-free mixing experiment. We, therefore, doubt that any experimental approach from studies mentioned above would have had the analytical time resolution of detecting such a short-lived phase, considering that, even with *in-situ* analytics applied herein, ACC was barely observable in the Mg-free system when starting from solutions rather than from dispersing ACC.

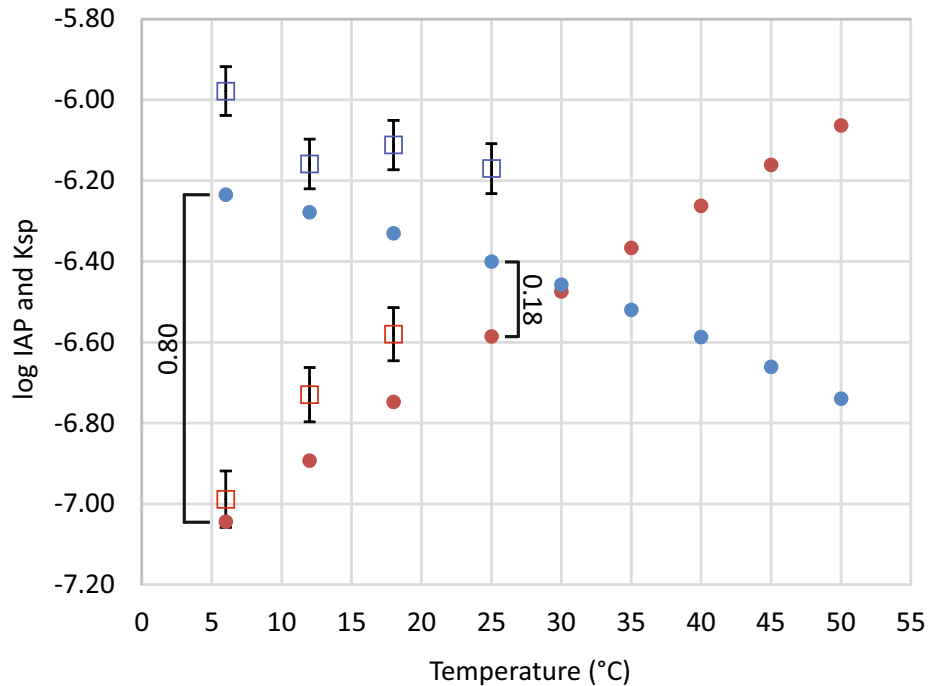


Figure 3.5. IAPs for ikaite and ACC from this study compared to the well-established solubility products from literature (Ksp). Notable is the shrinking difference between phase solubilities towards 30 °C, caused by the reverse temperature behaviour of ikaite getting more soluble at higher temperatures in contrast to ACC. • K_{ikaite} (Bischoff et al., 1993), • K_{ACC} (Brečević and Nielsen, 1989), □ IAP_{ACC} (this study), □ IAP_{ikaite} (this study).

3.4.2 Metastability and transformation of ACC at different temperatures

The mineral phase identification in solution through the *in-situ* technique together with solution sampling permits the unequivocal calculation of solubilities of metastable phases, like ACC and ikaite, which otherwise is often difficult to assign, considering the uncertainty of phase occurrences as well as phase transformations in aqueous fluids. The solubilities for ikaite and ACC thereby obtained are slightly higher compared to published data (Figure 3.5) (Brečević and Nielsen, 1989; Bischoff, Fitzpatrick, et al., 1993). A crucial difference, compared to these studies, is the solution chemistry, which is rich in Mg. As is well known, the solubility of e.g. calcites is increasing with the incorporation of Mg ions into the lattice (Bischoff et al., 1987; Busenberg and Plummer, 1989; Davis et al., 2000). This might be a reasonable explanation for the log IAPs obtained in this study as well, where the respected phases incorporated between 1-2 mol% of Mg (Table 3.1 and 3.2). Since ikaite found in nature is originating from a Mg-rich solution, and incorporates similar Mg amounts as observed in this study (Buchardt et al., 2001), we believe that the solubilities presented are applicable to natural surroundings.

Regarding the solubility of ACC, comparisons with naturally formed ACC are more difficult, as in addition to Mg, other foreign ions as well as organic ligands are incorporated into the

structure (Addadi et al., 2003; Gal et al., 2010; Habraken et al., 2015). However, the fact that the initially Mg-free ACC in this study contains Mg after dispersion into a Mg-rich solution clearly demonstrates that ACC dissolved and re-precipitated again as amorphous phase incorporating the Mg from the solution, thereby supporting dissolution and re-precipitation as the governing process. Comparing the solubility products of ikaite and ACC, the former phase shows a significant change with respect to the prevailing temperature. Such a dependency for ACC is not apparent from the data obtained (Figure 3.5). In contrast to the suggested temperature trend by Brečević and Nielsen (1989), the log IAPs of ACC obtained from the experiments in this study are rather fluctuating than following a temperature trend (Figure 3.5). This could stem from the slight differences in Mg incorporated in ACC (1.3-2.2 mol%) compared to ikaite, which is always the same (± 0.04 mol%) (Table 3.1), although no direct correlation with the amount of Mg is obvious. However, it could also suggest that over time the amorphous phase undergoes a structural rearrangement and becomes more ordered (Radha et al., 2010). This could be inferred by the temporal decrease of log IAPs prior to ACC's transformation (Table 3.2) and independent of prevailing temperatures or Mg in the lattice. Applying the solubility products for ACC and ikaite from literature (Brečević and Nielsen, 1989; Bischoff, Fitzpatrick, et al., 1993) shows that after the dispersion of ACC into the Mg-solutions, the latter become saturated with respect to the amorphous precursor until phase transformation, having an initial SI_{ACC} of 0.21 ± 0.06 non-correlated with the prevailing temperatures (Table 3.2). However, the presence of solely ACC in solution, as inferred by the saturation (Table 3.2) and as observed from *in-situ* Raman spectra (Table 3.1), was extended at elevated temperatures of the experiments ranging from 2 min at 6 °C up to 12 min at 25 °C (Figure 3.6). The supersaturations calculated for the anhydrous calcium carbonates show the same behaviour as ACC with no apparent differences with respect to the prevailing temperature (± 0.05) (Table 3.2). On the other hand, saturation indices of ikaite reveal marked differences ranging from SIs of 1.06 at 6 °C to 0.45 at 25 °C. As discussed, ikaite shows a reverse behaviour with respect to the solubility of calcium carbonates – getting more soluble with higher temperatures (Figure 3.5) – and undergoes a stronger impact of temperature on its solubility. Therefore, the timespan of ACC occurrence in solution is likely to be governed by the formation kinetics of ikaite, precipitating faster at lower temperatures driven by higher supersaturation. The prolonged metastability of ACC at 25 °C, where transformation occurred into calcite and to a minor extent into vaterite instead of ikaite, can then be reasonably explained by the inhibiting effect of magnesium in solution on the formation kinetics of the respective minerals (e.g. Rodriguez-Blanco et al., 2012).

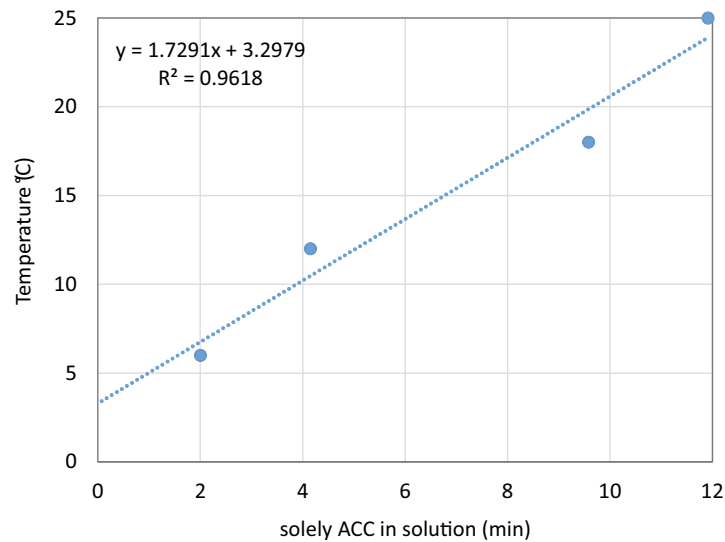


Figure 3.6. The sole occurrence of ACC in solution, respectively the time of incipient transformation, regardless of the crystallizing phase, shows a positive correlation with the prevailing experimental temperature and ranged up to 2 min at 6 °C and 12 min at 25 °C.

3.4.3 Formation of ikaite up to 18 °C and its transformation in air

The observation that ikaite is being formed from an amorphous precursor up to temperatures as high as 18 °C is an unexpected finding, considering that in the present study ikaite was formed from aqueous solutions at initial supersaturations and magnesium concentrations (in solution and in ikaite itself), which are comparable to natural environments (Bischoff, Stine, et al., 1993; Buchardt et al., 2001). The difference in solubility of ACC and ikaite is about 0.8 log units at 6 °C with ikaite being less soluble. This difference shrinks with increasing temperature to 0.18 log units at 25 °C (Figure 3.5). It is concluded that as a function of temperature the converging solubilities of these two calcium carbonate hydrates determine the limitations of ikaite formation. Hence, at higher temperatures (> 18 °C) ACC and ikaite are too close in solubility, such that the reaction kinetics skip the hexahydrate to precipitate directly calcite and vaterite, the formation dynamics of the latter being predominantly controlled by the prevailing aMg/aCa ratio of the solution (Blue et al., 2017; Purgstaller et al., 2017). The sampled ikaite from solution transformed under air exposure into predominantly calcite and to a minor extent into vaterite. Pseudomorphic replacements after ikaite, e.g. glendonitic calcites, as are commonly found in nature, were not observed in SEM images (Figure 3.3b). We attribute this to the transformation conditions being under air exposure and not in solution, where ikaite disintegrates in its own crystal water (Shearman and Smith, 1985; Bischoff, Stine, et al., 1993). Although Sánchez-Pastor et al. (2016), obtained glendonitic

calcites after the transformation of ikaite in air, the crystal sizes, grown by silica gel technique, were up to 100-1 000 times larger compared to the crystals obtained in the present study. This indicates that the increased surface area enhanced reaction kinetics as was observed by (Purgstaller, 2017). The same studies analysed the mineralogy after transformation of ikaite in air and report a correlation between the abundance of vaterite with increasing ΔT , the latter being defined as the difference between synthesis temperature of ikaite and temperature of the subsequent atmospheric drying. In our experiments no such correlation is observed, as only ikaite formed at 12 °C shows vaterite after transformation under air exposure (Table 3.1). However, ikaite synthesis temperatures and experimental conditions were significantly different in the referred studies. Sánchez-Pastor et al. (2016), precipitated large crystals in silica gel at 3 °C with controlled transformation conditions being held at 10 and 20 °C, while Purgstaller (2017), precipitated comparably small crystals at 6 and 12 °C with transformation at 25 °C. Considering that phase transformation processes are severely influenced by surface reactions, and, therefore, by the size of the particles, more experiments are necessary to verify such a correlation. This is particularly so, as both studies had different amounts of magnesium in their solution being partly incorporated into ikaite, which possibly alters the transformation behaviour as it has a higher dehydration energy known to affect stability and crystallization of Mg-ACC (Loste et al., 2003; Radha et al., 2012; Rodriguez-Blanco et al., 2012). Furthermore, ikaite's pronounced thermal expansion behaviour suggests differences in the crystal lattice with respect to the formation temperature, possibly influencing the transformation as well (Lennie et al., 2004).

3.5 Conclusions

The transformation of ACC into ikaite was monitored by *in-situ* Raman and complementarily by FTIR in aqueous solution from 6 to 18 °C. These results unequivocally reveal the possibility of ikaite being formed via an amorphous precursor. The observed prolongation of ACC's metastability in solution from 2 min at 6 to 12 min at 25 °C can be reasonably explained (i) by the slower formation kinetics of ikaite at higher temperatures caused by lower supersaturation, SI_{ikaite} being 1.01 at 6 °C and 0.45 at 25 °C and (ii) by the retarding effect of magnesium ions in solution on the precipitation of calcite. Due to the pronounced impact of temperature on the solubility of ikaite, its occurrence is limited to approximately 18 °C, as at higher temperatures the solubility products of ACC and ikaite are approaching a ΔK_{sp} of 0.18 at 25 °C. Therefore, the formation of ikaite at 25 °C could be skipped to precipitate directly one of the anhydrous calcium carbonates. Finally, the unexpected finding of ikaite being

formed up to a temperature as high as 18 °C at conditions applicable to natural environments in terms of magnesium concentration and initial supersaturation, questions the proposed use of ikaite as a reliable cold temperature indicator.

3.6 References

- Addadi L., Raz S. and Weiner S. (2003) Taking Advantage of Disorder: Amorphous Calcium Carbonate and Its Roles in Biomineralization. *Adv. Mater.* **15**, 959–970.
- Andersen F. and Brecevic L. (1991) Infrared spectra of amorphous and crystalline calcium carbonate. *Acta Chem. Scand* **45**, 1018–1024.
- Bischoff J. L., Fitzpatrick J. A. and Rosenbauer R. J. (1993) The solubility and stabilization of ikaite ($\text{CaCO}_3 \times 6\text{H}_2\text{O}$) from 0 - 25°C - environmental and paleoclimatic implications for thinolite tufa. *J. Geol.* **101**, 21–33.
- Bischoff J. L., Stine S., Rosenbauer R. J., Fitzpatrick J. A. and Stafford T. W. (1993) Ikaite precipitation by mixing of shoreline springs and lake water, Mono Lake, California, USA. *Geochim. Cosmochim. Acta* **57**, 3855–3865.
- Bischoff W. D., Mackenzie F. T. and Bishop F. C. (1987) Stabilities of synthetic magnesian calcites in aqueous solution: Comparison with biogenic materials. *Geochim. Cosmochim. Acta* **51**, 1413–1423.
- Blue C. R., Giuffre A., Mergelsberg S., Han N., De Yoreo J. J. and Dove P. M. (2017) Chemical and physical controls on the transformation of amorphous calcium carbonate into crystalline CaCO_3 polymorphs. *Geochim. Cosmochim. Acta* **196**, 179–196.
- Boch R., Dietzel M., Reichl P., Leis A., Baldermann A., Mittermayr F. and Pölt P. (2015) Rapid ikaite ($\text{CaCO}_3 \cdot 6\text{H}_2\text{O}$) crystallization in a man-made river bed: Hydrogeochemical monitoring of a rarely documented mineral formation. *Appl. Geochemistry* **63**, 366–379.
- Brečević L. and Nielsen A. E. (1989) Solubility of amorphous calcium carbonate. *J. Cryst. Growth* **98**, 504–510.
- Brooks R., Clark L. M. and Thurston E. F. (1950) Calcium Carbonate and Its Hydrates. *Philos. Trans. R. Soc. London. Ser. A, Math. Phys. Sci.* **243**, 145–167.
- Buchardt B., Israelson C., Seaman P. and Stockmann G. (2001) Ikaite Tufa Towers in Ikka Fjord, Southwest Greenland: Their Formation by Mixing of Seawater and Alkaline Spring Water. *J. Sediment. Res.* **71**, 176–189.
- Buchardt B., Seaman P., Stockmann G., Vous M., Wilken U., Düwel L., Kristiansen A., Jenner C., Whiticar M. J., Kristensen R. M., Petersen G. H. and Thorbjørn L. (1997) Submarine columns of ikaite tufa. *Nature* **390**, 129–130.

- Busenberg E. and Plummer L. N. (1989) Thermodynamics of magnesian calcite solid-solutions at 25°C and 1 atm total pressure. *Geochim. Cosmochim. Acta* **53**, 1189–1208.
- Coleyshaw E. E., Crump G. and Griffith W. P. (2003) Vibrational spectra of the hydrated carbonate minerals ikaite, monohydrocalcite, lansfordite and nesquehonite. *Spectrochim. Acta Part A Mol. Biomol. Spectrosc.* **59**, 2231–2239.
- Council T. C. and Bennett P. C. (1993) Geochemistry of ikaite formation at Mono Lake , California : Implications for the origin of tufa mounds. *Geology*, 971–974.
- Dana J. D. (1849) *United States Exploring Expedition. During the years 1838, 1839, 1840, 1841, 1842. Under the command of Charles Wilkes, U.S.N., v. X, Geology.*, Sherman, C, Philadelphia.
- Davis K. J., Dove P. M. and De Yoreo J. J. (2000) The Role of Mg²⁺ as an Impurity in Calcite Growth. *Science* **290**, 1134–1137.
- Dickens B. and Brown W. E. (1970) Crystal structure of calcium carbonate hexahydrate at about -120.deg. *Inorg. Chem.* **9**, 480–486.
- Dieckmann G. S., Nehrke G., Papadimitriou S., Göttlicher J., Steininger R., Kennedy H., Wolf-Gladrow D. and Thomas D. N. (2008) Calcium carbonate as ikaite crystals in Antarctic sea ice. *Geophys. Res. Lett.* **35**, L08501.
- Dieckmann G. S., Nehrke G., Uhlig C., Göttlicher J., Gerland S., Granskog M. A. and Thomas D. N. (2010) Brief Communication: Ikaite (CaCO₃·6H₂O) discovered in Arctic sea ice. *Cryosphere* **4**, 227–230.
- Field L. P., Milodowski A. E., Shaw R. P., Stevens L. A., Hall M. R., Kilpatrick A., Gunn J., Kemp S. J. and Ellis M. A. (2017) Unusual morphologies and the occurrence of pseudomorphs after ikaite (CaCO₃·6H₂O) in fast growing, hyperalkaline speleothems. *Mineral. Mag.* **81**, 565–589.
- Gabrielli C., Jaouhari R., Joiret S. and Maurin G. (2000) In situ Raman spectroscopy applied to electrochemical scaling. Determination of the structure of vaterite. *J. Raman Spectrosc.* **31**, 497–501.
- Gal A., Weiner S. and Addadi L. (2010) The stabilizing effect of silicate on biogenic and synthetic amorphous calcium carbonate. *J. Am. Chem. Soc.* **132**, 13208–11.
- Geilfus N. X., Galley R. J., Else B. G. T., Campbell K., Papakyriakou T., Crabeck O., Lemes M., Delille B. and Rysgaard S. (2016) Estimates of ikaite export from sea ice to the underlying seawater in a sea ice-seawater mesocosm. *Cryosphere* **10**, 2173–2189.
- Geisler T., Perdikouri C., Kasiopas A. and Dietzel M. (2012) Real-time monitoring of the overall exchange of oxygen isotopes between aqueous and H₂O by Raman spectroscopy.

- Geochim. Cosmochim. Acta* **90**, 1–11.
- Habraken W. J. E. M., Masic A., Bertinetti L., Al-Sawalmih A., Glazer L., Bentov S., Fratzl P., Sagi A., Aichmayer B. and Berman A. (2015) Layered growth of crayfish gastrolith: About the stability of amorphous calcium carbonate and role of additives. *J. Struct. Biol.* **189**, 28–36.
- Hu Y.-B., Wolf-Gladrow D. a., Dieckmann G. S., Völker C. and Nehrke G. (2014) A laboratory study of ikaite ($\text{CaCO}_3 \cdot 6\text{H}_2\text{O}$) precipitation as a function of pH, salinity, temperature and phosphate concentration. *Mar. Chem.* **162**, 10–18.
- Huggett J. M., Schultz B. P., Shearman D. J. and Smith A. J. (2005) The petrology of ikaite pseudomorphs and their diagenesis. *Proc. Geol. Assoc.* **116**, 207–220.
- Ito T. (1996) Ikaite from cold spring water at Shiowakka, Hokkaido, Japan. *J. Mineral. Petrol. Econ. Geol.* **91**, 209–219.
- Konrad F., Gallien F., Gerard D. E. and Dietzel M. (2016) Transformation of Amorphous Calcium Carbonate in Air. *Cryst. Growth Des.* **16**, 6310–6317.
- Larsen D. (1994) Origin and paleoenvironmental significance of calcite pseudomorphs after ikaite in the Oligocene Creede Formation, Colorado. *J. Sediment. Res.* **64**, 593–603.
- Last F. M., Last W. M., Fayek M. and Halden N. M. (2013) Occurrence and significance of a cold-water carbonate pseudomorph in microbialites from a saline lake. *J. Paleolimnol.* **50**, 505–517.
- Lennie A. R., Tang C. C. and Thompson S. P. (2004) The structure and thermal expansion behaviour of ikaite, $\text{CaCO}_3 \cdot 6\text{H}_2\text{O}$, from $T = 114$ to $T = 293$ K. *Mineral. Mag.* **68**, 135–146.
- Loste E., Wilson R. M., Seshadri R. and Meldrum F. C. (2003) The role of magnesium in stabilising amorphous calcium carbonate and controlling calcite morphologies. *J. Cryst. Growth* **254**, 206–218.
- Lu Z., Rickaby R. E. M., Kennedy H., Kennedy P., Pancost R. D., Shaw S., Lennie A., Wellner J. and Anderson J. B. (2012) An ikaite record of late Holocene climate at the Antarctic Peninsula. *Earth Planet. Sci. Lett.* **325–326**, 108–115.
- Mackenzie J. E. (1923) CCLXXIV.-Calcium Carbonate Hexahydrate. *J. chem. Soc.* **123**, 2409.
- Marland G. (1975) The stability of $\text{CaCO}_3 \cdot 6\text{H}_2\text{O}$ (ikaite). *Geochim. Cosmochim. Acta* **39**, 83–91.
- Oehlerich M., Mayr C., Griesshaber E., Lücke A., Oeckler O. M., Ohlendorf C., Schmahl W. W. and Zolitschka B. (2013) Ikaite precipitation in a lacustrine environment -

- implications for palaeoclimatic studies using carbonates from Laguna Potrok Aike (Patagonia, Argentina). *Quat. Sci. Rev.* **71**, 46–53.
- Parkhurst D. L. and Appelo C. A. J. (2013) Description of input and examples for PHREEQC version 3--A computer program for speciation, batch- reaction, one-dimensional transport, and inverse geochemical calculations: U.S. Geological Survey Techniques and Methods, book 6, chap. A43, 497 p.
- Pauly H. (1963) “Ikaite”, a New Mineral from Greenland. *Arctic* **16**, 263–264.
- Purgstaller B. (2017) The Role of Amorphous Precursors on the Formation of Calcium Carbonate Minerals. PhD Thesis, Graz University of Technology, Austria.
- Purgstaller B., Konrad F., Dietzel M., Immenhauser A. and Mavromatis V. (2017) Control of Mg^{2+}/Ca^{2+} Activity Ratio on the Formation of Crystalline Carbonate Minerals via an Amorphous Precursor. *Cryst. Growth Des.* **17**, 1069–1078.
- Purgstaller B., Mavromatis V., Immenhauser A. and Dietzel M. (2016) Transformation of Mg-bearing amorphous calcium carbonate to Mg-calcite – In situ monitoring. *Geochim. Cosmochim. Acta* **174**, 180–195.
- Putnis A. (2014) Why Mineral Interfaces Matter. *Science* **343**, 1441–1442.
- Radha A. V., Fernandez-Martinez A., Hu Y., Jun Y., Waychunas G. A. and Navrotsky A. (2012) Energetic and structural studies of amorphous $Ca_{1-x}Mg_xCO_3 \cdot nH_2O$ ($0 \leq x \leq 1$). *Geochim. Cosmochim. Acta* **90**, 83–95.
- Radha A. V, Forbes T. Z., Killian C. E., Gilbert P. U. P. A. and Navrotsky A. (2010) Transformation and crystallization energetics of synthetic and biogenic amorphous calcium carbonate. *Proc. Natl. Acad. Sci. U. S. A.* **107**, 16438–43.
- Rodriguez-Blanco J. D., Shaw S., Bots P., Roncal-Herrero T. and Benning L. G. (2012) The role of pH and Mg on the stability and crystallization of amorphous calcium carbonate. *J. Alloys Compd.* **536**, S477–S479.
- Rodríguez-Ruiz I., Veessler S., Gómez-Morales J., Delgado-López J. M., Grauby O., Hammadi Z., Candoni N. and García-Ruiz J. M. (2014) Transient Calcium Carbonate Hexahydrate (Ikaite) Nucleated and Stabilized in Confined Nano- and Picovolumes. *Cryst. Growth Des.* **14**, 792–802.
- Rysgaard S., Søgaard D. H., Cooper M., Pu&ccute;ko M., Lennert K., Papakyriakou T. N., Wang F., Geilfus N. X., Glud R. N., Ehn J., McGinnis D. F., Attard K., Sievers J., Deming J. W. and Barber D. (2013) Ikaite crystal distribution in winter sea ice and implications for CO₂ system dynamics. *Cryosph.* **7**, 707–718.
- Sánchez-Pastor N., Oehlerich M., Astilleros J. M., Kaliwoda M., Mayr C. C., Fernández-Díaz

- L. and Schmahl W. W. (2016) Crystallization of ikaite and its pseudomorphic transformation into calcite: Raman spectroscopy evidence. *Geochim. Cosmochim. Acta* **175**, 271–281.
- Selleck B. W., Carr P. F. and Jones B. G. (2007) A Review and Synthesis of Glendonites (Pseudomorphs after Ikaite) with New Data: Assessing Applicability as Recorders of Ancient Coldwater Conditions. *J. Sediment. Res.* **77**, 980–991.
- Shearman D. J. and Smith A. J. (1985) Ikaite, the parent mineral of jarrowite-type pseudomorphs. *Proc. Geol. Assoc.* **96**, 305–314.
- Slack J. G. (1980) Calcium carbonate hexahydrate: Its properties and formation in lime-soda softening. *Water Res.* **14**, 799–804.
- Spielhagen R. F. and Tripathi A. (2009) Evidence from Svalbard for near-freezing temperatures and climate oscillations in the Arctic during the Paleocene and Eocene. *Palaeogeogr. Palaeoclimatol. Palaeoecol.* **278**, 48–56.
- Suess E., Balzer W., Hesse K.-F., Muller P. J., Ungerer C. A. and Wefer G. (1982) Calcium Carbonate Hexahydrate from Organic-Rich Sediments of the Antarctic Shelf: Precursors of Glendonites. *Science* **216**, 1128–1131.
- Swainson I. P. and Hammond R. P. (2001) Ikaite, $\text{CaCO}_3 \cdot 6\text{H}_2\text{O}$: Cold comfort for glendonites as paleothermometers. *Am. Mineral.* **86**, 1530–1533.
- Tlili M. M., Amor M. Ben, Gabrielli C., Joiret S., Maurin G. and Rousseau P. (2001) Characterization of CaCO_3 hydrates by micro-Raman spectroscopy. *J. Raman Spectrosc.* **33**, 10–16.
- Wang D., Hamm L. M., Bodnar R. J. and Dove P. M. (2012) Raman spectroscopic characterization of the magnesium content in amorphous calcium carbonates. *J. Raman Spectrosc.* **43**, 543–548.

Chapter 4

Crystallization pathways and cation exchange during transformation of ACC in Me^{2+} -solutions

ABSTRACT: From the manifold studies existing about amorphous calcium carbonate (ACC), investigations on the transformation behaviour of ACC in differing metal-solutions apart from magnesium are rare. Nonetheless, such investigations are vital in terms of possible cation exchange reactions during transformation, eventually altering transformation pathways. Here, we present a study, where ACC was exposed to 0.1 M (heavy) Me^{2+} -rich solutions. The synthesis of additive-free ACC was thereby decoupled from the aging in the Me^{2+} -containing solutions, allowing to specifically study the influence of solution chemistry on the transformation. The results show that ACC transforms into orthorhombic aragonite [CaCO_3], solid-solutions of calcio-strontianite [$\text{Sr}_{(1-x)}\text{Ca}_x\text{CO}_3$] and calcio-witherite [$\text{Ba}_{(1-x)}\text{Ca}_x\text{CO}_3$] in the presence of Mg, Sr, and Ba. In accordance, rhombohedral otavite [CdCO_3], rhodochrosite [MnCO_3], and monoclinic hydrozincite [$\text{Zn}_5(\text{CO}_3)_2(\text{OH})_6$] were obtained as final products in the presence of Cd, Mn, and Zn in solution. In contrast, ACC exposed to a Ni-solution results in amorphous nickel carbonate. The exchange rate of (heavy) Me^{2+} -ions from solution into the solid throughout ACC transformation was generally high, e.g. 30 mol% for Mn and nearly 100 mol% for Zn, where accordingly in the latter case Ca from ACC was almost completely released into the reactive solution. Contrarily, the exchange of ACC with Mg was strongly limited. The present study demonstrates that - besides potential temperature or ACC pre-structuring effects - the reactive solution chemistry is strongly influencing the transformation pathway of ACC and is controlling the chemical compositions of the reaction products. This has to be considered if the formation of ACC and its subsequent transformation occurs in the same fluid and thus, may explain occurring discrepancies of obtained ACC reaction products in the literature. Implications of the observed Me^{2+} exchange behaviour and final mineral formation throughout ACC transformation are discussed in the scope of reconstruction of environmental precipitation conditions in the past, tailored mineral synthesis routes, and trapping of heavy metals within aqueous media.

4.1 Introduction

The incorporation of metal (Me)-ions in crystalline calcium carbonates is known to depend on the physicochemical parameters, like temperature, pH or precipitation rate (Lea, 2013). Prominent examples are the incorporation of Sr into coralline aragonite as a function of temperature (Beck et al., 1992) or the incorporation of Mg in calcite as a function of growth rate and pH (Immenhauser et al., 2010; Mavromatis et al., 2013). For amorphous carbonate precursors, information on incorporation behaviour of Me-ions are limited to studies on the uptake of Mg, Sr or Ba during nucleation from Ca/Mg- (Loste et al., 2003; Blue and Dove, 2015; Rodriguez-Blanco et al., 2015; Purgstaller et al., 2016) or Ca/Sr (and Ba)-rich solutions (Matsunuma et al., 2014; Cam et al., 2015; Littlewood et al., 2017). However, insights into the elemental exchange between Ca of ACC with dissolved Me^{2+} -ions in solution during the transformation of the amorphous phase and its impact on the reaction product are missing. Experimental approaches are highly required to reveal novel carbonate formation pathways and to understand reaction mechanisms behind carbonate mineral formation via an amorphous precursor and the thereof resulting implications for natural and technical environments, e.g. to reconstruct formation conditions, to synthesise distinct carbonate minerals or to trap/release dissolved Me^{2+} -ions.

In general, the effect of the chemical composition of the reactive solution on the transformation behaviour of ACC into distinct crystalline products is not yet fully understood. Metastability of ACC and the crystalline reaction products are often suggested to be governed by the primary incorporation of foreign cations and organic ligands (Raz et al., 2000; Addadi et al., 2003; Habraken et al., 2015). However, increasing evidences arise that the solution chemistry is a major parameter in determining the transformation pathway and metastability of amorphous carbonate phases (Blue et al., 2017; Purgstaller et al., 2017). The difficulty unveiling the individual influences of solid and solution composition results from the highly variable environmental settings and chemical compositions of natural biogenic ACC (Addadi et al., 2003) as well as from the high metastability of ACC and the therefrom devised experimental approaches using additives in the synthesis process (e.g. Blue et al., 2017 and therein). Additive-free ACC is usually transforming in solution within minutes after its formation (Ogino et al., 1987; Shen et al., 2006). Hence, for retarding the ACC transformation process, it is mostly synthesized in the presence of Mg and left in the same solution of synthesis until complete transformation (Blue and Dove, 2015; Rodriguez-Blanco et al., 2015; Purgstaller et al., 2016). However, as Mg gets incorporated into ACC during synthesis and is present in solution, any clear assertions as to the individual contributions in the transformation

process are problematic. Studies on crystallization behaviour of ACC by re-introducing the amorphous powder into a solution are rare, as are studies on cation exchange of ACC interacting with different Me-solutions (Zhang et al., 2012).

Here, we separated the formation of ACC and the transformation of the latter in a Me^{2+} -containing solution. By re-introducing additive-free ACC into one of a Mg-, Sr-, Ba-, Cd-, Mn-, Ni- and a Zn-rich solution and for reference into *pure* water, it was investigated whether ACC (i) changes its transformation pathways in dependence of the individual solution chemistry and (ii) whether Ca is expelled from ACC in favour of another element during/after the transformation.

4.2 Experimental

4.2.1 Synthesis of ACC and experimental setup

As reported more comprehensively in an earlier study (Konrad et al., 2016), ACC was obtained by mixing 0.250 M solutions containing calcium chloride dihydrate and sodium carbonate (ACS, from Roth). After vacuum-filtration and washing of the filter cake, the precipitated ACC was placed into a Virtis Benchtop 3 dm³ freeze dryer (-58 °C condenser temperature and 10 mbar partial vacuum), sublimating the non-structurally bound H₂O. Until usage, the obtained additive and physisorbed water-free material was stored under gastight conditions to inhibit crystallization. Powder X-ray diffraction (PXRD) did not reveal any distinct peaks and from secondary electron microscopy (SEM) images, it is suggested the synthesized powder consists of individual spherules with an estimated mean particle size of about 90 nm (Figure S4.1) (Konrad et al., 2016). In a subsequent step, fractions of 0.138 g of the amorphous powder were re-suspended into vials containing 0.025 dm³ of various Me^{2+} -chloride solutions, as well as *pure* water as a comparison. The 0.1 M Me^{2+} -stock solutions were prepared by using Milli-Q water (18.2 MΩcm) and the following analytical grade chlorides: magnesium chloride hexahydrate, barium chloride dihydrate, nickel chloride hexahydrate, manganese chloride tetrahydrate, and anhydrous zinc chloride from Roth, strontium chloride hexahydrate from Emsure and cadmium chloride monohydrate from Riedel-de Haën. In total, 24 vials containing the experimental solutions and dispersed ACC were prepared and placed on a KS15 compact shaker (Edmund Buehler) for reaction times of 1 d, 8 d and 22 d (d = day(s)). At the end of the experimental time, the reactive solutions were vacuum-filtered through a membrane cellulose acetate filter (0.2 μm pore size) and the filtrate solution, as well as separated solids, prepared for analyses.

4.2.2 Analytics

The pH of the reactive solutions was measured with a SenTix 940 gel electrode from WTW, calibrated against NIST standard buffers at pH 4.01, 7.00 and 10.00. Measurements of total alkalinity were performed with a Schott TitroLine alpha plus titrator using a 1×10^{-3} M HCl solution. Subsamples of separated solids and solutions were digested in 6% HNO₃ for analyses of ion concentrations with inductively coupled plasma optical emission spectroscopy (ICP-OES) on a Perkin Elmer Optima 8300 DV with an analytical error for Ca and Mg of $\pm 3\%$ (2σ) and for Sr, Ba, Cd, Mn, Ni and Zn of $\pm 5\%$ (2σ).

Solid phase characterisation of the separated solids were conducted by Fourier transform infrared spectroscopy (FTIR) in attenuated total reflection (ATR) mode from 650-4 000 cm⁻¹ at a resolution of 4 cm⁻¹, and by powder X-ray diffraction (PXRD) performed on a PANalytical X'Pert Pro diffractometer, equipped with a Co target and a solid-state real time multiple strip (RTMS) detector (measurement parameters: 40 kV, 40 mA, 0.008° step, 40 s/step ranging 4-80° in 2θ). Subsequent identification, and quantification, of the resulted mineral phases was accomplished by using the inorganic crystal structure database (ICSD) and by Rietveld analysis using the fundamental parameter approach, respectively (Rietveld, 1969; Cheary et al., 2004). Phase identification for FTIR was accomplished by band assignments of literature data (Table 4.1). Images of the reaction products were obtained by using a ZEISS DSM 982 Gemini scanning electron microscope (SEM) equipped with a field emission gun operated at 5 kV.

Table 4.1. Chemical formulas and solubility data from literature as well as FTIR-bands of the synthesized ACC and resulting carbonate phases via ACC transformation, including references used for phase identification in FTIR (± 2 cm⁻¹). *Note:* the ν_4 -band of barytocalcite from literature is reported at 725 cm⁻¹ compared to 717 cm⁻¹ obtained in this study, indicating, in accordance with PXRD results, a non-stoichiometric phase with a Ba/Ca ratio > 1; solubility products are reported for end-member carbonates.

mineral	chemical formula	solubility products (log Ksp) at 25°C	assigned FTIR-bands (cm ⁻¹)				references
			CO ₃ ν_4	CO ₃ ν_2	H ₂ O ν_1, ν_3	OH-bending	
calcite	CaCO ₃	-8.48 Plummer and Busenberg (1982)	712	870-873	-	-	Meiron et al. (2011); Andersen and Brečević (1991)
aragonite	CaCO ₃	-8.30 Plummer and Busenberg (1982)	700, 713	853	-	-	Andersen and Brečević (1991)
calcio-strontianite	Sr _x Ca _(1-x) CO ₃	-9.27 Busenberg et al. (1984)	700, 707	854	-	-	Alía et al. (1997)
calcio-witherite	Ba _x Ca _(1-x) CO ₃	-8.57 Busenberg and Plummer (1986)	693	854	-	-	Pasierb et al. (2001)
otavite	CdCO ₃	-12.10 Stipp et al. (1993)	721	858	-	-	Bucca et al. (2009)
rhodochrosite	MnCO ₃	-10.58 Johnson (1982)	725	862	-	-	Böttcher et al. (1992)
zarattite	Ni ₃ CO ₃ (OH) ₄ •4H ₂ O	- no data available	-	833	2 600-3 700	-	García-Guinea et al. (2013)
(nickel hydroxycarbonate)							Minkova et al. (1984)
hydrozincite	Zn ₅ (CO ₃) ₂ (OH) ₆	-8.70 Preis and Gamsjäger (2001)	708, 737	833	3 292	950, 1 046	Frost and Hales (2007)
barytocalcite (shifted)	BaCa(CO ₃) ₂	-8.54 Garrels et al. (1960)	717	871	-	-	Frost and Dickfos (2008); Scheetz and White (1977)
monohydrocalcite	CaCO ₃ •H ₂ O	-7.05 Kralj and Brečević (1995)	700, 727	873	3 235	-	Neumann and Epple (2007)
ACC	CaCO ₃ •0.42H ₂ O	-6.39 Brečević and Nielsen (1989)	695, 725	859	2 600-3 700	-	Konrad et al. (2016)

4.3 Results and Discussion

4.3.1 Formation of alkaline earth metal carbonate minerals from ACC

In our control experiment, additive-free ACC reacting with MilliQ-water (MQ) for 1 d transformed into calcite (CaCO_3), as can be observed in PXRD- and FTIR-measurements (Figure 4.1 and Table 4.2) as well as SEM images showing euhedral calcite rhombohedra of 3-5 μm in size (Figure 4.2). Vaterite, a common intermediate phase throughout the ACC transformation pathway to calcite, was not detected. This suggests that the reaction time of 1 d was sufficient for complete transformation of ACC into calcite. This is in accordance with the experiments of Bots et al. (2012) who reported that complete transformation of ACC into calcite via intermediate vaterite takes up to 9 h.

Table 4.2. Reaction time of sampling, pH, alkalinity, chemical composition of fluid and solid as well as results from mineralogical analyses of ACC transformation experiments. cc: calcite, ara: aragonite, mhc: monohydrocalcite, ca-str: calcio-strontianite, ca-wit: calcio-witherite, ba-cc: barytoalcite, ot: otavite, ANC: amorphous nickel carbonate, rhod: rhodochrosite, hyzi: hydrozincite, smi: smithsonite.

samples	time (days)	pH	alkalinity mmol dm^{-3}	fluid mmol dm^{-3}		solid mol%		FTIR	PXRD
				Ca	Me^{2+}	Ca	Me^{2+}		
MQ-stock		7.60							
MQ-1d	1	10.27	2.0	0.0	-	100.0	-	cc	cc: 100.0 wt%
MQ-8d	8	10.28	2.0	0.1	-	100.0	-	cc	cc: 100.0 wt%
MQ-22d	22	8.21	2.1	0.2	-	100.0	-	cc	cc: 100.0 wt%
Mg-stock		5.60			95.5				
Mg-1d	1	9.51	4.4	2.4	94.2	98.8	1.2	ara, cc, mhc	ara: 58.1 wt%, cc: 19.4, mhc: 22.5 wt%
Mg-8d	8	9.25	2.5	1.2	96.0	98.9	1.1	ara, cc	ara: 95.4 wt%, cc: 4.6 wt%
Mg-22d	22	9.33	2.7	1.0	96.2	99.0	1.0	ara	ara: 100 wt%
Sr-stock		5.34			97.0				
Sr-1d	1	9.19	1.7	31.6	59.5	26.3	73.7	ca-str	ca-str: 100.0 wt%
Sr-8d	8	7.72	1.3	35.0	58.6	20.0	80.0	ca-str	ca-str: 100.0 wt%
Sr-22d	22	6.01	1.3	38.6	58.1	21.5	78.5	ca-str	ca-str: 100.0 wt%
Ba-stock		5.35			95.0				
Ba-1d	1	9.69	2.1	25.3	79.2	50.9	49.1	ca-wit	ca-wit: 22.6 wt%, ba-cc: 77.4 wt%
Ba-8d	8	9.22	1.4	38.8	70.0	23.5	76.5	ca-wit	ca-wit: 55.9 wt%, ba-cc: 44.1 wt%
Ba-22d	22	6.56	1.3	46.8	65.2	9.2	90.8	ca-wit	ca-wit: 100 wt%
Cd-stock		2.96			97.6				
Cd-1d	1	6.44	2.0	35.3	71.1	41.9	58.1	ot, cc	ot: 69.0 wt%, cc: 31.0 wt%
Cd-8d	8	6.40	1.4	32.6	71.5	40.6	59.4	ot, cc	ot: 70.8 wt%, cc: 29.2 wt%
Cd-22d	22	5.15	1.2	24.1	77.3	54.0	46.0	ot, cc	ot: 56.4 wt%, cc: 43.6 wt%
Mn-stock		5.48			93.4				
Mn-1d	1	6.68	1.7	16.0	76.1	73.4	26.6	rhod, cc	rhod: 39.6 wt%, cc: 60.4 wt%
Mn-8d	8	6.61	1.4	18.3	81.4	69.6	30.4	rhod, cc	rhod: 46.4 wt%, cc: 53.6 wt%
Mn-22d	22	6.47	1.4	20.0	81.3	63.3	36.7	rhod, cc	rhod: 49.8 wt%, cc: 50.2 wt%
Ni-stock		5.52			96.8				
Ni-1d	1	7.09	9.4	37.4	72.3	34.1	65.9	ANC, cc	ANC, cc (not quantified)
Ni-8d	8	7.09	7.3	38.3	70.0	29.9	70.1	ANC, cc	ANC, cc (not quantified)
Ni-22d	22	7.09	6.3	40.2	66.8	24.4	75.6	ANC, cc	ANC, cc (not quantified)
Zn-stock		5.64			93.3				
Zn-1d	1	5.97	5.7	47.6	44.4	0.9	99.1	hyzi	hyzi: 96.2 wt%, smi: 3.8 wt%
Zn-8d	8	5.91	3.0	44.7	45.9	0.0	100.0	hyzi	hyzi: 97.6 wt%, smi: 2.4 wt%
Zn-22d	22	5.84	1.8	40.8	40.9	0.4	99.6	hyzi	hyzi: 97.5 wt%, smi: 2.5 wt%

By dispersing ACC into a 0.1 M MgCl₂-solution, the transformation product incorporated 1 mol% of Mg. The transformation pathway, however, changed completely compared to the control experiment. PXRD and FTIR show that after 1 d of reaction time a mix of aragonite, monohydrocalcite [CaCO₃•H₂O] and calcite were present (Figure S4.2). These reaction products were transforming entirely to aragonite, with needles up to 10 μm in length, after 22 d of reaction time (Figure 4.2 and Table 4.2). High concentrations of Mg in solution are known to inhibit calcite and to promote aragonite formation (Mucci and Morse, 1983; Astilleros et al., 2010). Purgstaller et al. (2017) observed that Mg-ACC sampled during an experiment transformed under air exposure into different CaCO₃ polymorphs compared to the same Mg-ACC kept in a Mg-rich solution. Although no measurements were conducted directly after filtration, it is assumed that ACC was still present after 1 d in the Mg-rich solution, considering the stabilizing effect of Mg in solution for the lifetime of ACC, as was observed and discussed in Chapter 2. Hence, it is suggested that the obtained calcite in the present experiments results from the transformation of ACC under air exposure after filtration. This is supported by SEM, displaying nm-sized particles akin to the amorphous phase instead of idiomorphic rhombohedral crystals as in the control experiment (Figure S4.2). Konrad et al. (2016) made the same morphological observations for the transformation of ACC in air. The formation of intermediate monohydrocalcite from ACC and its transformation to aragonite is likely resulting from the high Mg-concentration in respect to reaching a high $a\text{Mg}^{2+}/a\text{Ca}^{2+}$ ratio in the reactive solution (Blue et al., 2017; Purgstaller et al., 2017 and Chapter 2).

In the experiments, where ACC was dispersed into Sr and Ba solutions, the orthorhombic aragonitic structure evolved from ACC, as observed for the Mg-solution experiments (Figure 4.1). However, in contrast to Mg, the Sr and Ba ions were readily incorporated into the final reaction product and calcium was released into the reactive solution (Table 4.2). The initial ACC transformed into calcio-strontianite and calcio-witherite with about 80 mol% of Sr and 90 mol% of Ba in the respective solid after 22 d of reaction time. In both experiments aragonite-type single solid-solution phases are formed at ambient temperatures, which was in former studies only achieved at elevated temperatures > 75 °C for calcio-strontianite respectively is not reported at all for calcio-witherite (Plummer and Busenberg, 1987; Lucas-Girot et al., 2007). Studies on the solid-solution of the latter are absent. SEM images show up to 3 μm long and 1 μm thick spindle-shaped crystals as well as thin needles up to 2 μm of calcio-strontianite and calcio-witherite crystals (Figure 4.2). While in the Sr-solution experiment the orthorhombic calcio-strontianite was already present as a single solid-solution

phase after 1 d of reaction time, ACC in the Ba-solution transformed initially into two distinct solid solutions: calcio-witherite and barytocalcite $[\text{BaCa}(\text{CO}_3)_2]$. PXRD and FTIR measurements suggest that the barytocalcite is disordered (Figure S4.2). The diffractograms and spectra show shifted peak and band-positions with respect to reference data (Scheetz and White, 1977; Frost and Dickfos, 2008) and from Rietveld refinement, larger cell volumes of 269.6 \AA^3 in the sample Ba_1d and 271 \AA^3 in the sample Ba_8d are obtained compared to a value of 266.4 \AA^3 found in the literature (Dickens and Bowen, 1971). This indicates that the barytocalcite is disordered and non-stoichiometric with a greater Ba- than Ca-content (Figure S4.2).

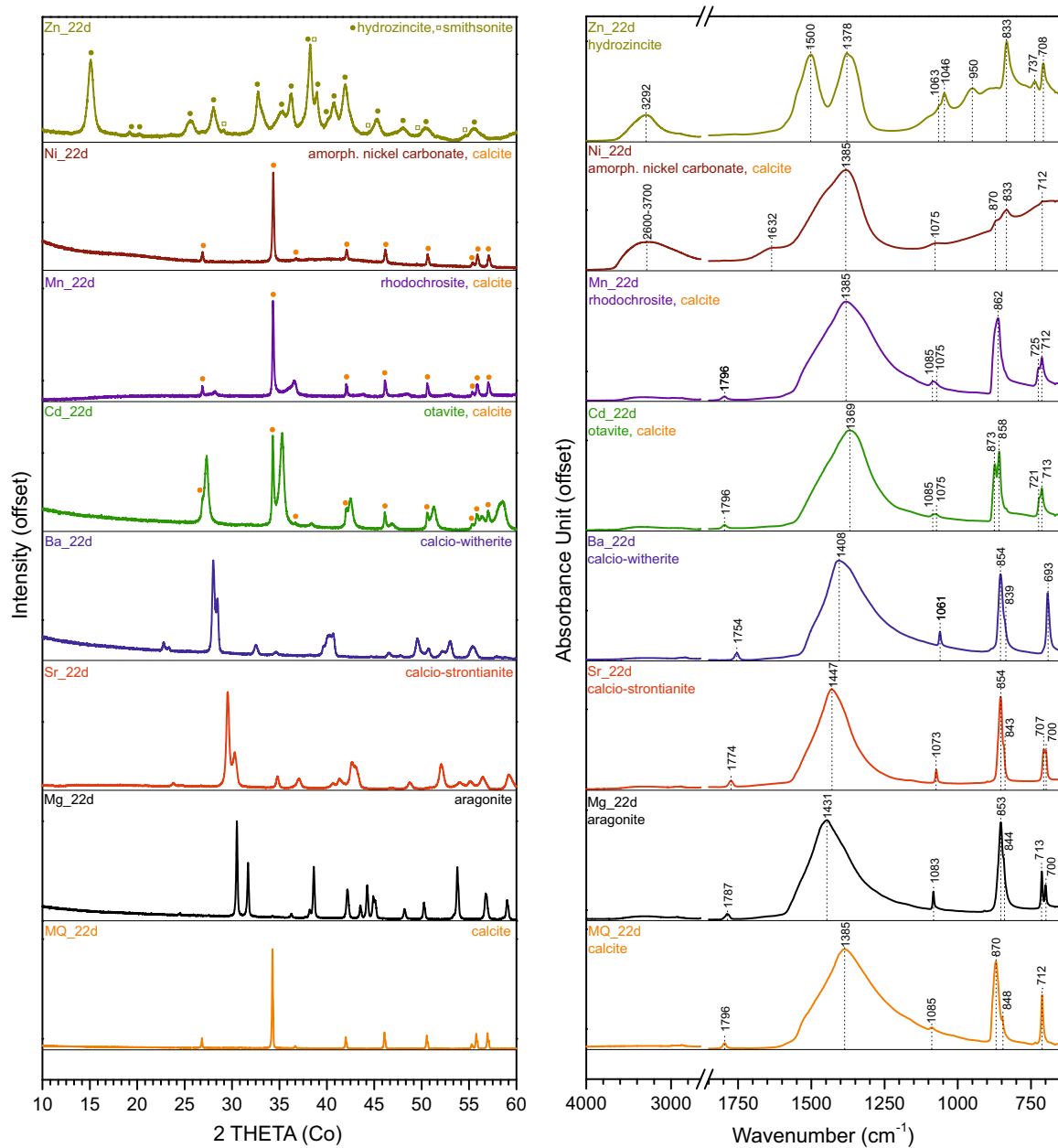


Figure 4.1. PXRD- and FTIR-measurements of final reaction products obtained after 22 d from the transformation of ACC in Me^{2+} -rich solutions as well as in reference solution using Milli-Q water (MQ).

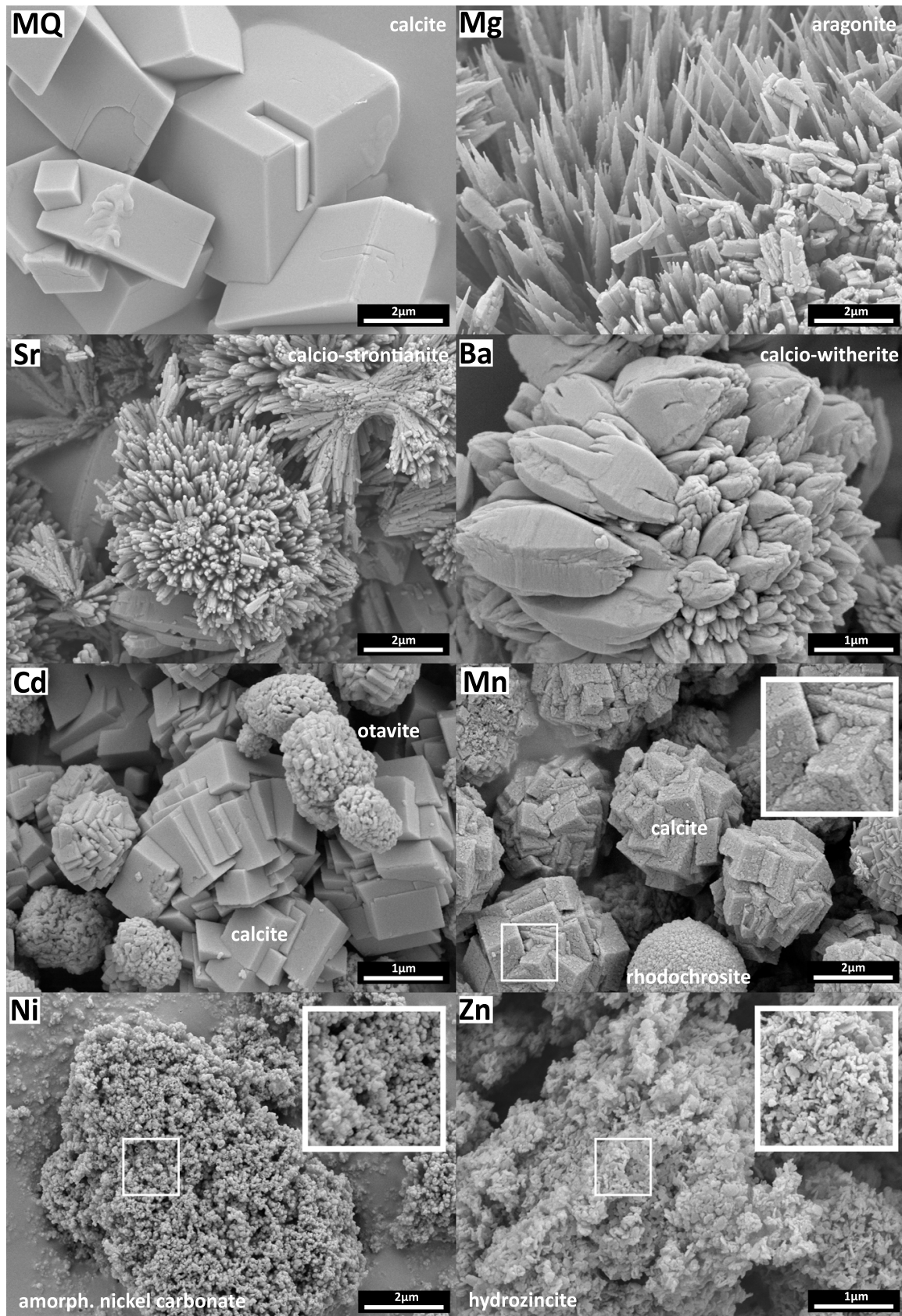


Figure 4.2. SEM images of final reaction products after 22 d show orthorhombic crystals from the transformation of ACC in Mg-, Sr- and Ba-solutions. In the control experiment with Milli-Q water (MQ) as well as in the Cd- and Mn-experiments rhombohedral crystals are obtained and in the Ni- and Zn-solutions spherical nanoparticles and platy-crystals from the formation of hydrated amorphous and crystalline carbonates were observed.

4.3.2 Formation of transition metal carbonate minerals from ACC

ACC dispersed in a Cd- and a Mn-rich solution was observed to transform into the end-member minerals otavite and rhodochrosite together with calcite (Figure 4.1). Throughout the transformation of ACC up to 60 mol% respectively up to 37 mol% of Ca were released into the respected solution and replaced in the final reaction products with the dissolved Cd- and Mn-ions (Table 4.2). Otavite formed about 1 μm sized spherical aggregates, composed of 100 nm rhombohedra, differing from calcite which formed 2 μm large flower-like aggregates of euhedral calcite crystals (Figure 4.2). Rhodochrosite crystallized into spheres of 1-2 μm in diameter, composed of rhombohedral crystals of 100 nm in size (Figure 4.2). The calcite, which formed together with rhodochrosite, shows 4 μm large flower-like structures of rhombohedral crystals with unusual surface characters, which could imply that step movement was inhibited during growth (Figure 4.2) as a result of adsorbed Mn-complexes. Similar observations are reported in an AFM study by Vinson et al. (2007) who investigated the inhibition of calcite dissolution in the presence of Mn^{2+} in solution.

ACC dispersed into a Ni-rich solution transformed into an X-ray amorphous nickel carbonate simultaneously with calcite, verified by the amorphous hump in the diffractograms (Figure 4.1). The amorphism of the nickel carbonate is furthermore indicated from the characteristic absence of the ν_4 -band as well as presence of a broad H_2O -band at 2 600-3 700 cm^{-1} in the FTIR spectrum (Figure 4.1) (Minkova et al., 1984; García-Guinea et al., 2013). Up to 76 mol% of the Ca originally bound in the ACC phase was released into the reactive solution and substituted by Ni. The particles are spherical in shape and show maximum particle sizes up to 100 nm (Figure 4.2). The FTIR spectrum suggests the amorphous reaction product may correspond to a nickel hydroxycarbonate mineral phase commonly referred to as zaratite ($\text{Ni}_3\text{CO}_3(\text{OH})_4 \cdot 4\text{H}_2\text{O}$; Table 4.1). However, the International Mineralogical Association (IMA) has classified the phase as questionable in terms of describing a distinct mineral phase, due to their low crystallinity and different hydration states (García-Guinea et al., 2013). Accordingly, the present reaction product is referred to as amorphous nickel carbonate (ANC).

A hydrated mineral phase is forming as well when dispersing ACC into a Zn-containing solution, namely hydrozincite. Hydrozincite is forming 200 nm platy-crystals (Figure 4.2) with minor amounts of smithsonite (ZnCO_3), where the latter is only detectable in PXRD (Table 4.2 and Figure 4.1). These two Zn-carbonate phases are the only products of the transformation of ACC in the Zn solution. Throughout this transformation process almost the entire Ca content in the ACC was released into the reactive solution being exchanged by

dissolved Zn-ions to form zinc carbonate minerals at a close to 100 % level. Ni- and Zn-ions are strongly hydrated in aqueous media and thus known for their high dehydration energy. Anhydrous carbonate minerals of these two Me-ions are, therefore, unlikely reaction products at ambient temperatures and pressures and are commonly not found under these physicochemical conditions in natural environments, resulting in the formation of hydrous Me-carbonates instead (Zachara et al., 1991; Hoffmann and Stipp, 2001; Pokrovsky and Schott, 2002).

4.3.3 Conditioning transformation pathways of ACC by solution chemistry

The observed transformation pathways in this study demonstrate the importance of the solution chemistry on the fate of ACC in aqueous media. The observed exchange of elements during ACC transformation is a strong indicator for progressive dissolution of ACC and subsequent re-precipitation of distinct solid carbonate phases. On another point of view, the observed high exchange rates of dissolved Me^{2+} -ions from the solution into the solid are unlikely to be obtained via ion diffusion considering a solid-state transformation, especially for such short reaction times at ambient conditions (Rodríguez-Navarro et al., 2015). Our results discard a significant influence of formerly reported proto-structures of the used ACC on its transformation pathway (Gebauer et al., 2008; Gebauer et al., 2010), as orthorhombic carbonates were forming in solutions containing larger cations than Ca (Ba and Sr) and rhombohedral structures were found precipitating in solutions with smaller cations than Ca (Mn and Cd). However, exceptions were obtained for the ACC transformation behaviour in the presence of the strongly hydrated cations Ni and Zn, forming hydrated carbonate phases, and for Mg. Mg is the only cation observed in this study, which did not readily incorporate into the precipitating solid, but nonetheless effectively determined CaCO_3 polymorph development to form aragonite, via the formation of monohydrocalcite, instead of calcite. This supports the governing role of solution chemistry on carbonate mineral formation via an amorphous precursor in all our experimental runs (Figure 4.3). The, in most cases, significant incorporation of Me^{2+} -ions into the precipitated solid throughout ACC transformation might be explained by the high surface area of ACC in contrast to crystalline calcium carbonates enhancing favourable exchange reactions (Kim et al., 2014) and by the sparse solubility of the studied Me^{2+} -carbonates compared to ACC and calcite (Table 4.1). The final reaction products are at least two magnitudes less soluble than ACC as well as less soluble than calcite.

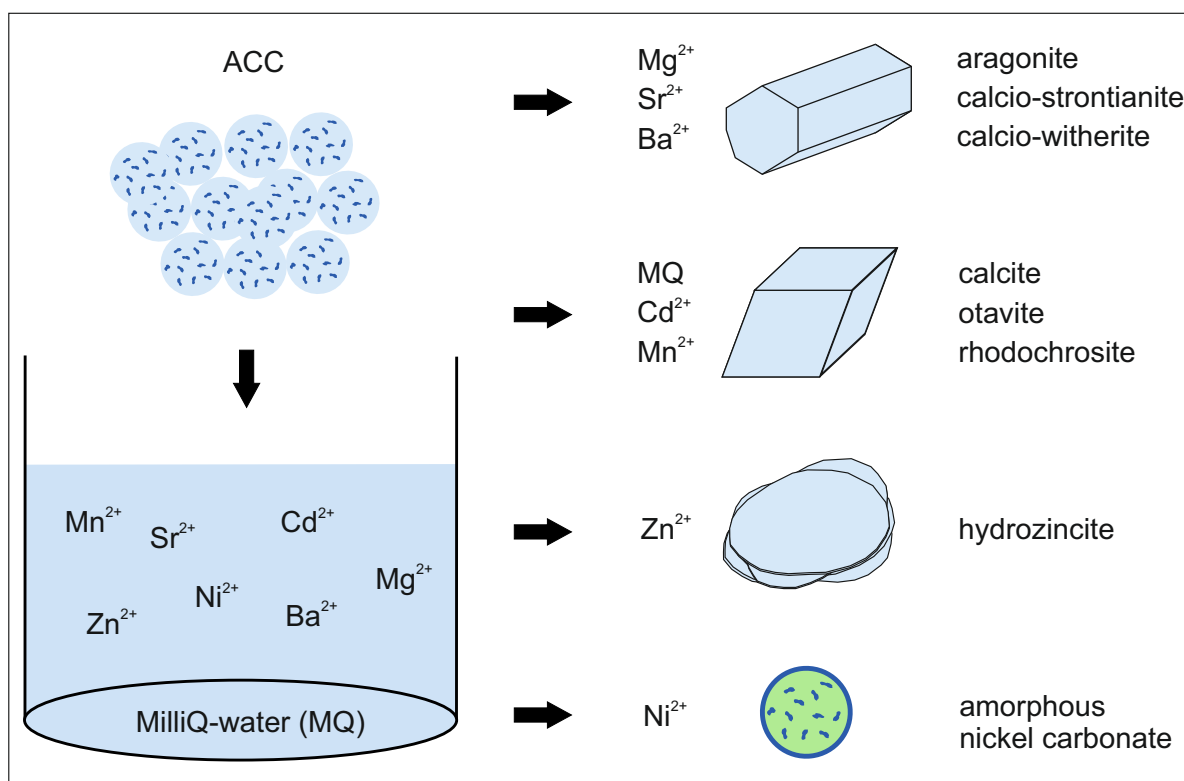


Figure 4.3. The dispersion of additive-free ACC into Me^{2+} -rich solutions as well as into reference MQ water without metals, reveal that crystallization pathways and chemical composition of the transformed phase are conditioned by solution chemistry. Thus, precipitated carbonate phases from ACC transformation are not preserving the elemental signatures of ACC formation but record the prevailing environmental conditions during the transformation process.

In this study, the investigation on the transformation behaviour of ACC in a Me^{2+} -rich solution shows differences compared to the distinct uptake of metals during the formation of amorphous carbonates. The incorporation of metals during amorphous carbonate precipitation is well studied for elements like Sr, Fe and rare earth elements (REE), and in particular for Mg (Sel et al., 2012; Rodriguez-Blanco et al., 2014; Blue et al., 2017; Littlewood et al., 2017). As these amorphous precursor form from highly supersaturated solutions without distinct long range ordering, they seem to discriminate between Me^{2+} -ions at a very low level. This can be illustrated in the case of Mg, where any composition of $\text{Ca}_x\text{Mg}_{(1-x)}$ can be formed as amorphous carbonate by co-precipitation of Mg and Ca (Radha et al., 2012), resulting after transformation in (high) Mg-calcites (Loste et al., 2003). On the other hand, by using classical experimental approaches, the direct precipitation of Mg-calcite from a saturated solution is not exceeding 3 mol% of Mg and at elevated Mg/Ca ratios, aragonite instead of Mg-calcite is formed (Politi et al., 2010). In analogy, the transformation experiments in this study show that additive-free ACC does not incorporate large amounts of Mg even during transformation in a Mg-rich solution, but results in the formation of aragonite via monohydrocalcite, which might

be attributed to the difference in supersaturation. While the formation of an amorphous carbonate occurs in highly supersaturated solutions, the dispersion of ACC in an initially undersaturated solution leads to dissolution of the amorphous phase until its saturation is reached (see [Chapter 2](#) and [3](#)). The subsequent transformation in a highly supersaturated solution is therefore much more vigorous than in a saturated one, in which the most stable phase has time to be formed. Similar observations can be made for Sr, where high Sr-calcites were obtained from a Sr-rich ACC precursor, while direct precipitation triggers the formation of aragonite-type structures, with Sr incorporating in calcite at a comparatively low concentration level ([Matsunuma et al., 2014](#); [Littlewood et al., 2017](#)).

4.3.4 Implications for natural environments and technical applications

The presented experiments reveal that the composition of the amorphous phase is not necessarily preserved in the reaction product after transformation in an aqueous media with differing solution chemistry compared to the time of precursor formation. This could have implications for the reconstruction of paleo-environmental conditions from biominerals, where the chemical environment of certain tissues within an organism in which amorphous precursor are formed, may differ from the aqueous environment where transformation occurs, (e.g. body fluid vs. seawater) ([Beniash et al., 1999](#); [Raz et al., 2003](#); [Vidavsky et al., 2014](#); [Devol et al., 2015](#)). This must be considered when using elemental or isotopic signatures in biogenic carbonates originating from an amorphous precursor. The presented results imply that the reaction product records rather the condition of the transformation environment than the condition of the amorphous precursor formation ([Giuffre et al., 2015](#); [Immenhauser et al., 2016](#); [Mavromatis et al., 2017](#)).

On a technical aspect, this screening experiment demonstrates the potential of amorphous carbonates to be used as blank precursor material, as it was illustrated that ACC can be triggered by physicochemical conditions of the solution to crystallize into specific carbonate polymorphs. This synthesis route, via an amorphous precursor, shows a prospective possibility to forge novel composite materials with desired particle shapes and compositions, where e.g. the formation of calcio-strontianite or calcio-witherite solid solutions can be achieved at ambient temperatures. Furthermore, the high exchange rates observed for Ca from ACC with Me^{2+} -ions in solution throughout transformation, reveal a great potential for ACC to be used as a remediation material, in particular, when compared to crystalline carbonates as it shows considerably higher cation exchange rates throughout transformation ([Fukushi et al., 2011](#)).

4.4 Conclusions

The decoupling of the formation step of ACC and its transformation in Me^{2+} -rich solutions, enabled to study the distinct influence of the solution chemistry on respective transformation kinetics and mechanisms. Our experiments reveal that the transformation pathway of additive-free ACC is strongly determined by the solution chemistry. Thus, proto-structures in the ACC material, if present, have no significant influence on the crystal structure of the final precipitate. In general, cations with large ion radius, like Sr and Ba, triggered the formation of orthorhombic carbonate minerals. Cations smaller in size compared to Ca, like Mn and Cd, precipitated rhombohedral carbonate minerals. The strongly hydrated cations Zn and Ni formed hydrated crystalline and amorphous carbonates, respectively. Mg was the only element not being readily incorporated into the reaction product, but nonetheless poised the calcite formation and triggered the formation of aragonite via intermediate monohydrocalcite. The results clearly demonstrate that throughout transformation, the chemical composition of the amorphous precursor must not be passed on to the crystalline reaction product but changes dependent on solution chemistry at time of transformation. On the other hand, the results also demonstrate that the amorphous precursor can be triggered to form distinct carbonate minerals and further reveal an enhanced and fast exchange rate with dissolved (heavy) Me^{2+} -ions in the course of transformation compared to its crystalline counterparts.

4.5 Supporting Information

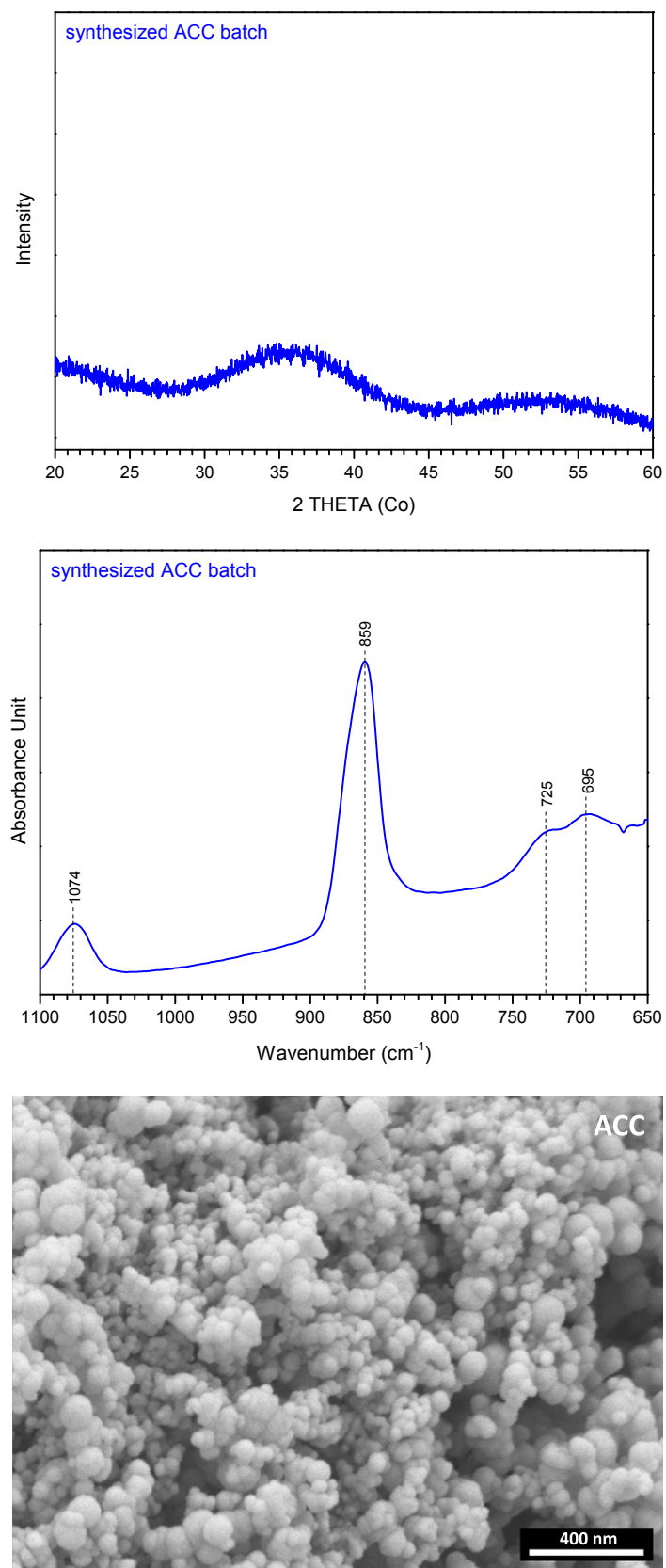


Figure S4.1. PXRD, FTIR and SEM analyses of the synthesized ACC, displaying a non-X-ray-diffracting hydrated calcium carbonate forming 30-200 nm large spherical particles.

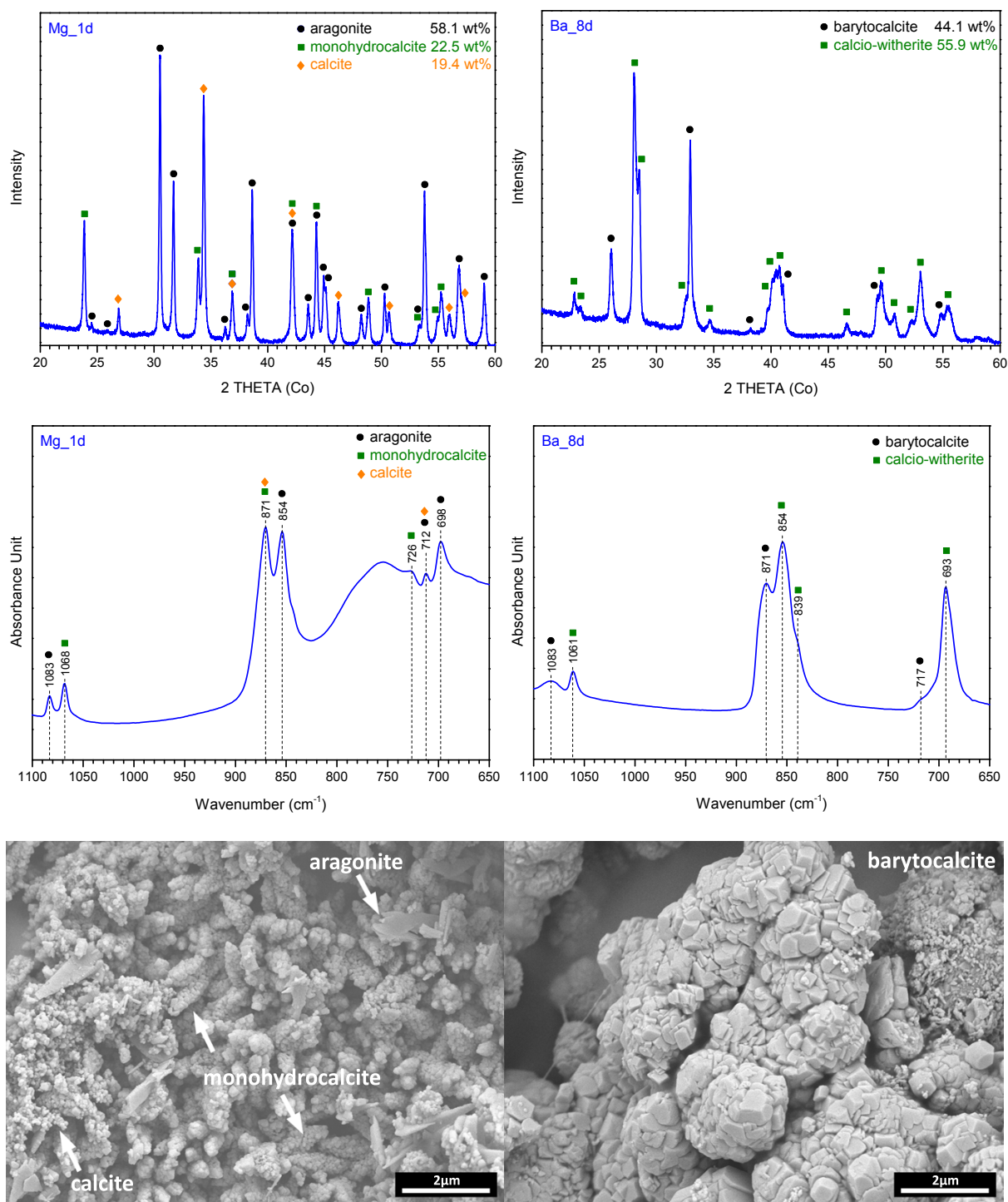


Figure S4.2. Intermediate reaction products were obtained in the experiments with Mg and Ba in solution. *Left:* the dispersion of ACC into a Mg-rich solution revealed the formation of intermediate monohydrocalcite and calcite next to aragonite after 1 d in solution prior to the complete transformation into aragonite. The formation of calcite is suggested to be an artefact caused by the transformation of ACC under air exposure (see discussion). *Right:* in the Ba-rich solution, ACC transformed initially into rhombohedral barytocalcite and calcio-witherite prior to the complete transformation into calcio-witherite. PXRD and FTIR measurements suggest the barytocalcite is disordered and non-stoichiometric with a greater Ba than Ca content in its structure.

4.6 References

- Addadi L., Raz S. and Weiner S. (2003) Taking Advantage of Disorder: Amorphous Calcium Carbonate and Its Roles in Biomineralization. *Adv. Mater.* **15**, 959–970.
- Alía J. M., de Mera Y. D., Edwards H. G. M., Martín P. G. and Andres S. L. (1997) FT-Raman and infrared spectroscopic study of aragonite-strontianite ($\text{Ca}_x\text{Sr}_{1-x}\text{CO}_3$) solid solution. *Spectrochim. Acta Part A Mol. Biomol. Spectrosc.* **53**, 2347–2362.
- Andersen F. and Brecevic L. (1991) Infrared spectra of amorphous and crystalline calcium carbonate. *Acta Chem. Scand* **45**, 1018–1024.
- Astilleros J. M., Fernández-Díaz L. and Putnis A. (2010) The role of magnesium in the growth of calcite: An AFM study. *Chem. Geol.* **271**, 52–58.
- Beck J. W., Edwards R. L., Ito E., Taylor F. W., Recy J., Rougerie F., Joannot P. and Henin C. (1992) Sea-Surface Temperature from Coral Skeletal Strontium/Calcium Ratios. *Science* **257**, 644–647.
- Beniash E., Addadi L. and Weiner S. (1999) Cellular Control Over Spicule Formation in Sea Urchin Embryos: A Structural Approach. *J. Struct. Biol.* **125**, 50–62.
- Blue C. R. and Dove P. M. (2015) Chemical controls on the magnesium content of amorphous calcium carbonate. *Geochim. Cosmochim. Acta* **148**, 23–33.
- Blue C. R., Giuffre A., Mergelsberg S., Han N., De Yoreo J. J. and Dove P. M. (2017) Chemical and physical controls on the transformation of amorphous calcium carbonate into crystalline CaCO_3 polymorphs. *Geochim. Cosmochim. Acta* **196**, 179–196.
- Bots P., Benning L. G., Rodriguez-Blanco J.-D., Roncal-Herrero T. and Shaw S. (2012) Mechanistic Insights into the Crystallization of Amorphous Calcium Carbonate (ACC). *Cryst. Growth Des.* **12**, 3806–3814.
- Böttcher M. E., Gehlken P. L. and Usdowski E. (1992) Infrared spectroscopic investigations of the calcite-rhodochrosite and parts of the calcite-magnesite mineral series. *Contrib. to Mineral. Petrol.* **109**, 304–306.
- Brečević L. and Nielsen A. E. (1989) Solubility of amorphous calcium carbonate. *J. Cryst. Growth* **98**, 504–510.
- Bucca M., Dietzel M., Tang J., Leis A. and Köhler S. J. (2009) Nucleation and crystallization of otavite, witherite, calcite, strontianite, hydrozincite, and hydrocerussite by CO_2 membrane diffusion technique. *Chem. Geol.* **266**, 143–156.
- Busenberg E. and Plummer L. N. (1986) The solubility of $\text{BaCO}_3(\text{cr})$ (witherite) in $\text{CO}_2\text{-H}_2\text{O}$ solutions between 0 and 90°C , evaluation of the association constants of $\text{BaHCO}_3^+(\text{aq})$ and $\text{BaCO}_3^0(\text{aq})$ between 5 and 80°C , and a preliminary evaluation of the

- thermodynamic properties of $\text{Ba}^{2+}(\text{aq})$. *Geochim. Cosmochim. Acta* **50**, 2225–2233.
- Busenberg E., Plummer L. N. and Parker V. B. (1984) The solubility of strontianite (SrCO_3) in CO_2 - H_2O solutions between 2 and 91°C, the association constants of $\text{SrHCO}_3^+(\text{aq})$ and $\text{SrCO}_3^0(\text{aq})$ between 5 and 80°C, and an evaluation of the thermodynamic properties of $\text{Sr}^{2+}(\text{aq})$ and $\text{SrCO}_3(\text{cr})$ at 25°C and 1atm total. *Geochim. Cosmochim. Acta* **48**, 2021–2035.
- Cam N., Georgelin T., Jaber M., Lambert J. F. and Benzerara K. (2015) In vitro synthesis of amorphous Mg-, Ca-, Sr- and Ba-carbonates: What do we learn about intracellular calcification by cyanobacteria? *Geochim. Cosmochim. Acta* **161**, 36–49.
- Cheary R. W., Coelho A. a. and Cline J. P. (2004) Fundamental parameters line profile fitting in laboratory diffractometers. *J. Res. Natl. Inst. Stand. Technol.* **109**, 1.
- Devol R. T., Sun C. Y., Marcus M. A., Coppersmith S. N., Myneni S. C. B. and Gilbert P. U. P. A. (2015) Nanoscale Transforming Mineral Phases in Fresh Nacre. *J. Am. Chem. Soc.* **137**, 13325–13333.
- Dickens B. and Bowen J. S. (1971) The crystal structure of $\text{BaCa}(\text{CO}_3)_2$ (barytocalcite). *J. Res. Natl. Bur. Stand. Sect. A Phys. Chem.* **75A**, 197.
- Frost R. L. and Dickfos M. J. (2008) Raman and infrared spectroscopic study of the anhydrous carbonate minerals shortite and barytocalcite. *Spectrochim. Acta Part A Mol. Biomol. Spectrosc.* **71**, 143–146.
- Frost R. L. and Hales M. C. (2007) Synthesis and vibrational spectroscopic characterisation of synthetic hydrozincite and smithsonite. *Polyhedron* **26**, 4955–4962.
- Fukushi K., Munemoto T., Sakai M. and Yagi S. (2011) Monohydrocalcite: a promising remediation material for hazardous anions. *Sci. Technol. Adv. Mater.* **12**, 64702.
- García-Guinea J., Iglesia A. La, Crespo-Feo E., González Del Tánago J. and Correcher V. (2013) The status of zaratite: investigation of the type specimen from Cape Ortegal, Galicia, Spain. *Eur. J. Mineral.* **25**, 995–1004.
- Garrels R. M., Thompson M. E. and Siever R. (1960) Stability of some carbonates at 25 degrees C and one atmosphere total pressure. *Am. J. Sci.* **258**, 402–418.
- Gebauer D., Gunawidjaja P. N., Ko J. Y. P., Bacsik Z., Aziz B., Liu L., Hu Y., Bergström L., Tai C., Sham T.-K., Edén M. and Hedin N. (2010) Proto-Calcite and Proto-Vaterite in Amorphous Calcium Carbonates. *Angew. Chemie Int. Ed.* **49**, 8889–8891.
- Gebauer D., Völkel A. and Cölfen H. (2008) Stable prenucleation calcium carbonate clusters. *Science* **322**, 1819–1822.
- Giuffrè A. J., Gagnon A. C., De Yoreo J. J. and Dove P. M. (2015) Isotopic tracer evidence

- for the amorphous calcium carbonate to calcite transformation by dissolution-reprecipitation. *Geochim. Cosmochim. Acta* **165**, 407–417.
- Habraken W. J. E. M., Masic A., Bertinetti L., Al-Sawalmih A., Glazer L., Bentov S., Fratzi P., Sagi A., Aichmayer B. and Berman A. (2015) Layered growth of crayfish gastrolith: About the stability of amorphous calcium carbonate and role of additives. *J. Struct. Biol.* **189**, 28–36.
- Hoffmann U. and Stipp S. L. S. (2001) The behavior of Ni²⁺ on calcite surfaces. *Geochim. Cosmochim. Acta* **65**, 4131–4139.
- Immenhauser A., Buhl D., Richter D., Niedermayr A., Riechelmann D., Dietzel M. and Schulte U. (2010) Magnesium-isotope fractionation during low-Mg calcite precipitation in a limestone cave – Field study and experiments. *Geochim. Cosmochim. Acta* **74**, 4346–4364.
- Immenhauser A., Schöne B. R., Hoffmann R. and Niedermayr A. (2016) Mollusc and brachiopod skeletal hard parts: Intricate archives of their marine environment. *Sedimentology* **63**, 1–59.
- Johnson K. S. (1982) Solubility of rhodochrosite (MnCO₃) in water and seawater. *Geochim. Cosmochim. Acta* **46**, 1805–1809.
- Kim Y., Schenk A. S., Ihli J., Kulak A. N., Hetherington N. B. J., Tang C. C., Schmahl W. W., Griesshaber E., Hyett G. and Meldrum F. C. (2014) A critical analysis of calcium carbonate mesocrystals. *Nat. Commun.* **5**, 1–14.
- Konrad F., Gallien F., Gerard D. E. and Dietzel M. (2016) Transformation of Amorphous Calcium Carbonate in Air. *Cryst. Growth Des.* **16**, 6310–6317.
- Kralj D. and Brečević L. (1995) Dissolution kinetics and solubility of calcium carbonate monohydrate. *Colloids Surfaces A Physicochem. Eng. Asp.* **96**, 287–293.
- Lea D. W. (2013) *Elemental and Isotopic Proxies of Past Ocean Temperatures*. 2nd ed., Elsevier Ltd.
- Littlewood J. L., Shaw S., Peacock C. L., Bots P., Trivedi D. and Burke I. T. (2017) Mechanism of Enhanced Strontium Uptake into Calcite via an Amorphous Calcium Carbonate Crystallization Pathway. *Cryst. Growth Des.* **17**, 1214–1223.
- Loste E., Wilson R. M., Seshadri R. and Meldrum F. C. (2003) The role of magnesium in stabilising amorphous calcium carbonate and controlling calcite morphologies. *J. Cryst. Growth* **254**, 206–218.
- Lucas-Girot A., Hernandez O. and Oudadesse H. (2007) Re-examination of the structural properties of solid solutions Sr_xCa_{1-x}CO₃. *Mater. Res. Bull.* **42**, 1061–1068.

- Matsunuma S., Kagi H., Komatsu K., Maruyama K. and Yoshino T. (2014) Doping Incompatible Elements into Calcite through Amorphous Calcium Carbonate. *Cryst. Growth Des.* **14**, 5344–5348.
- Mavromatis V., Gautier Q., Bosc O. and Schott J. (2013) Kinetics of Mg partition and Mg stable isotope fractionation during its incorporation in calcite. *Geochim. Cosmochim. Acta* **114**, 188–203.
- Mavromatis V., Purgstaller B., Dietzel M., Buhl D., Immenhauser A. and Schott J. (2017) Impact of amorphous precursor phases on magnesium isotope signatures of Mg-calcite. *Earth Planet. Sci. Lett.* **1**, 1–10.
- Meiron O. E., Bar-David E., Aflalo E. D., Shechter A., Stepensky D., Berman A. and Sagi A. (2011) Solubility and bioavailability of stabilized amorphous calcium carbonate. *J. Bone Miner. Res.* **26**, 364–72.
- Minkova N., Krusteva M. and Nikolov G. (1984) Spectroscopic Study of Nickel Hydroxide, Nickel Carbonate-Hexahydrate and Nickel Hydroxocarbonate. *J. Mol. Struct.* **115**, 23–26.
- Mucci A. and Morse J. W. (1983) The incorporation of Mg^{2+} and Sr^{2+} into calcite overgrowths: influences of growth rate and solution composition. *Geochim. Cosmochim. Acta* **47**, 217-233.
- Neumann M. and Epple M. (2007) Monohydrocalcite and Its Relationship to Hydrated Amorphous Calcium Carbonate in Biominerals. *Eur. J. Inorg. Chem.* **2007**, 1953–1957.
- Ogino T., Suzuki T. and Sawada K. (1987) The formation and transformation mechanism of calcium carbonate in water. *Geochim. Cosmochim. Acta* **51**, 2757–2767.
- Pasierb P., Gajerski R., Komornicki S. and Rękas M. (2001) Structural Properties and Thermal Behavior of Li_2CO_3 – $BaCO_3$ System by DTA, TG and XRD Measurements. *J. Therm. Anal. Calorim.* **65**, 457–466.
- Plummer L. N. and Busenberg E. (1982) The solubilities of calcite, aragonite and vaterite in CO_2 - H_2O solutions between 0 and 90°C, and an evaluation of the aqueous model for the system $CaCO_3$ - CO_2 - H_2O . *Geochim. Cosmochim. Acta* **46**, 1011–1040.
- Plummer L. N. and Busenberg E. (1987) Thermodynamics of aragonite-strontianite solid solutions: Results from stoichiometric solubility at 25 and 76°C. *Geochim. Cosmochim. Acta* **51**, 1393–1411.
- Pokrovsky O. S. and Schott J. (2002) Surface Chemistry and Dissolution Kinetics of Divalent Metal Carbonates. *Environ. Sci. Technol.* **36**, 426–432.
- Politi Y., Batchelor D. R., Zaslansky P., Chmelka B. F., Weaver J. C., Sagi I., Weiner S. and

- Addadi L. (2010) Role of magnesium ion in the stabilization of biogenic amorphous calcium carbonate: A structure-function investigation. *Chem. Mater.* **22**, 161–166.
- Preis W. and Gamsjäger H. (2001) (Solid + solute) phase equilibria in aqueous solution. XIII. Thermodynamic properties of hydrozincite and predominance diagrams for ($\text{Zn}^{2+} + \text{H}_2\text{O} + \text{CO}_2$). *J. Chem. Thermodyn.* **33**, 803–819.
- Purgstaller B., Konrad F., Dietzel M., Immenhauser A. and Mavromatis V. (2017) Control of $\text{Mg}^{2+}/\text{Ca}^{2+}$ Activity Ratio on the Formation of Crystalline Carbonate Minerals via an Amorphous Precursor. *Cryst. Growth Des.* **17**, 1069–1078.
- Purgstaller B., Mavromatis V., Immenhauser A. and Dietzel M. (2016) Transformation of Mg-bearing amorphous calcium carbonate to Mg-calcite – In situ monitoring. *Geochim. Cosmochim. Acta* **174**, 180–195.
- Radha A. V., Fernandez-Martinez A., Hu Y., Jun Y., Waychunas G. A. and Navrotsky A. (2012) Energetic and structural studies of amorphous $\text{Ca}_{1-x}\text{Mg}_x\text{CO}_3 \cdot n\text{H}_2\text{O}$ ($0 \leq x \leq 1$). *Geochim. Cosmochim. Acta* **90**, 83–95.
- Raz S., Hamilton P. C., Wilt F. H., Weiner S. and Addadi L. (2003) The Transient Phase of Amorphous Calcium Carbonate in Sea Urchin Larval Spicules: The Involvement of Proteins and Magnesium Ions in Its Formation and Stabilization. *Adv. Funct. Mater.* **13**, 480–486.
- Raz S., Weiner S. and Addadi L. (2000) Formation of High-Magnesian Calcites via an Amorphous Precursor Phase: Possible Biological Implications. *Adv. Mater.* **12**, 38–42.
- Rietveld H. M. (1969) A profile refinement method for nuclear and magnetic structures. *J. Appl. Crystallogr.* **2**, 65–71.
- Rodriguez-Blanco J. D., Shaw S. and Benning L. G. (2015) A route for the direct crystallization of dolomite. *Am. Mineral.* **100**, 1172–1181.
- Rodriguez-Blanco J. D., Vallina B., Blanco J. A. and Benning L. G. (2014) The role of REE^{3+} in the crystallization of lanthanites. *Mineral. Mag.* **78**, 1373–1380.
- Rodriguez-Navarro C., Kudłacz K., Cizer Ö. and Ruiz-Agudo E. (2015) Formation of amorphous calcium carbonate and its transformation into mesostructured calcite. *CrystEngComm* **17**, 58–72.
- Scheetz B. E. and White W. B. (1977) Vibrational spectra of the alkaline earth double carbonates. *Am. Mineral.* **62**, 36–50.
- Sel O., Radha a. V., Dideriksen K. and Navrotsky A. (2012) Amorphous iron (II) carbonate: Crystallization energetics and comparison to other carbonate minerals related to CO_2 sequestration. *Geochim. Cosmochim. Acta* **87**, 61–68.

- Shen Q., Wei H., Zhou Y., Huang Y., Yang H., Wang D. and Xu D. (2006) Properties of amorphous calcium carbonate and the template action of vaterite spheres. *J. Phys. Chem. B* **110**, 2994–3000.
- Stipp S. L. ., Parks G. A., Nordstrom D. K. and Leckie J. O. (1993) Solubility-product constant and thermodynamic properties for synthetic otavite, $\text{CdCO}_3(\text{s})$, and aqueous association constants for the $\text{Cd}(\text{II})\text{-CO}_2\text{-H}_2\text{O}$ system. *Geochim. Cosmochim. Acta* **57**, 2699–2713.
- Vidavsky N., Addadi S., Mahamid J., Shimoni E., Ben-Ezra D., Shpigel M., Weiner S. and Addadi L. (2014) Initial stages of calcium uptake and mineral deposition in sea urchin embryos. *Proc. Natl. Acad. Sci.* **111**, 39–44.
- Vinson M. D., Arvidson R. S. and Luttge A. (2007) Kinetic inhibition of calcite (1 0 4) dissolution by aqueous manganese(II). *J. Cryst. Growth* **307**, 116–125.
- Zachara J. M., Cowan C. E. and Resch C. T. (1991) Sorption of divalent metals on calcite. *Geochim. Cosmochim. Acta* **55**, 1549–1562.
- Zhang Z., Xie Y., Xu X., Pan H. and Tang R. (2012) Transformation of amorphous calcium carbonate into aragonite. *J. Cryst. Growth* **343**, 62–67.

Chapter 5

Perspectives

5.1 Synthesis of amorphous metal carbonates and co-precipitation of different metal ions with ACC

Literature on amorphous carbonates can be found in ever-growing number, but as the minerals of the calcium endmember are by far the most encountered carbonates on Earth, the main focus lies on ACC. Studies on endmember precursors of other metal-carbonates are still rare with reported syntheses confined only to the cases of Mg (Blue et al., 2017), Fe (Sel et al., 2012) and for some rare earth elements (Rodriguez-Blanco et al., 2014). Nonetheless, the synthesis and transformation behaviour of other metal precursors might be vital to understand chemical compositions found in biominerals, as the latter are hardly pure calcium carbonates, but contain, beside Mg, a range of different cations, such as Sr or Ba. This is especially important as the co-precipitation of different metal ions into an amorphous carbonate likely shows a completely different partitioning behaviour to that found in crystalline carbonates. In general, as an amorphous phase has no long-range order, and, therefore, no definitive atomic structure, discrimination between different elements seems less pronounced (Cam et al., 2015). Sr or Ba, which are often considered as incompatible in the calcite structure, have been reported to show an enhanced incorporation into calcite, when formation was occurring via an amorphous calcium precursor containing Sr (Littlewood et al., 2017). Future studies on co-precipitation of different elements with ACC is essential to understand better the chemical compositions of biogenic crystalline carbonate minerals derived thereof. This again is crucial as the incorporation of metals into carbonates is often used to deduce the prevalent environmental conditions at time of formation. Hence, the knowledge obtained from developing a synthesis routine for ACC and from the transformation behaviour of ACC in different metal-solutions, as presented in this thesis, facilitates the design of constrained experimental setups with favourable conditions for the synthesis of other amorphous metal-carbonates and to investigate partitioning behaviour of elements with respect to the amorphous phase.

5.2 Unveiling the individual effects of solid and solution composition on the transformation of amorphous carbonate phases

Most studies that investigate the transformation behaviour of ACC into crystalline carbonates deduce their information from an experimental approach where the synthesis and aging of ACC occurs in the same solution (Blue et al., 2017 and therein). For example, the synthesis of Mg-ACC from highly supersaturated Mg/Ca-rich solutions and the subsequent monitoring of crystallization behaviour occurs in the same Mg/Ca-rich solution. Hence, the distinct influence of either Mg-content in ACC or aqueous Mg species in the experimental solution on observed metastabilities of the amorphous phase and on the different crystallization pathways is difficult to ascertain. The decoupling of ACC synthesis from the transformation in solution, as presented in this thesis, is a novel approach that allowed the specific study of the influence of solution chemistry on the transformation behaviour of ACC. The observation that a maximum of about 4 mol% of Mg is incorporated into ACC when being dispersed and subsequently dissolved until saturation was reached (Chapter 2), suggests that incorporation of large amounts of Mg in ACC are only accomplished during the synthesis from highly supersaturated solutions with respect to ACC. Therefore, a complementary study comes to mind, dispersing ACC with different Mg-content into pure water, which would facilitate the investigation of the sole influence of solid Mg-content in ACC on its transformation behaviour. As it is often suggested that observed metastabilities of ACC originate from the Mg-content therein, the experiment would allow clarification of such an assumption.

5.3 The importance of *in-situ* observation of reaction processes in aqueous solution

The *in-situ* Raman monitoring made it possible to visualize and uncover reaction steps, which would have otherwise been lost, in turn allowing reaction processes to be proven rather than inferred. This novel technique has not been widely applied and has a great potential, especially when dealing with metastable phases, where it is not clear for how long the respected phase is present in solution. This advantage can help in obtaining finally a reliable solubility product constant (K_{sp}) for ACC, for which different values are proposed (Brečević and Nielsen, 1989; Clarkson et al., 1992). An experimental study trying to unveil the K_{sp} of ACC, must always face the criticism of not being able to assess if the metastable phase in

solution was present the whole time as a single mineral phase. As already inferred in [Chapter 3](#), solution sampling together with the certainty of knowing at any time the mineral phase being present in solution through *in-situ* monitoring, helps to conduct an experimental study that delivers a reliable K_{sp} . In particular, as it was demonstrated, Mg in solution prolongs the lifetime of dispersed ACC while being saturated, but at the same time does not change the solid composition considerably.

5.4 Adsorption capacity and controlled transformation of ACC

The enhanced sorption capacity of ACC for dissolved metal ions with respect to the formation of crystalline carbonates shows great potential for being used as remediation material in industrial effluents and contaminated sites, e.g. for the fast removal of radiogenic strontium. More importantly, the experiments in this thesis reveal that ACC can be used as blank starting material, retaining the ability to be subsequently triggered to transform into distinct crystalline carbonates with defined compositions, particle shapes and size distribution controlled by the physiochemical conditions (temperature, chemical composition) of the reactive solution. These results give confidence for further studies in the future to design novel functional materials with application specific properties.

5.5 References

- Blue C. R., Giuffre A., Mergelsberg S., Han N., De Yoreo J. J. and Dove P. M. (2017) Chemical and physical controls on the transformation of amorphous calcium carbonate into crystalline CaCO_3 polymorphs. *Geochim. Cosmochim. Acta* **196**, 179–196.
- Brečević L. and Nielsen A. E. (1989) Solubility of amorphous calcium carbonate. *J. Cryst. Growth* **98**, 504–510.
- Cam N., Georgelin T., Jaber M., Lambert J. F. and Benzerara K. (2015) In vitro synthesis of amorphous Mg-, Ca-, Sr- and Ba-carbonates: What do we learn about intracellular calcification by cyanobacteria? *Geochim. Cosmochim. Acta* **161**, 36–49.
- Clarkson J. R., Price T. J. and Adams C. J. (1992) Role of metastable phases in the spontaneous precipitation of calcium carbonate. *J. Chem. Soc. Faraday Trans.* **88**, 243.
- Littlewood J. L., Shaw S., Peacock C. L., Bots P., Trivedi D. and Burke I. T. (2017)

Mechanism of enhanced strontium uptake into calcite via an amorphous calcium carbonate (ACC) crystallisation pathway Mechanism of enhanced strontium uptake into calcite via an amorphous calcium carbonate (ACC) crystallisation pathway.

Rodriguez-Blanco J. D., Vallina B., Blanco J. A. and Benning L. G. (2014) The role of REE³⁺ in the crystallization of lanthanites. *Mineral. Mag.* **78**, 1373–1380.

Sel O., Radha a. V., Dideriksen K. and Navrotsky A. (2012) Amorphous iron (II) carbonate: Crystallization energetics and comparison to other carbonate minerals related to CO₂ sequestration. *Geochim. Cosmochim. Acta* **87**, 61–68.

Chapter 6

Afterword

6.1 Acknowledgement

First and foremost, I would like to thank my supervisors Martin Dietzel and Florian Gallien for being always supportive to new ideas and for spending so many hours discussing with me and giving me advice on the realization of these ideas. I would also like to thank Omya International AG for their financial support and in giving me the opportunity to obtain a PhD in the first place by founding this project. I am particularly grateful for the scientific discussions I had at Oftringen with Patrick Gane, Joachim Schoelkopf, Dan Gerard, Thomas Staehrfeldt and many more. For providing analytical access of *in-situ* Raman probe, I thank the Research Center Pharmaceutical Engineering and the Austrian Centre for Electron Microscopy and Nanoanalysis in Graz for conducting TEM- and SEM-measurements. Andre Baldermann is thanked for ICP-OES measurements and Katja Goetschl and particularly Maria Hierz for their assistance in the laboratory.

I am immensely grateful to Bettina Purgstaller and Vasileios Mavromatis for their valuable comments and endless discussions on the topic of ACC and more. For providing me with the best office environment one can possibly have, I owe special thanks to my colleagues and friends Cyrill Grengg, Anja Fuger and Jessica Stammerer. It has been a great pleasure to work with all the people from the Institute of Applied Geosciences and to get to know them personally. Thank you for having been a part of an exciting period in my life.

6.2 Curriculum Vitae

Florian Konrad was born on June 3rd 1986 in Hallein. After his high school diploma obtained from the Bundeshandelsakademie Hallein in 2006 and completion of his military service, he enrolled in 2007 at the Leopold Franzens University in Innsbruck to study Geo- and Atmospheric Sciences with specialization in Earth Sciences. He completed his bachelor in 2010 with a thesis in petrology entitled "*Crystal chemistry of heavy metal-rich rutiles and titanites of a manganese quartzite from the Rhodopes/ N-Greece*" and with a thesis in sedimentary geology entitled "*Changes of carbonate-rocky talus slopes of Tyrol over a period of 50-60 years*". For his master, he enrolled for studying Earth Sciences at the Institute of Mineralogy and Petrography in Innsbruck, where he was employed as University Project Assistant. In 2013, he finished with his studies with specialization in Mineralogy with a thesis entitled "*Quantitative phase analysis of Bauxite via NIR-Spectroscopy*", in which the applicability of near-infrared spectroscopy for continuous bauxite mineral quantification on a conveyor belt was tested in close cooperation with industry. In 2014, Florian Konrad started his PhD at Graz University of Technology working in the group of Martin Dietzel at the Institute of Applied Geosciences as University Project Assistant, being part of an industry financed project, in which the synthesis and stabilization of amorphous calcium carbonate and its controlled transformation into crystalline carbonates is investigated.

6.3 Statutory declaration

I declare that I have authored this thesis independently, that I have not used other than the declared sources / recourses, and that I have explicitly marked all material which has been quoted either literally or by content from the used sources.

Date

Signature